UC Berkeley
UC Berkeley Electronic Theses and Dissertations

Title
An experimental study of smoldering-to-flaming transition and emissions from wildland vegetative fuels

Permalink
https://escholarship.org/uc/item/9345z665

Author
Garg, Priya

Publication Date
2023

Peer reviewed|Thesis/dissertation

eScholarship.org Powered by the California Digital Library
University of California

An Experimental Study of Smoldering-to-Flaming Transition and Emissions from Wildland Vegetative Fuels

By

Priya Garg

A dissertation submitted in partial satisfaction of the

requirements for the degree of

Doctor of Philosophy

in

Engineering - Mechanical Engineering

in the

Graduate Division

of the

University of California, Berkeley

Committee in charge:

Professor Michael J. Gollner, Chair
Professor Carlos Fernandez-Pello
Professor Allen Goldstein

Summer 2023

An Experimental Study of Smoldering-to-Flaming Transition and Emissions from Wildland Vegetative Fuels

Copyright 2023
by
Priya Garg

Abstract

An Experimental Study of Smoldering-to-Flaming Transition and Emissions from Wildland Vegetative Fuels

by

Priya Garg

Doctor of Philosophy in Engineering - Mechanical Engineering

University of California, Berkeley

Professor Michael J. Gollner, Chair

Wildfires have increased in frequency and severity over recent decades, resulting in serious impacts on both the environment and human lives. These fires are often fueled by dry conditions, high temperatures, and strong winds, making them difficult to contain. The consequences of these extreme wildfires are enormous, leading to the destruction of vast forested areas, the loss of biodiversity, and the release of harmful gases and particulate matter into the atmosphere. These emissions pose a serious health threat to nearby populations and firefighters who are tasked with controlling the fire.

In this study, the concentration of gaseous and particulate matter emissions resulting from flaming and smoldering combustion of different wildland fuels found across the United States is characterized. Furthermore, the effect of fuel moisture content (FMC) on these emissions is explicitly studied, which has not been considered in the literature before. To achieve this, a custom linear tube-heater apparatus is constructed, enabling the steady production of emissions in different combustion modes across a wide range of FMC. The results obtained demonstrate that smoldering combustion exhibits increased emissions of CO, particulate matter, and unburned hydrocarbons when compared to flaming combustion. Moreover, it is observed that the concentrations of CO and particulate matter in the flaming mode are significantly correlated with FMC, while FMC has little influence on emissions during smoldering mode combustion when considering the dry mass of fuel burned. These variations are observed in certain vegetative fuel species but not others, highlighting the importance of fuel type. Additionally, Fourier-transform infrared (FTIR) spectroscopy is employed to provide detailed characterization of the unburnt hydrocarbons.

Secondly, this study quantifies the limiting conditions for the smoldering-to-flaming (StF) transition, a commonly observed phenomenon during wildfire events, specifically focusing on cellulose powder, which constitutes approximately 50% of vegetative wildland fuel. It is discovered that the external heat flux required for the StF transition increases as the oxygen (O_2) concentration decreases from 21% to 10% at fixed flow velocities. However, for a constant O_2 concentration, an increase in flow velocity leads to a higher required heat flux

due to the growing significance of convective heat losses. Under the experimental conditions, an oxidizer flow velocity of 5 cm/s is determined to be a limiting value for the StF transition. Finally, the efficacy of six different respiratory protection (RP) materials commonly worn during wildland fire events is tested against simulated wildland fire smoke. The findings indicate that cloth bandanas, currently the most commonly used RP material, offer minimal benefits in terms of reducing both particulate matter (PM) and gaseous emissions. On the other hand, all other filter materials demonstrate significant advantages. N95, P95, and P100 filters prove highly effective in removing PM and show some effectiveness in filtering certain gaseous species, particularly those with nuisance volatile organic compound (VOC) capabilities, although this effect may not be sustained over longer durations.

To my parents, family, friends, and everyone who made this possible.

Thank you to all those who have supported and encouraged me throughout my academic journey. I am truly grateful to my parents for their unwavering love and support. It is because of their continuous encouragement and assistance that I have been able to achieve the milestone of obtaining a PhD. Additionally, I would like to extend a special thanks to my brother for his constant support, encouragement, and mentorship. This significant accomplishment would not have been possible without the collective support of my loved ones.

Love,
Priya

Contents

List of Figures

List of Tables

Acknowledgments

This dissertation owes its completion primarily to the unwavering support of my supervisor, Professor Michael J. Gollner. Throughout my graduate studies, he has been a constant presence, providing guidance and encouragement during both the highs and lows. From the moment I joined his group, he granted me the freedom to choose a research project that captivated my interest. Alongside this independence, he offered continuous guidance to help me achieve the objectives of our project. Through his mentorship, I acquired the skills to approach scientific problems systematically and solve them proficiently. He played a pivotal role in shaping me into a proficient researcher, instilling confidence in my ability to make sound scientific decisions. Professor Gollner's work ethics and unwavering curiosity in tackling new challenges serve as a personal aspiration for my career.

I would like to express my heartfelt gratitude to the esteemed members of my doctoral committee: Professor Carlos Fernandez-Pello, Professor Allen Goldstein, Professor Chris Dames, and Professor Van P. Carey. Their invaluable contributions and insights have greatly enhanced the quality of my PhD research work. I consider myself fortunate to have had the opportunity to benefit from their vast knowledge and experience.

I am truly thankful to my colleagues, Dr. Maria Thomsen, Dr. James L. Urban, and Dr. Lauren Gagnon, who have not only acted as mentors but have also provided invaluable support at every step of my academic journey. Dr. Xingyu Ren and Dr. Mohammadhadi Hajilou have been great friends and sources of support throughout my PhD. I am grateful that this friendship will last a lifetime.

I would like to extend my gratitude to everyone in Hesse Hall and the Berkeley Fire lab for being great friends, mentors, and colleagues, and for making the lab an enjoyable place. Special thanks go to Michael Neufer, Daniel Paragas, Tom Clark, Alex Jordan, and Scott McCormick for their assistance in setting things up in the lab and providing continuous support. I am also thankful to all my lab mates: Dr. Sriram Bharath Hariharan, Dr. Luca Carmignani, Dr. Charles Scudiere, Dr. Xiaoyu Ju, Dr. Dwi Marhaendro Jati Purnomo, Dr. Maryam Zamanialaei, Dr. Wuquan Cui, Dr. Shaorun Lin, Cristina Liveretou, Joseph Dowling, Maria Theodori, Kelly Clevenson, Mackenzie Conkling, Siyan Wang, Bryce Bathras, Ingrid Shan, and Alina Rai. I would also like to thank the collaborators from Northestern University, Prof. Jessica M. Oakes, Prof. Chiara Bellini, Matthew J. Eden, and Jacqueline Matz, for their valuable inputs and discussions. Furthermore, I would like to express my gratitude Sara McAllister and Chelsea Philips from the USFS for their assistance in acquiring fuels.

I convey my thanks to the staff at the Mechanical Engineering department, including Yawo Dagbevi Akpawu, Isabel Blanco, Sheila Caguiat, and Ana Preza-Gregg, for their assistance throughout the administrative formalities.

I would also like to acknowledge the Department of Homeland Security (DHS)/Federal Emergency Management Funds (FEMA) Fire Prevention and Safety Grant program for funding this work under award number EMW-2017-FP-00446. This work was also supported by the National Institute of Environmental Health Sciences of the National Institutes of

Health under award number R01ES033792, as well as the California Energy Commission – Energy Program Investment Charge (EPIC) program under grant number EPC-18–026. Additionally, I acknowledge the support from the Ralph A. Seban Heat Transfer Fellowship and the Ernest and Marjory Starkman Fellowship offered by the Mechanical Engineering department at the University of California, Berkeley.

Above all, the never-ending support and encouragement from family and friends have propelled me throughout my academic journey. Most of all, I would like to thank Mukul, who has stood by me and appreciated my achievements.

Chapter 1

Introduction

1.1 Motivation and Scope

Wildland fires play a crucial role in maintaining ecological processes, but they can also pose serious threats to the economy, environment, and human health [10–12]. The risks associated with these fires have been amplified by climate change and changes in land-use and management practices, leading to significant losses for communities [10, 12]. On top of the more direct impacts imposed, the enormous volume of emissions released during wildland fires contributes to both climate change and a variety of adverse health effects on nearby populations. These exposure can be particularly high for firefighters who actively respond to these incidents or engage in mitigation efforts [10, 13–16].

To comprehensively understand and quantify the emissions of gaseous and particulate matter (PM) resulting from wildland fires, it is crucial to understand how emissions vary between different vegetative fuels and the state under which they are burned. As the diversity of wildland fuels, including their loading and fuel states, as well as ambient conditions can vary, emissions under different burning conditions can span a wide range and are not yet well characterized for these diverse conditions. At the fine scale, conditions affecting combustion of specific wildland fuels may include the fuel size and shape, loading, moisture content, ambient wind velocity, local oxygen concentrations, external heating, etc., resulting in combustion occurring under either flaming or smoldering conditions. Experiments are often run with larger fuel complexes or mixtures of fuels with varying conditions at different locations in the fire, making it challenging to identify the specific source of measured emissions. Nonetheless, being able to predict emissions from wildland fuels burning under different conditions remains a goal within the scientific community, which if achieved, can be used to improve air quality predictions, to better comprehend the health effects associated with smoke inhalation, feed into climate models and make better smoke-informed decisions on active or prescribed fires.

The objective of this dissertation is therefore to investigating the emissions of gaseous and particulate matter from different vegetative fuels. This research will examine how these

emissions vary under different moisture contents and combustion conditions, with a particular emphasis on comparing flaming and smoldering. Measurements are conducted in the laboratory using a new apparatus applicable to both direct emissions measurements and mouse-model studies on health effects associated with smoke inhalation [17].

It is also important to understand the effectiveness of mitigation measures to reduce smoke exposure, such as various respiratory protection materials which could be worn by the public or firefighters during these events. In this dissertation, different respiratory protection materials will be tested against the smoldering combustion of vegetative fuel to determine their efficacy and provide enhanced recommendations to wildland fire managers, enabling them to make informed decisions.

As emissions vary drastically between flaming and smoldering conditions, a fundamental study was also conducted to better understand the limiting conditions that can trigger the transition from smoldering to flaming during a wildland fire event. Specifically, factors such as varying oxygen concentration, wind speed, and external heat flux will be examined, with a focus on cellulose powder, a major component of vegetative fuels. Understanding the Smoldering to Flaming (StF) transition contributes to advancing our fundamental knowledge and provides valuable insights to guide the prevention of extreme fire events.

By addressing these research objectives, this dissertation contributes to a comprehensive understanding of wildland fire emissions, the efficacy of respiratory protection materials, and transition from smoldering combustion to flaming during such events. The findings will inform fire management strategies, help mitigate the risks associated with wildland fires, and support decision-making processes to safeguard the environment, economy, and human health.

1.2 Background

1.2.1 Emissions

In recent decades, there has been a significant increase in the frequency, severity, and extent of wildfires in various parts of the world [18–20]. The United States has experienced these escalating trends due to a combination of factors, including a historical approach of aggressively suppressing wildfires, which has led to the accumulation of higher fuel loads. Additionally, climate change has contributed to longer fire seasons, earlier snow melts, and extended periods of drought [19–21]. The influx of people into wildland-urban interface (WUI) areas has further increased the number of individuals vulnerable to the adverse impacts of fires and has also raised the potential for ignition sources. In addition to the direct destruction caused by wildfires, they also release substantial amounts of gaseous emissions and particulate matter (PM) into the atmosphere as seen in Fig. 1.1. The composition of these emissions depends on factors such as the type of vegetation, moisture content, and the state of combustion [22, 23]. As the smoke from these wildfires can travel long distances, it can significantly affect air quality and have broader implications for the earth-climate system

[24]. Wildland firefighters and nearby populations face the risk of exposure to these wildfire-related pollutants, potentially leading to various health effects. Firefighters, in particular, experience high concentrations of smoke exposure, often repeatedly within the same fire season, due to their occupation [10, 25]. In contrast, the exposure patterns of surrounding populations differ, as they typically face location-based exposures and have access to more mitigation measures such as masks or indoor filtration systems.

Figure 1.1: Wildland fire emitting particulate matter and gaseous emissions into the environment. Image Credit: Salam2009. Website: https://en.wikipedia.org/wiki/File:Wildfire From The Air.jpg

The extent to which this smoke exposure impacts both first responders and surrounding populations has been widely studied in literature. Adetona et al. [10] performed a thorough literature review on the health effects of wildfires on both firefighters and the public. Short-term health effects observed from these emissions includes asthma exacerbation, coughing, headache, hypertension, and breathlessness [26–28], while long-term health effects include respiratory and cardiovascular illness [11, 12, 17, 29].

Numerous studies have quantified emissions from wildfires [3, 30, 31], prescribed fires [32], and smaller-scale laboratory experiments [33–35]. Experiments on both wildland and prescribed fires have thus far been unable to distinguish between modes of combustion, fuel type, and fuel composition whereas some laboratory studies [23, 36, 37] have considered the mode of combustion and fuel type as an important parameter.

Estimating emissions of various effluents from wildland fires typically involves two steps. First, the amount of biomass consumed out of the initial available biomass is calculated, often termed ‘fuel consumption’ [3]. Then, the amount of effluent produced is estimated using an emission factor (EF),

$$\text{EF } (g/kg) = \frac{\text{mass}_i}{\text{mass}_{d,fuel}} \tag{1.1}$$

where mass_i represents the mass of species emitted in grams and $\text{mass}_{d,fuel}$ is the mass of dry fuel consumed in kg. While this representation only provides time-averaged results, it is a useful framework which is commonly used alongside time-varying measurements.

Urbanski [38] sampled emissions over three wildfires and a prescribed fire that occurred in mixed conifer forests of the northern Rocky Mountains using airborne instruments measuring concentrations of carbon monoxide (CO), carbon dioxide (CO_2), methane (CH_4), and PM. The study is believed to be first to apply in-flight technology to characterize the emissions for open biomass burning in a natural environment. They concluded that fuel composition and combustion conditions play an important role in EF variability. Numerous laboratory studies [4–6, 35, 39] have been performed at the Missoula Fire Sciences Laboratory, Rocky Mountain Research Station, USDA Forest Service, in Missoula, Montana, U.S.A., quantifying emissions from various vegetation in pile burns using FTIR sampling in the exhaust duct of a large overhead hood. The first study in this series, performed in 1996 [39], suggested that combustion conditions and fuel type strongly effects emissions.

It is well known that emissions can vary depending on both the mode of combustion and fuel type; however, there are very few studies addressing these changes alongside varying fuel moisture content (FMC). Mobley [40] found fuel arrangement and moisture content are significant factors affecting the resulting emission factors (EFs) within similar fuel types. Studies conducted in the field including wildfire and prescribed fire emissions are unable to distinguish between modes of combustion, fuel type, and fuel conditions. Moreover, it is difficult to determine an appropriate location for instrumentation to sample emissions that is representative of total emissions from a fire. Emissions may also vary from location to location during a wildland fire as mixing and secondary combustion takes place within the plume. To fill these gaps, it is crucial to study emissions that result from each specific fuel type and combustion condition. The work performed in this dissertation is conducted in a small-scale laboratory apparatus which has the benefit of burning under controlled conditions, where properties of the fuel (like chemical composition, mass, shape, size) are known, the environment is very well controlled, and the emissions are fully captured, measured, and analysed.

Emission factors are strongly dependent on burning conditions, moisture content, and type of fuel [23]. Fuel moisture content is often defined based on the wet, M_W vs. dry mass, M_D of the sample,

$$\text{FMC} = \frac{M_W - M_D}{M_W} * 100. \tag{1.2}$$

The percentage of water or other liquid compounds that evaporate during the determination of dry fuel mass is essentially what is referred to as Fuel Moisture Content (FMC). It is important to note that the definition of FMC used in this context is distinct from that used in some wildland fire studies, where the denominator in equation 1.2 is replaced with the

dry mass, resulting in FMC ranging from 55% to 180% [36, 37]. To differentiate between different modes of combustion, i.e. flaming and smoldering, a modified combustion efficiency is frequently employed,

$$\mathrm{MCE} = \frac{\Delta \mathrm{CO}_2}{(\Delta \mathrm{CO}_2 + \Delta \mathrm{CO})} * 100 \tag{1.3}$$

where it is assumed that $\Delta \mathrm{CO}_2$ and $\Delta \mathrm{CO}$ are the excess concentrations of CO and CO_2. A full mass balance including all carbon-based species would be ideal; however, it has been found that this simplified version works well to distinguish modes of combustion, because CO and CO_2 are the primary effluents by mass ($> 94\%$) [3].

Numerous studies have extensively investigated the impact of FMC on smoldering combustion in peat fires and organic soils. This focus stems from their prolonged burning duration, generation of effluents, and associated detrimental health effects. In experiments conducted by Hu et al. [36, 37], peat was found to sustain smoldering combustion at high FMC levels of up to 61%. On the other hand, McMahon et al. [41] conducted laboratory-scale experiments on wet and dry soil samples and observed low emissions of NO_x, but high levels of particulate matter (PM) emissions during smoldering combustion. However, none of these studies conducted a comprehensive analysis of the comparison between smoldering and flaming combustion of various fuel types under different FMC. This serves as a primary motivation for the present work.

1.2.2 Smoldering to Flaming (StF) transition

Emissions from burning wildland vegetation can vary drastically depending on the combustion conditions. Smoldering combustion accompanies almost all wildland fire spread either under limiting ambient conditions or as post-frontal combustion behind the flaming front. Smoldering is a slow, low-temperature, flameless mode of combustion, differing from gas-phase flaming combustion in terms of chemistry, transport processes, time scales, and emissions. For both smoldering and flaming, pyrolysis is a common prerequisite, generating gaseous pyrolyzate and solid char that are both susceptible to subsequent oxidative reactions. Smoldering is more specifically a heterogeneous oxidation reaction where oxygen molecules directly react with the hot surface of fuel or char, whereas flaming is a homogeneous oxidation reaction of pyrolyzate and ambient oxygen.

More importantly, smoldering can be initiated by a weak heat source [42] commonly present during a wildland fire event or even self-ignition [43], providing a shortcut to flaming through smoldering-to-flaming (StF) transition, which is a rapid initiation of homogeneous gas-phase ignition (i.e., flaming) induced by a heterogenous solid surface reaction (i.e., smoldering). In this transition process, the smolder reaction acts both as the source of pyrolyzate and ignition heating. This process can lead to severe consequences through a sudden increase in spread rate, heat release, and subsequent safety hazards [44]. StF transition also contributes to rapid fire spread during wildland-urban-interface fires by lofting embers (i.e.,

firebrands). These accumulating and often smoldering embers can initiate local smoldering ignition which may later exhibit StF transition that leads to fire spread far beyond the original fire point [44–47]. Despite its important hazard, our understanding of the precise conditions for StF transition and controlling mechanisms remains limited.

In this work, we also aim to quantify the limiting conditions of the StF transition of cellulose powder, which is the major component of ($\sim 50\%$) of vegetative wildland fuel and provide the value of radiant heat flux required at varying oxygen concentrations and oxidizer flow velocities. The limiting external heat fluxes required for StF transition is an important research topic as it is commonly seen in wildland fires.

1.2.3 Health Effects

Particulate matter (PM) produced during a wildland fire event is often considered the most important constituent to predict the health hazard of smoke, especially to surrounding populations, where there is more time and distance for effluent dilution. PM is classified by aerodynamic diameter: coarse (aerodynamic diameter between 2.5 and 10 μm), fine (< 2.5 μm), and ultra-fine (< 0.1 μm) [48]. Literature shows that wildland smoke is dominated by respirable particles, i.e., < 4 μm [10, 25]. Previous studies performed during periods of wildland fire events [10, 49] have measured fine PM (≤ 2.5 μm) and respirable PM (≤ 4 μm) which are small enough to penetrate into the lungs. The maximum occupational exposure limit for respirable PM by the Occupational Safety and Health Administration (OSHA) is 5,000 $\mu g/m^3$; however, concentrations surrounding wildland fire events are often very high (12.5 mg/m^3 as reported by Alves et al. [50] in the immediate vicinity of fire) compared to this limit [10].

Gaseous species emitted are also a significant concern, especially closer to the fire source, as some of them are carcinogenic and can cause major health issues. Species of major concern include carbon monoxide (CO), sulfur dioxide (SO_2), nitrogen dioxide (NO_2), ozone (O_3), acrolein (C_3H_4O), formaldehyde (CH_2O), benzene (C_6H_6), toluene (C_7H_8), and xylene (C_8H_{10}) [10]. Exposure to these species beyond the established exposure limits could be deadly. OSHA in the United States has defined exposure limits for these species which should be taken into consideration by firefighters when working for days or weeks in the field [51]. For instance, CO easily binds with hemoglobin to form carboxyhemoglobin (COHb), limiting the oxygen carrying capacity of blood, resulting in short term effects like headache, dizziness, disorientation, and weakness [52]. Acrolein and formaldehyde are respiratory irritants and exposure beyond the limit can cause lung injury. Formaldehyde and benzene are classified as carcinogens and nitrogen dioxide causes a decrease in pulmonary responses [10]. Additionally, high concentrations of ozone and other gases formed downstream the fire location are also associated with acute cardiovascular effects and respiratory illness [53]. A few studies at prescribed fires and wildfires have reported measured emissions of gaseous species below the exposure limits, but this result largely depends on the location of sampling [10, 32, 54, 55].

Knowing the potential health effects of smoke exposure, it is very important for nearby populations and firefighters to protect themselves when conditions warrant by wearing proper

Figure 1.2: Wildland firefighter working close to fire during an event of Wildland fire. Website: https://www.dhs.gov/science-and-technology/wildland-fire-fighter-uniform-redesigned

respiratory protection (RP) equipment. Wildland firefighters work in very close proximity of fire fronts as shown in Fig. 1.2 and often remain at locations which can experience heavy smoke for extended periods of time, for instance during inversion events. Therefore, having proper RP equipment can be necessary to preserve their health.

Wildland firefighters, however, are often observed wearing either bandanas or no covering over their nose and mouth. In contrast to structural firefighters, who employ self-contained breathing apparatus (SCBA) that adhere to National Fire Protection Association standards [49, 56], wildland firefighters lack standardized respirators. The use of SCBA in wildland settings is impractical due to limited air supply duration and the weighty cylinders, which pose challenges during high temperatures and physically demanding work. The prevalence of masks and respirators has significantly increased during the COVID-19 pandemic [57, 58], yet their specific effectiveness against wildland fire smoke remains unstudied in the literature. Therefore, this study aims to examine the efficacy of various respiratory protection materials in the context of wildland firefighting.

1.3 Outline of the Dissertation

This dissertation explores the emissions of gaseous and particulate matter from various vegetative fuels found in wildland fires, which are burned using a small-scale laboratory setup. The details of the experimental setup developed for this specific research and the diagnostic techniques employed are presented in Chapter 2. The chapters following Chapter 2 are organized roughly based on the journal articles that comprise this dissertation. Each chapter

contains a separate introduction and literature review. A comprehensive list of references is provided as a bibliography. Chapter 3 presents the effects of FMC on gaseous and particulate emissions from flaming and smoldering combustion of four different vegetative fuels under varying FMC found across the United States. The data is further compared with real wildland fires and prescribed fires, and discussed in the chapter. Chapter 4 presents the detailed gaseous species measured using FTIR for two vegetative fuels under two different FMCs and two combustion conditions. Chapter 5 presents the limiting conditions required for the Smoldering to Flaming (StF) transition of cellulose powder, which is a major component of vegetative fuel. These limiting conditions include heat flux, oxygen concentration, and oxidizer flow velocity. Finally, Chapter 6 discusses the effectiveness of various respiratory protection materials used by wildland firefighters against the emissions produced from vegetative fuels. A conclusion and future research directions are presented in Chapter 7. Additional figures, raw data, and details of FTIR measurements are included in the Appendices.

1.4 Summary

This study aims to address three distinct issues that arise during wildland fire events: quantification of emissions in relation to changes in vegetative fuel type, FMC, and combustion conditions; investigating the transition from smoldering to flaming (StF) combustion for cellulose powder; and evaluating the effectiveness of different respiratory protection materials against wildland fire smoke. By conducting these investigations, we aim to gain a deeper understanding of the variations in emissions, the propagation of wildland fires, and their impact on human health.

Chapter 2

Experimental Setup

2.1 Vegetative fuels

In this work, various different vegetative fuels representation of those consumed in US wildland fires are used, and a broad explanation of each fuel type is provided in this chapter. Subsequent chapters will briefly discuss the fuel type that was used and its state during the experiments.

Four fire-prone species were chosen for testing in this work: Douglas fir (*Pseudotsuga menziesii* (Mirb.) Franco), mountain laurel (*Kalmia latifolia*), lodgepole pine (*Pinus contorta* Douglas ex Loudon), and pitch pine (*Pinus rigida* Mill.), as shown in Fig. 2.1. These species were selected because of their availability and prevalence in fire-prone ecosystems. Lodgepole pine and Douglas fir were shipped from Missoula, Montana, providing a representation of wildland fires in western United States forests. Mountain laurel and pitch pine were shipped from New Jersey, with the Pine Barrens there representing a subset of fires in oak pine forests of the United States.

Fuels were picked live from trees, placed in sealed plastic bags and shipped overnight to the University of California, Berkeley. Samples were immediately placed in a refrigerator to avoid decomposition until experiments were performed. Samples were prepared so that continuous flaming conditions could be reached during testing. Lodgepole and pitch pine needles were cut into ~ 3 cm segments. Mountain laurel leaves were crushed before testing, and Douglas fir needles were burned without any further processing.

2.2 Moisture content

Three different drying conditions were investigated, referred to as 'live', 'wet', and 'dry', based on the duration of drying before testing (0 h, 3 h, and 72 h respectively), resulting in approximately $52.9\% \pm 4.20\%$, $11.9\% \pm 1.43\%$, and $2.88\% \pm 0.91\%$ FMC respectively, where the error range represents the standard deviation between different test averages. Leaves and needles were first removed from branches to form a single layer over a perforated aluminium

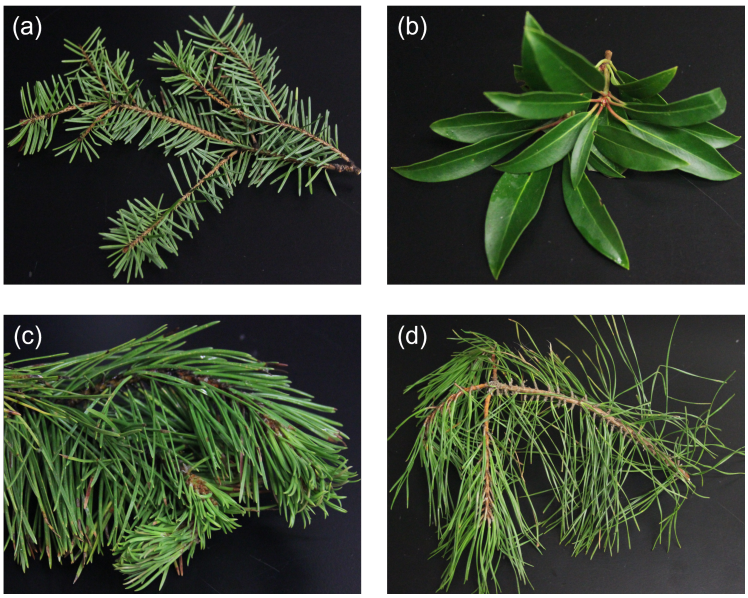

Figure 2.1: Various vegetative fuels i.e., (a) Douglas fir, (b) mountain laurel, (c) lodgepole pine, and (d) pitch pine used in this study.

tray and placed in a laboratory convection oven at 70°C for approximately the duration noted earlier. It is hypothesised that the loss of volatile constituents mainly depends on drying parameters and, by using a lower drying temperature, a wet condition is achieved such that it retains some, but not all, volatiles and other characteristics of live fuels [59–61]. Towards the end of the drying duration, a subset of samples was removed, and their moisture content was analysed using an A&D MF-50 moisture analyser, which rapidly heats samples over a micro-balance using a quartz heater. FMC was continuously checked on multiple samples before testing.

2.3 Apparatus

Combustion of wildland fuels was conducted in a custom-made linear tube-heater apparatus based on DIN 53436 [62, 63], shown in Fig. 2.2. This apparatus is relatively new for wildland fuels and consists of a 182 cm long quartz tube with an inner diameter of 3.5 cm and a narrow, annular ceramic heater with a length of 15.2 cm and an inner diameter of 7.6 cm. The ceramic heater surrounding the quartz tube was mounted on a Velmex linear actuator that moved along the outside of the quartz tube at a controllable speed. The heater travelled in the direction opposite to the primary airflow in the tube (counter-current direction), and it was employed with the lowest heating rate that exhibited continuous flaming without preheating the upstream fuel throughout the test duration. Moreover, the traverse rate of the heater

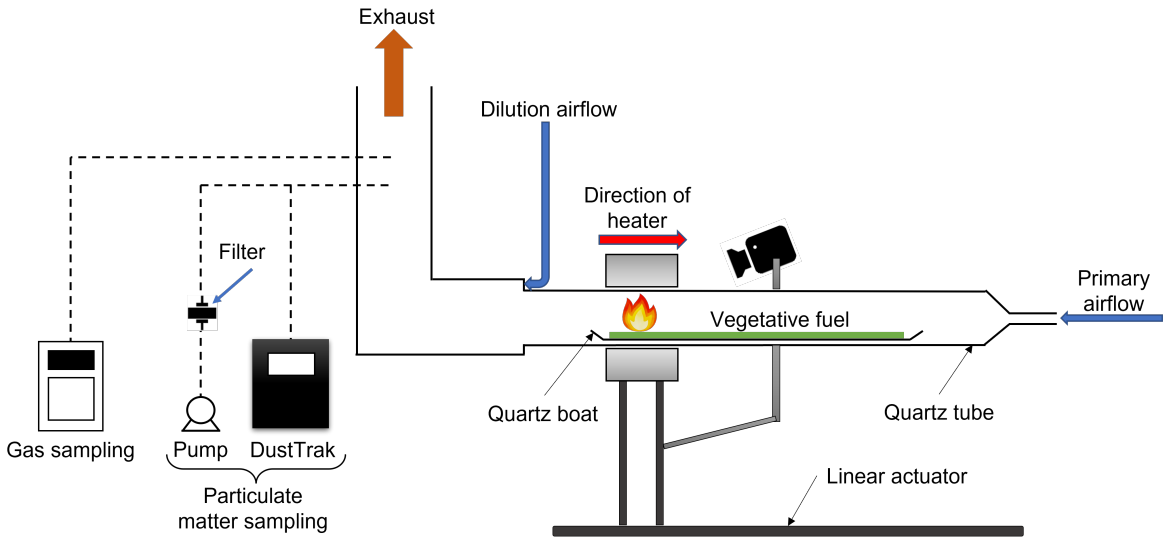

Figure 2.2: Schematic diagram of the linear tube-heater smoke generator apparatus (not to scale – dimensions are mentioned in the text).

was determined after performing several preliminary experiments at each condition such that it did not accelerate the burning process of the fuel. A similar experimental setup was used recently [64]; however, the heater was travelling in the same direction as the primary airflow (co-current direction), resulting in mixed flaming and smoldering combustion, potentially re-burning pyrolysed fuels in the flaming mode. DIN 53436 was designed to provide a continuous and constant concentration of species over a long duration of time ($>$ 60 min), a condition that is unachievable in the steady-state tube furnace [65]. The electrically heated ceramic can reach a temperature as high as 1200°C; controllable using a K-Type thermocouple placed adjacent to the ceramic heater. Radiant heat flux on the top fuel surface from the heater was measured by a radiometer aligned at the center of the quartz tube. The temperature of the heater was increased from 50 °C to 700 °C in the increment of 25 °C and the corresponding equivalent external heat flux was recorded. An empirical correlation between the temperature of the heater and equivalent radiant heat flux was formulated as $\dot{q}''_e = 2.8exp(0.005T)$, with $R^2 = 0.98$ as shown in Fig. 2.3. The temperature was set in the range of 450–475°C ($\sim$ 25.5 - 28.8 kW/m^2 of external heat flux) for smoldering and in the range of 625–650 °C ($\sim$ 60.1 - 67.9 kW/m^2 of external heat flux) for flaming experiments. After combustion, heating tape set to 100°C was placed over the quartz tube, minimising deposition of particulates on the tube.

Conditions such as the amount of fuel, airflow, operating temperature, and translation speed were optimised to achieve fully flaming or smoldering combustion for each test condition (see Table 2.1). The fuel was evenly distributed along the 80 cm long quartz boat, which was then placed in the quartz tube. One end of the quartz tube was supplied with

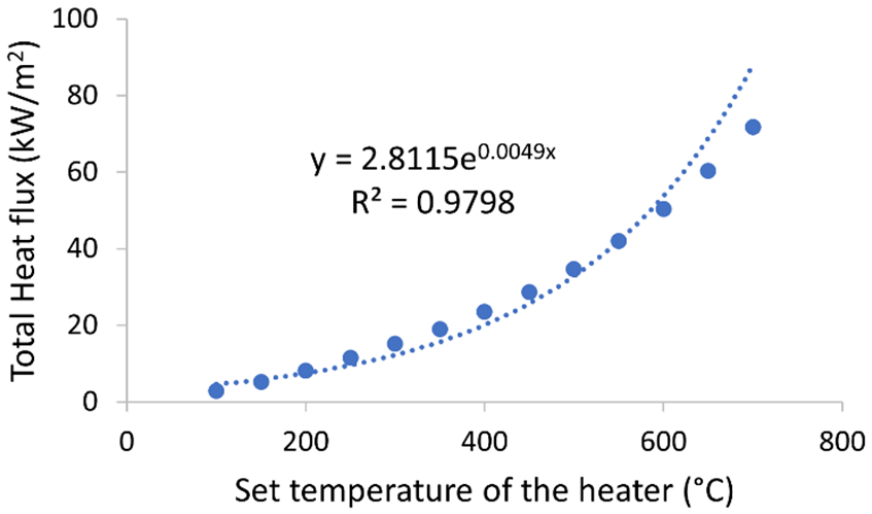

Figure 2.3: Total heat flux corresponding to set temperature of the heater.

Table 2.1: Control parameters for continuous flaming and smoldering experiments. DF, Douglas fir; LPP, lodgepole pine; PP, pitch pine; ML, mountain laurel

Fuel	Air Flow (L/min)		Amount of Fuel (g)		Heater rate (cm/min)	
	Primary	Dilution	Flaming	Smoldering	Flaming	Smoldering
DF	3	15	15	7.5	3	2
LPP	3	12	15	7.5	3	2
PP	3	15	10	5	3	2
ML	3	15	10	5	3	2

dry air and the other end was either attached to a 7.62 cm diameter steel exhaust port, where emissions were diluted using dilution air before leaving to the exhaust or was directly connected to the instrumentation. Both primary and dilution airflow rates were controlled using Alicat flow controllers; flow rates varied depending on burning conditions (see Table 2.1). A stainless-steel sampling tube, 9.24 mm inner diameter with 2 mm holes spaced 12.7 mm apart along the length, was inserted through the diameter of the steel exhaust, ensuring enough length for fully-developed flow and mixing. Effluents were drawn from both ends of the sampling probe by a 6.35 mm tubing connected to the gaseous and particulate matter diagnostic instruments. Due to the low saturation limits of the instruments, the smoke was diluted a third time before analysis of smoldering experiments. Only when performing Fourier-transform infrared (FTIR) spectroscopy was the the smoke not diluted, with the instrument probe inserted directly into the outlet of the quartz tube . Figure 2.4 shows the actual experimental setup in the laboratory.

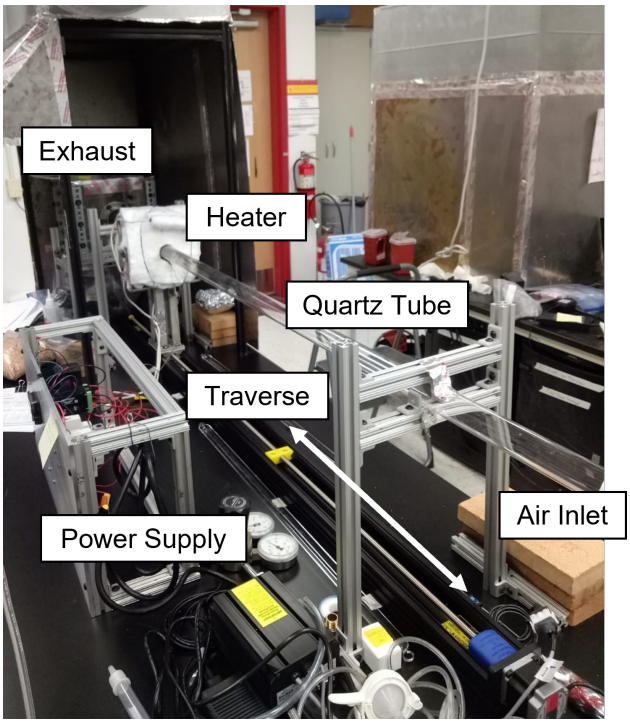

Figure 2.4: Actual setup in the laboratory

2.4 Instrumentation

2.4.1 Gaseous Sampling

Two different gaseous sampling devices were used depending on the sampling technique desired. Both are described in detail below.

2.4.1.1 Fourier-transform infrared (FTIR)spectroscopy

Real-time concentrations of different gas species were measured from a heated probe positioned directly at the outlet of the quartz tube during experiments using a Thermo Scientific Nicolet iG50 Fourier-transform infrared (FTIR) spectroscopy, as shown in Fig. 2.5. FTIR is a powerful technique utilized to obtain the infrared absorption spectrum of a gas. The absorption in the infrared range arises from the vibrational-rotational transitions of gas molecules. Through the comparison of measured spectra with reference spectra of the gas in question, taken under well-defined conditions of temperature, pressure, and concentration, the FTIR instrumentation enables the retrieval of trace gas concentrations.

The FTIR used in this work has a 2 m pathlength gas cell, along with a deuterated triglycine sulfate (DTGs) detector. Experiments were performed at 0.5 cm^{-1} resolution with

Figure 2.5: Image of Thermo Scientific Nicolet iG50 Fourier-transform infrared (FTIR) spectroscope placed on a cart.

a sampling frequency of 0.025 Hz. Gases were continuously sampled throughout the duration of the experiment. All the ducts were constantly heated to 100°C to avoid gas condensation. The FTIR was thoroughly purged with dry air before every experiment and background concentrations were subtracted from the results. Based on the gas calibration and built-in least square algorithm of the FTIR, the real time concentration of 26 gaseous species which are commonly reported in fire literature were measured: carbon dioxide (CO_2), carbon monoxide (CO), sulfur dioxide (SO_2), nitric oxide (NO), nitrogen dioxide (NO_2), ammonia (NH_3), methanol (CH_3OH), hydrogen cyanide (HCN), hydrogen chloride (HCl), hydrogen fluoride (HF), hydrogen bromide (HBr), nitrous acid (HNO_2), acetic acid (CH_3COOH), formic acid (CH_2O_2), acrolein (C_3H_4O), formaldehyde (CH_2O), methane (CH_4), water (H_2O), acetylene (C_2H_2), ethane (C_2H_6), propane (C_3H_8), butane (C_4H_{10}), isobutene (C_4H_8), ethene (C_2H_4), propene (C_3H_6), and isoprene (C_5H_8). The reference spectra of these 26 targeted gases were used to determine concentrations at the sampled conditions, 100°C and 650 torr, using a full-gas factory calibration. Table A.1 (Appendix A) provides the details of spectral bands used during calibration of various gaseous species, along with the interferences.

Figure 2.6: Image of (a) Enerac 700 [1] and (b) DustTrak DRX Aerosol Monitor 8534 [2].

2.4.1.2 Enerac 700

An Enerac 700 shown in Fig. 2.6(a) provided real-time concentrations of oxygen (O_2), nitrogen oxide (NO), nitrogen dioxide (NO_2), oxides of nitrogen (NO_x), and sulfur dioxide (SO_2) using an electrochemical sensor and the concentrations of carbon dioxide (CO_2), carbon monoxide (CO), and unburnt hydrocarbons (HC) using a nondispersive infrared (NDIR sensor, which was calibrated against propane for the concentration of HC, all with an acquisition frequency of 1 Hz. The internal pump flow rates were set at 1.5 L/min and 1 L/min for flaming and smoldering conditions respectively. Electrochemical sensors used for CO_2 and CO measurement can accurately detect low-range concentrations, up to three digits. When exposed to higher concentrations, these sensors utilize a dilution air to facilitate measurement. By combining the readings from the sample oxygen sensor and the dilution oxygen sensor, an accurate concentration of CO_2 and CO can be obtained for the higher ranges [1]. However, it should be noted that transitioning from the low range to the high range requires time and caution. During testing, measures were taken to prevent the Enerac 700 from switching to the high range, as this could result in data loss.

2.4.2 Particulate Matter (PM) Sampling

A DustTrak DRX Model 8534 with a concentration range of 0.001–150 mg/m^3 and a flow rate of 3 L/min was used for real-time measurements of PM with an acquisition frequency of 1 Hz as shown in Fig. 2.6(b). Although the device could distinguish different size ranges (e.g. PM_1, $PM_{2.5}$, PM_{10}, and TPM), little variation was observed, so only TPM has been reported in this study. Moreover, experiments were performed with caution in order to avoid over-saturating the DustTrak beyond 150 mg/m^3. Gravimetric analysis was performed to calibrate readings from the DustTrak and to provide time-averaged PM mass measurements using a 0.8 µm pore size mixed cellulose ester filter placed in a 37 mm filter cassette, connected to the pump running at 2 L/min. During an experiment, filters that are exposed to

particulate matter will acquire a static charge. Prior to weighing the filters, the static charge was neutralized using an NRD 2U500 Staticmaster Ionizing Cartridge. The weight of the filters before and after neutralization was measured using a Sartorius CPA225D scale with a maximum weighing capacity of 220 mg and a resolution of 0.01 mg.

Additionally, experiments were continuously recorded using a GoPro camera to help explain sudden peaks in PM and CO, often attributed to a transition between smoldering and flaming.

Chapter 3

Effect of moisture content and fuel type on emissions

3.1 Introduction

The occurrence of wildland fires is increasing every year, resulting in the release of substantial amounts of gaseous and particulate matter into the atmosphere. These emissions have detrimental effects on human health, emphasizing the critical need to comprehend and study these pollutant releases while distinguishing them based on fuel type, fuel moisture content (FMC), and combustion conditions. Emission measurements for a wide variety of field burns are available in the literature. However, it is challenging to accurately determine the source of emissions due to large-scale land burning and the dependence of precise measurements on the location of the instrumentation. Additionally, literature also provides emission measurements from laboratory experiments and pile burns, but they do not always isolate the effect of individual features such as FMC.

This study explores the effect of FMC on gaseous and particulate emissions from flaming and smoldering combustion of four different wildland fuels found across the United States. A custom linear tube-heater apparatus was built to steadily produce emissions in different combustion modes over a wide range of FMC. A selected set of chemical species have been examined in this study, including carbon-based species, oxygen (O_2), nitrogen oxide (NO), nitrogen dioxide (NO_2), oxides of nitrogen (NO_x), sulfur dioxide (SO_2), and unburnt hydrocarbon (HC). Four of these (CO, PM, SO_2, and NO_2) belong to the six 'criteria air pollutants' as identified by the United States Environmental Protection Agency (EPA).

Results showed that when compared with flaming combustion, smoldering combustion showed increased emissions of CO, particulate matter, and unburned hydrocarbons, corroborating trends in the literature. The emissions of CO and particulate matter during flaming mode combustion exhibited a strong correlation with the FMC, whereas FMC had minimal impact on emissions during smoldering mode combustion when considering the dry mass of burned fuel. These variations were observed across different types of vegetative fuel,

suggesting that the fuel type is a crucial factor. The dissimilarities in emissions could be attributed to the chemical composition of moist and recently live fuels, which are analyzed and compared with previous findings in the existing literature.

3.2 Background

Wildland fires emit a mixture of gaseous and particulate emissions during combustion that impacts the health of first responders, nearby populations, and the earth-climate system. Recent studies have shown both short- and long-term health effects from these emissions [10], in particular to the pulmonary and cardiovascular systems [11, 12, 29]. In addition, earth-climate simulations rely on estimates of global carbon production from fires [66]. Numerous studies have quantified emissions from wildfires, prescribed fires [30, 32, 67, 68], and smaller-scale laboratory experiments [34, 35]. Ward [69] developed a model for predicting particulate matter emission rates as a function of fireline intensity and flame length for prescribed fires. Freeborn et al. [34] measured a wide range of effluents from flaming laboratory fires of numerous fuels with fixed fuel moisture content (FMC). Reinhardt and Ottmar [30, 68] tracked time-averaged exposure of gases and particulates to wildland firefighters operating on several tasks in the field, finding the highest exposure levels during prescribed fires, most likely due to increased FMC and smoldering conditions. Effluents measured included benzene, acrolein, formaldehyde, CO, CO_2, respirable particulate matter (PM), and total particulate matter (TPM). Despite higher levels measured during prescribed fires, all measurements were still determined to be within permissible levels, even though wildland firefighters do not generally wear respiratory protection [30, 68]. Fuels in the field ranged from completely live to dead, with modified combustion efficiency (MCE) ranging from 75% to 95% [3].

It is well known that smoldering and flaming combustion dramatically differ in emissions behaviour; however, there are few studies addressing changes in emissions for different burning conditions such as changes in fuel type, FMC, and mode of combustion. Within similar fuel types, fuel arrangement and moisture content are known to strongly influence resulting emission factors (EFs) [70]. Chen et al. [71] studied the effect of moisture content on emissions from litter, duff, soil, and aboveground shrub vegetation in laboratory-scale experiments. They first completely dried the fuels and then re-wetted them to obtain a desired moisture content. They concluded that the overall combustion efficiency decreases as the FMC increases. They also saw change in EFs as the FMC changed, but no prominent trend was reported. May et al. [23] performed a laboratory examination of the effect of FMC on sugar gum eucalyptus (Eucalyptus cladocalyx), mountain laurel (Kalmia latifolia), and northern bayberry (Myrica pensylvanica). Laboratory experiments of fire spread over a 1 m^2 test surface showed that FMC had a drastic impact on production of PM, CO, and CO_2. It was hypothesised that some of this was due to the presence of volatile oils in recently-live, moist samples, especially eucalyptus. Using a cone calorimeter, Possell and Bell [72] also showed a large effect on emissions with changes in FMC of eucalyptus. Emission factors of

CO and PM were observed to correlate with decreasing FMC, though the peak heat-release rate (HRR) increased. Hayashi et al. [73] performed experiments on the residue of three cereal crops, that is, rice, wheat, and barley at two moisture contents (dry and wet) and measured gas and particle emissions from open burning. They saw differences in emissions and combustion conditions with crop type, as wheat straw underwent long-duration smoldering, whereas rice and barley straw underwent long-duration flaming. They concluded an increase in carbon species emitted occurred with an increase in FMC; similar results were also found for loblolly needle beds burned in the laboratory [70].

The effect of FMC on smoldering combustion has been well studied for peat fires [36, 37] and organic soils [41] due to their large production of effluents, impacts on health, and extended burning durations. Hu et al. [36, 37] performed experiments at eight different FMCs and showed that peat can self-sustain smoldering combustion with FMC as high as 61%. McMahon et al. [41] performed laboratory-scale experiments on wet (75% FMC) and dry (6.63% FMC) soil samples and found very low emissions of NO_x. PM emissions during smoldering combustion were particularly high, which is important as PM can lead to various respiratory and cardiovascular diseases [11, 29]. PM emissions were measured for different size ranges by Hu et al. [36, 37] using a staged cascade impactor. Variations in the production rate of PM were observed for different FMC under the same burning conditions. Hu et al. [36, 37] also observed different particles, namely blackish carbon particles during flaming combustion and a yellowish haze during smoldering combustion, which is characteristic of haze aerosols from wildland fire smoke with diameters less than 1 µm. McMahon et al. [41] also found a similar bright yellow colour on the glass fibre filters designed to capture particulates from experiments and reported that they were most likely oil droplets from smoldering combustion, concluding no soot particles were evident. None of the aforementioned studies performed a detailed analysis on the filters to identify the chemical compounds present.

Recent studies [74–76] have shown that emission data are multivariate and relative in nature as the amount of mass burned and released (in terms of smoke emissions, residual char and ash) are fixed by conservation of mass. They propose a new Compositional Data Analysis (CoDA) technique that considers the relative nature of data, which is ignored in commonly used statistical techniques in the literature. However, the present study is performed on a custom-made linear tube-heater apparatus, and it becomes important to compare and validate the results with literature where traditionally statistical techniques are used. So, in this study, data is expressed as an average ± standard deviation between averages from different experiments.

3.3 Experimental Method

In this work, four vegetation fuel species shown in Fig. 2.1 have been tested at 3 different fuel moisture contents referred to as ‘live’, ‘wet’, and ‘dry’, resulting in approximately 52.9% ± 4.20%, 11.9% ± 1.43%, and 2.88% ± 0.91% FMC respectively. Four different diagnostic

techniques were used. An Enerac 700, DustTrak, Gravimetric filters, and a GoPro camera. Numerous preliminary experiments were conducted to characterise the experimental setup and achieve a continuous flaming condition. The amount of fuel and the heater speed were varied for different fuels and FMC to achieve continuous flaming, as reported in Table 2.1. Gas sampling for all experiments were repeated four times: two times alongside a filter cassette and two times with a DustTrak. Caution was applied not to cause the Enerac 700 to switch from a low range to a high range during testing, which would result in data loss, or to over-saturate the DustTrak beyond 150 mg/m^3. Any saturated data, which amounted to a small fraction of what was recorded in any one experiment, was removed during post processing. This process did not appreciably affect the reported results.

3.4 Results

3.4.1 Time-dependent burning process

Time-dependent concentrations of gaseous emissions from representative tests of flaming Douglas fir at 10% FMC are shown in Fig. 3.1. Emissions remain relatively constant throughout the test duration, with a small increase in CO and a very small decrease in TPM over time. The former is possibly due to the time required to achieve steady-state conditions, and the latter due to deposition onto the quartz tube. CO and CO_2 are clearly the primary effluents with smaller contributions of HC, NO_x and SO_2. HRR is also shown, calculated using CO_2 production [77] due to its greater sensitivity than O_2 measurements. Other fuel types similarly emitted a constant concentration of gaseous emissions with time; average values from these tests are reported in Table 3.1.

Flaming and smoldering combustion results in different emissions, most dramatically in CO and TPM production. Fig. 3.2 shows the influence of FMC on CO production during both flaming and smoldering combustion of Douglas fir. As the FMC decreases, the CO concentration increases for smoldering combustion. This may be attributed to differences in the makeup of the moisture in the fuel, which could include volatiles that enhance combustion efficiency; however, such differences are not observed when time- and mass-averaged EFs are calculated (see next section). For flaming combustion, dry and live conditions produce the most CO emissions, with wet conditions generating significantly less CO. It is important to note that these results do not incorporate the influence of a reduced burning rate for wetter fuels and that the flame and heater move at different rates for flaming and smoldering combustion (see Table 2.1) which results in a shorter test duration for flaming versus smoldering. Smoldering tests with live fuels are an exception, where readings cannot be maintained for the full test duration due to changes between the high/low range of the Enerac sensor.

Table 3.1: Characteristics of the biomass smoke emitted from the tube-heater apparatus

FLAMING								
Sample	MCE	TPM (mg/m^3)	CO (ppm)	CO_2 (%)	HC (ppm)	NO_x (ppm)	SO_2 (ppm)	HRR (W)
DF - L	97.3±0.85	57.8±3.78	2091±536	7.74±0.48	0	154±38.2	5.82±2.82	562±33.0
DF - W	99.4±0.43	114±35.9	655±40.98	12.2±0.18	1.68±2.10	225±6.72	28.3±8.70	883±15.1
DF - D	99.1±0.28	168±48.3	1119±357	12.8±0.78	14.0±15.5	196±31.3	27.8±14.7	929±57.7
PP - L	-	-	-	-	-	-	-	-
PP - W	99.2±0.27	107±20.7	819±275	1008±2.28	0	219±32.8	15.4±12.0	730±1.8
PP - D	99.3±0.12	119±1.62	733±132	1082±12.5	11.8±13.6	225±36.3	13.7±15.5	785±3.48
LPP - L	97.9±0.98	50.0±0.75	1030±100	6.40±0.05	0	144±15.4	10.7±4.35	462±3.4
LPP - W	99.5±0.30	117±14.8	456±18.7	11.9±0.05	0	257±6.75	28.5±4.85	720±4.65
LPP - D	99.6±0.02	68.5±15.6	544±30.1	12.9±0.15	0	256±8.95	38.9±2.20	785±10.6
Kalmia - W	99.4±0.03	26.8±1.98	554±30.7	9.36±0.06	0	220±36.2	24.5±3.36	675±3.30
Kalmia - D	99.5±0.03	95.6±46.8	511±16.3	9.42±0.60	0	245±19.5	20.3±3.18	681±47.2
SMOLDERING								
Sample	MCE	TPM (mg/m^3)	CO (ppm)	CO_2 (%)	HC (ppm)	NO_x (ppm)	SO_2 (ppm)	HRR (W)
DF - L	77.6±1.22	1525±21.12	4481±844	1.56±0.18	383±58.7	64.8±29.9	0	128±17.0
DF - W	81.9±0.05	2203±88.7	6833±645	3.12±0.30	675±104	114±8.58	0	243±36.0
DF - D	81.4±1.81	2641±710	8332±883	3.66±0.06	843±216	121±12.7	0	298±0.24
PP - L	77.9±20.0	821±257	3741±414	1.08±0.18	165±15.2	57.7±69.2	0.72±1.02	89.5±27.8
PP - W	79.3±1.22	1547±97.4	6274±241	2.40±0.06	347±10.1	35.6±16.9	0	198±5.34
PP - D	77.3±0.77	1909±195	7436±213	2.52±0.06	363±7.80	60.2±17.6	0	213±2.04
LPP - L	74.9±13.3	1370±125	5656±1131	1.70±0.35	302±60.3	78.9±15.8	0	99.8±27.5
LPP - W	82.4±2.64	2213±407	7283±948	3.40±0.20	536±46.7	103±25.6	0	230±7.85
LPP - D	79.9±0.32	2494±325	9198±326	3.65±0.05	607±6.75	98.8±10.7	0	252±4.60
Kalmia - W	79.8±7.01	1432±76.3	6385±754	2.52±0.30	398±49.6	117±17.5	24.0±18.8	169±53.8
Kalmia - D	83.2±0.12	1830±265	5590±269	2.76±0.18	443±16.9	78.7±18.9	0	191±56.8

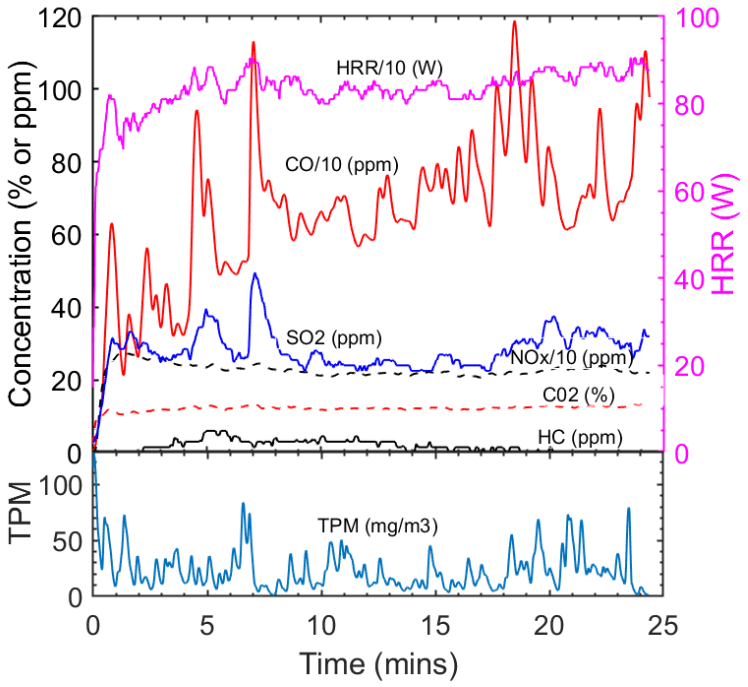

Figure 3.1: Average concentrations of CO (ppm/10), CO_2 (%), HC (ppm), NO_x (ppm/10), SO_2 (ppm), HRR (W/10), and TPM (mg/m^3) from 10% MC Douglas fir emissions as measured directly out of the quartz tube. Note the use of both %, ppm, and scaling by a factor of 10 in order to highlight all species on one graph.

3.4.2 Cumulative emissions

Fig. 3.3 shows the EF of various species at three different FMC. It was not possible to achieve a continuous flame for live pitch pine and mountain laurel leaves (50% FMC), suggesting some chemical differences between the remaining liquids or structural differences in the way compounds evaporate from leaves versus needles. This behaviour has been observed previously during convective ignition experiments [78], but it has not been reported in regards to sustained flaming or emission conditions. A similar behaviour was also observed by Engstrom et al. [79] and Fletcher et al. [80] while testing live fuel species using a flat-flame burner; however, resulting emissions were not a focus of either study.

For flaming combustion, between species, Douglas fir and lodgepole pine show elevated EFs of TPM between 50% (live) and 10% (wet) FMC conditions, followed by a decrease from the 10% (wet) to the 2% (dry) conditions, whereas EFs of CO first decrease and then slowly increase. CO production is also notably higher for live conditions, which may be due to incomplete combustion, with the MCE dropping from 99% to 97% for this condition. Total production of CO and TPM was less for dry fuels compared with that for live and wet

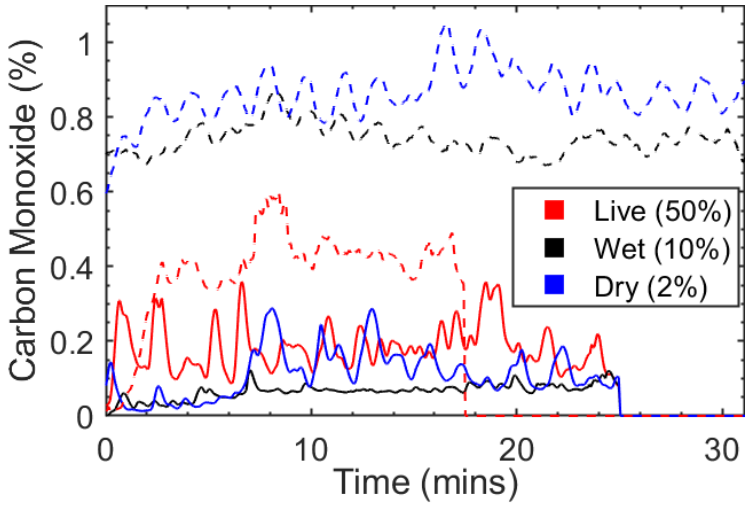

Figure 3.2: CO emissions for Douglas fir with varying MC under flaming (solid line) and smoldering (dashed line) condition as measured directly out of the quartz tube.

fuels, which is to be expected as the energy provided by the heater is spent in vaporising the moisture of live plants, thus delaying the complete combustion of the pyrolysis species. Pitch pine and mountain laurel, however, have opposite trends compared with Douglas fir and lodgepole pine, which may have occurred due to differences in the chemical makeup of the fuels. NO and NO_2 have been combined to NO_x due to the negligible amount of NO_2 detected. It is decreasing with decrease in FMC, except for mountain laurel.

Possell and Bell [72] performed experiments on eucalyptus with varying FMC, and the peak CO released during mass-loss calorimetry followed a similar trend as our tests on conifers from Montana, Douglas fir and lodgepole pine. Conifers from the New Jersey Pine Barrens, however, behave in a different manner, with pitch pine and mountain laurel showing little variation in emissions between wet and dry fuels.

Hydrocarbon emission factors were not presented for flaming conditions because they were negligible and within the sensitivity of the instrument (resolution of ± 4 ppm). SO_2 was also below 0.5 g/kg of fuel for all flaming conditions. McMeeking et al. [7] previously observed SO_2 EF in the range of $0 - 1$ g/kg of fuel, so values reported here are in a similar range.

Unlike flaming, EFs from smoldering combustion are relatively uniform, regardless of FMC condition. EF of various species at three different FMC are reported for only lodgepole pine in Fig. 3.3e (Plots of other vegetative species is presented in Appendix B). EFs, MCE and average concentration for the fuel species under various FMC are reported in Table 3.1. Emissions of TPM, CO, HC, and NO_x are higher for smoldering compared with those for flaming. CO_2 production during smoldering is lower than that for flaming by an order of magnitude, corresponding to a reduction in HRR. Further, statistical analysis supported the

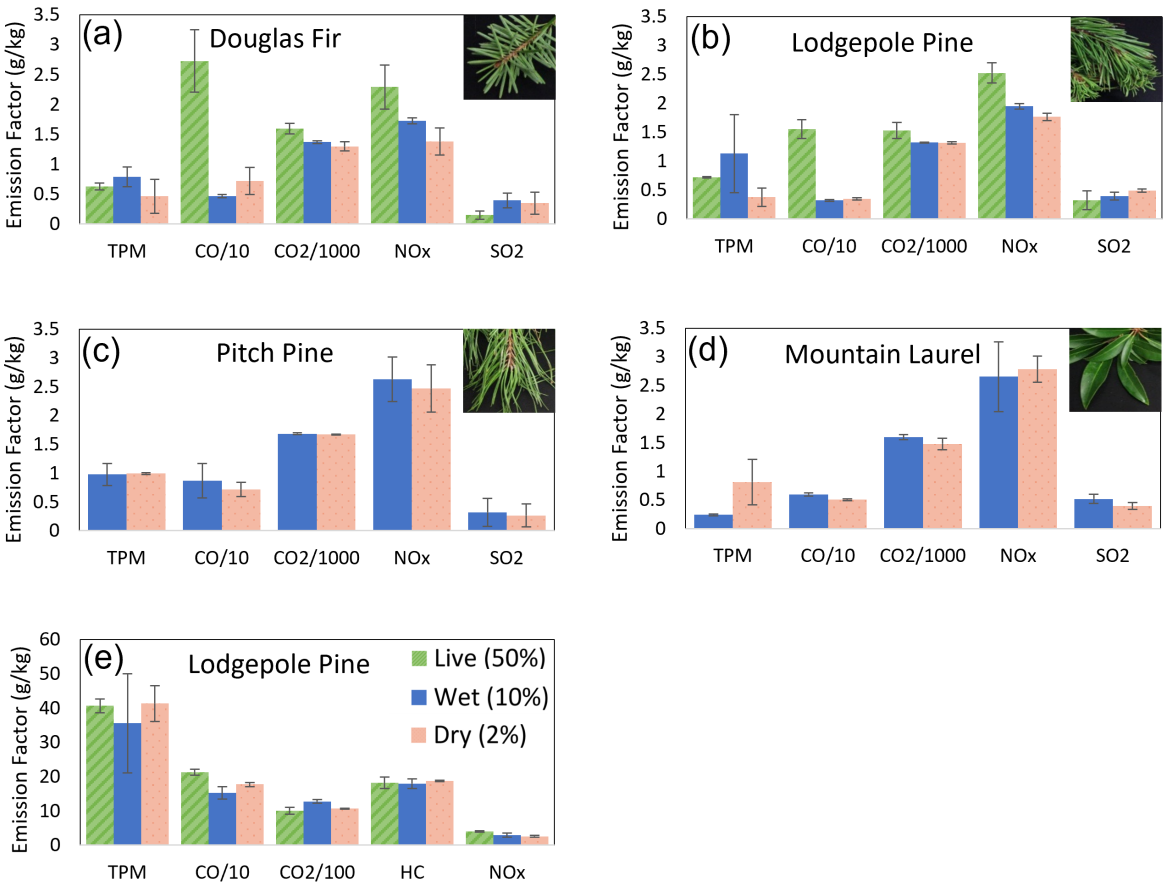

Figure 3.3: (a-d) Average EFs of different species during flaming combustion of different fuels at 3 FMC conditions, (e) Average EFs of species during smoldering combustion of lodgepole pine at 3 FMC conditions. Error bars represent the standard deviation between averages from different tests.

observed differences between flaming and smoldering combustion. A paired sample t-test was performed on the average values of the EFs, and the value of P was obtained as 1.05e–9, 4.25e–9, and 1.87e–4 for TPM, CO, and CO_2 respectively, signifying greater variation of emission species among two different combustion conditions. SO_2 is not reported due to negligible levels detected.

A small decrease in TPM and CO EFs is observed for the wet condition in smoldering Douglas fir and lodgepole pine fuels, similarly seen in MCE. Pitch pine also has the lowest CO EF for wet fuel, but the CO EF for live fuel is almost three times that of the wet and dry conditions. The NO_x EF follows the same trend as CO for pitch pine, whereas it is relatively uniform for other fuel types. An increased mass of fuel was used for lodgepole pine compared with that for pitch pine, yet the TPM EF is comparatively lower than that for pitch pine. With small decreases in the TPM and CO EFs for the wet condition, there is a small increase in the CO_2 EF. The opposite trend of the CO and CO_2 EFs can be explained by the oxygen supply and carbon content present in the controlled emissions setup. Smoldering of the type of vegetation chosen in this study has previously been discussed in the literature, but Hu et al. [36, 37] is the only one to have explored the effect of FMC, and for that study only on smoldering peat fires. It is interesting to note that the CO EF for previous studies of peat fires did not vary much with FMC, similar to what was observed in this study for Douglas fir, lodgepole pine and mountain laurel. The average HC EF for different fuels is around 20 g/kg, and this value is comparable to those reported by McMeeking et al. [7].

3.5 Discussion

A major requirement of the new apparatus built in this study was to produce steady emissions from vegetative fuels under different burning conditions. The time-dependent emissions behaviour of wet Douglas fir (Fig. 3.1) showed the resulting adaptability of the apparatus as the emissions produced are relatively constant throughout the test duration and a similar trend was found for all other fuel types under both flaming and smoldering combustion conditions. Control over the amount of fuel, ambient airflow, heater temperature, and moving rate makes this setup versatile allowing for emissions to be measured from a vast array of fuels varying in FMC, size (long versus short pine needles), and shape (needles versus leaves) under different combustion conditions (flaming, smoldering, pyrolysis (in an inert atmosphere) and even mixed modes of combustion).

Emissions were found to vary between both species and the FMC of the vegetation. The MCE, which roughly characterises a transition between flaming and smoldering, was determined to be $\sim 99\% \pm 0.8\%$ for flaming experiments and $\sim 80 \pm 2.5\%$ for smoldering experiments. Field observations from wildland fires have reported a MCE between 85% and 95%, as there is a mix of both flaming and smoldering [3, 38]. As expected, HRR increases with decreasing FMC for both smoldering and flaming. Our apparatus, in essence, achieves extreme conditions, that is, fully flaming and fully smoldering, which is helpful to better understand and characterise the source of these emissions. Unlike most previous

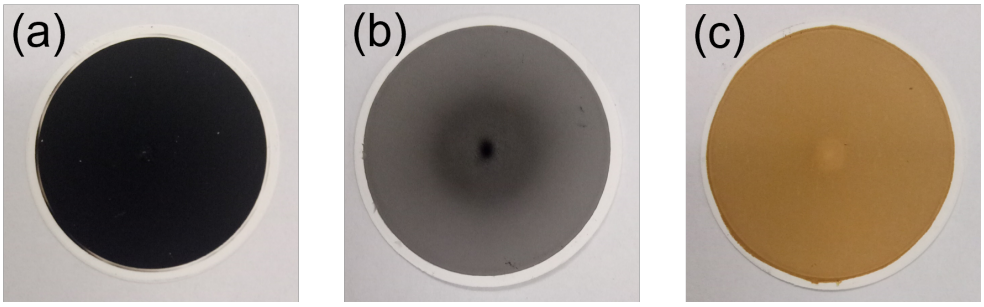

Figure 3.4: Particles emitted from (a) flaming DF, LPP, and PP, (b) flaming ML, and (c) smoldering combustion conditions.

experiments, fuels were dried at low temperatures to preserve liquid volatiles, rather than completely drying them at first and then rehydrating them to introduce FMC [71, 81]. The presence of this liquid both inhibits combustion by requiring additional energy for vaporisation and, in some cases, may contribute to heat release through remaining liquid volatiles.

Both CO and HC EFs for smoldering combustion remain relatively constant for all fuels, whereas for flaming combustion variations are observed for CO as a function of both fuel type and FMC. The CO concentration decreases with increased FMC for smoldering combustion, but for flaming it shows a small reduction and then increases with increase in the FMC (see Fig. 3.2). This is similar to what Hu et al. [36] observed for experiments over smoldering peat fires and Possell and Bell [72] for flaming eucalyptus experiments. TPM measurements generally followed similar trends. These trends no longer appear for smoldering combustion when considering fuel consumption in the EF (see Fig. 3.3e, similar to Hu et al. [36, 37]). Gravimetric filter samples also appeared starkly different after tests with flaming versus smoldering samples as shown in Fig. 3.4. Flaming experiments resulted in what appeared to be black carbon particles, whereas smoldering experiments had a yellowish colour, indicating the presence of aerosols that should be chemically analysed in the future. McMahon et al. [41] and Hu et al. [36, 37] have also reported the similar difference between filters but did not analyse them chemically. Differences in the colour of filters was also observed among the fuel species. As shown in Fig. 3.4(a,b), Douglas fir, pitch pine, and lodgepole pine produce much darker particles than mountain laurel under flaming experiments, and all four fuel types resulted in yellow colour filters under smoldering combustion.

Video observations also reveal further differences between fuel types. Douglas fir exhibits a ‘popping’ behaviour during flaming combustion that is not observed with other fuels. This behaviour was previously noted by McAllister and Finney [78], who observed ‘bursting’ of vapours from recently-live pine needles under convective heating. Engstrom et al. [79] and Fletcher et al. [80] also reported bubbling/bursting of leaf surfaces that contain a high moisture content. This highlights the effect not only of volatiles that could be present in

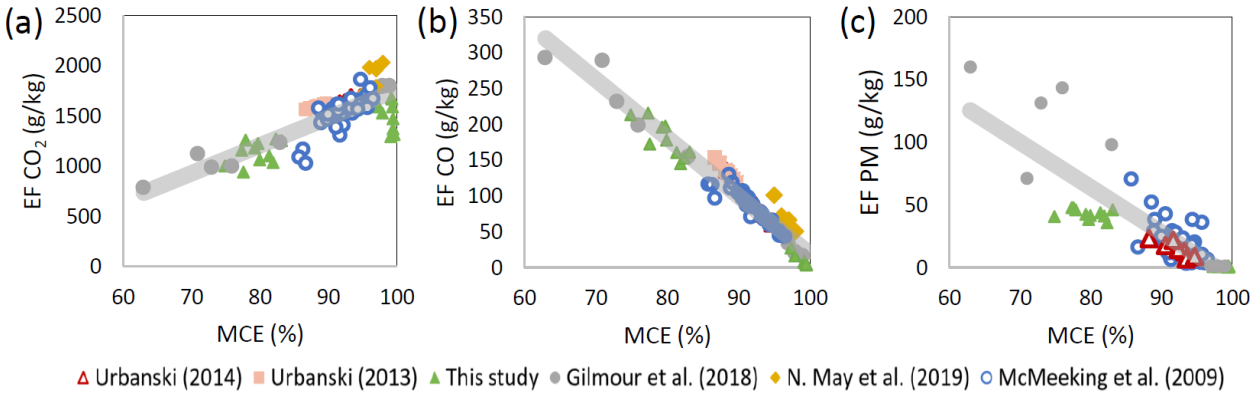

Figure 3.5: A comparison of EFs of different species during flaming and smoldering combustion vs. MCE. Results from previous studies are also shown.

the fuel, but also of structural differences that change the manner in which the volatiles are released. These differences may together contribute to the variability in EFs across species. For flaming combustion, the EF of CO for both mountain laurel and pitch pine is about half that of Douglas fir and lodgepole pine under wet conditions and 1/3 of that for NO_x. The fact that pitch pine and mountain laurel could not sustain flaming combustion under a nearly-live (50% FMC) condition further highlights these differences.

It is known in the field of fire toxicity that scale will affect emissions and not all the results can be replicated at the small scale. Previous studies have found strong correlations between calculated EFs and MCE. To validate the results obtained using this tube-heater apparatus, EFs for CO, CO_2, and PM were compared with published EFs from previous biomass combustion studies. Here we compare our results with five different studies in the literature, out of which two were prescribed fires [3, 38], two were open combustion experiments in a laboratory [7, 23], and one study was performed in a similar apparatus but run in an opposite, concurrent configuration [64]. Among these studies, only May et al. [23] have explicitly varied FMC. Fig. 3.5 shows how the EFs are linearly dependent on MCE. These linear trends are fitted with a linear function with R^2 values of 0.60, 0.94, and 0.70 for CO_2, CO, and PM respectively. CO has the strongest correlation with MCE. It is interesting to note that field studies generally lie between fully smoldering and flaming conditions, as achieved in this and one previous study [64], indicating that real fires typically incorporate mixed modes of combustion that cannot always be well documented in the field but can be very well studied in the small-scale setup developed in this study.

3.6 Conclusions

It is clear that the new apparatus built to steadily generate emissions from vegetative fuels highlighted the strong effect of FMC on emissions from fires in many cases. Decreased FMC often results in higher heat release during combustion and lower heating rates needed to achieve sustained flaming combustion. As expected, smoldering combustion resulted in significantly increased CO, PM, and HC emissions compared with flaming for all the fuel types. For flaming combustion, CO production decreases from live to wet and slightly increases from wet to dry for Douglas fir and lodgepole pine, but little variation is observed with FMC between pitch pine and mountain laurel. Higher FMC, therefore, does not always result in different emissions; it depends on the nature of the fuel. For smoldering combustion, emissions are similar between wet and dry fuels, in contrast to what was observed in previous peat studies.

FMC effects on emissions have not been well documented in the past, due in part to difficulties acquiring and testing large quantities of fuels. This new approach, with small fuel samples under controlled environments, provides a platform from which to deduce effects of fuel species, FMC and burning conditions on produced effluents. Although differences between laboratory-scale tests and field conditions will always occur, trends observed in the laboratory can be useful to highlight variations that are observable in the field, including those relevant to human health. Open questions remain, such as capturing a broader spectrum of effluents, understanding the chemical composition of different vegetation, investigating the filter colour difference from flaming and smoldering combustion, increasing the number of different FMC conditions, and assessing the variation in emissions between experiments at different scales.

3.7 Acknowledgements

Data from this chapter, in part, has been published in *International Journal of Wildland Fire*, “Effect of moisture content and fuel type on emissions from vegetation using a steady state combustion apparatus”, by P. Garg, T. Roche, M. Eden, J. Matz, J. M. Oakes, C. Bellini, and M.J. Gollner (2022) 31, 14 - 23. The thesis author is the primary investigator in this publication.

Chapter 4

Broader spectrum of gaseous emissions using FTIR

4.1 Introduction

Wildland fires are both an essential ecological process and a potential hazard leading to devastating impacts on the economy, environment, and human health [10–12]. Risks from large-scale wildland fires have increased due to climate change and evolving land-use and management practices, leading to the damage or destruction of homes, businesses, and other infrastructure. This has lead to significant economic losses including the cost for recovery and rebuilding. Billions of US dollars are spent every year for wildland fire management activities including preparedness, suppression, and fuel management. The impact of wildland fires, however, spread far beyond immediately threatened areas.

Wildland fires are also significantly coupled to climate change, both directly and indirectly. When a wildland fire occurs, it releases large amounts of carbon dioxide and other greenhouse gases into the atmosphere. This contributes to the accumulation of greenhouse gases in the atmosphere, which is the primary driver of global warming and climate change. Additionally, these fires can have a feedback effect on climate change. As global temperatures rise, many regions are experiencing longer and more severe dry seasons, which increases the risk of fires [13–16]. Moreover, vast amounts of gaseous and particulate emissions are released into the atmosphere, posing a significant risk to surrounding populations. Firefighters, who are at the front lines responding to these disasters or mitigation efforts such as prescribed burning, are particularly vulnerable to exposure from these emissions, which can have a variety of long-term health effects, in particular to the pulmonary and cardiovascular systems [10, 12, 82, 83]. So, it becomes really important to understand and quantify these gaseous and particulate matter emissions.

In this chapter, the concentration and emission factors of 20 different gaseous species and total particulate matter (TPM) have been measured for two different vegetative fuel species with varying fuel moisture contents (FMC) burned under both flaming and smoldering com-

bustion conditions. Data in this study are expressed as an average ± the standard deviation between averages from different experiments.

4.2 Literature Review

Emissions from burning wildland vegetation can vary drastically depending on the conditions under which combustion occurs. While wildland fires are often pictured as towering flames, smoldering combustion accompanies almost all wildland fire spread either under limiting ambient conditions or as post-frontal combustion behind the flaming front. Smoldering is a slow, low-temperature, flameless mode of combustion, differing from gas-phase flaming combustion in terms of chemistry, transport processes, time scales, and emissions. For both smoldering and flaming, pyrolysis is a common prerequisite, generating gaseous pyrolyzate and solid char that are both susceptible to subsequent oxidative reactions. Smoldering is more specifically a heterogeneous oxidation reaction where oxygen molecules directly react with the hot surface of fuel or char, whereas flaming is a homogeneous oxidation reaction of pyrolyzate and ambient oxygen. Smoldering fires therefore occur without flames at lower temperatures, resulting in incomplete combustion and the production of large amounts of particulate matter and other pollutants such as carbon monoxide and volatile organic compounds [39]. In contrast, flaming combustion occurs when fuels burn at high temperatures with visible flames, resulting in more complete combustion and lower concentration of particulate matter and other pollutants. During a wildland fire event, both smoldering and flaming co-exist making it difficult to understand the source of these emissions. Numerous studies have quantified emissions from wildfires [3, 30, 31], prescribed fires [32], and laboratory experiments of burning vegetation [33–35, 47]. Experiments on both wildland and prescribed fires have thus far been unable to distinguish between modes of combustion whereas some laboratory studies [36, 37] have considered the mode of combustion as an important parameter.

Urbanski [38] sampled emissions over three wildfires and a prescribed fire that occurred in mixed conifer forests of the northern Rocky Mountains using airborne instruments measuring concentrations of carbon monoxide (CO), carbon dioxide (CO_2), methane (CH_4), and PM. They concluded that fuel composition and combustion conditions play an important role in EF variability. Guerette et al. [84] characterised 25 gaseous species from Australian temperate forest prescribed fires using Open-path Fourier-transform infrared spectroscopy (OP-FTIR). The EF of various gaseous species such as formaldehyde, acetic acid, methanol, etc. exhibited significant dependence on the Modified Combustion Efficiency (MCE), which will be described later. Scharko et al. [85] identified for the first time naphthalene, methyl nitrite, allene, acrolein, and acetaldehyde using FTIR at prescribed fires in longleaf pine stands. They compared the results with emissions recorded using other sampling techniques such as gas chromatography–mass spectrometry (GC-MS) and proton-transfer-reaction time-of-flight mass spectrometer (PTR-ToF-MS), and concluded that variation among the studies is due to multiple factors including different fuel types, varying analytical methods, sampling

techniques, and experimental conditions. Akagi et al. [86] reported emissions from three pine-understory prescribed fires conducted in the Southern United States (South Carolina), using airborne FTIR. They reported numerous known air toxins and suggested that peak exposures are more likely to challenge permissible exposure limits for wildland fire personnel than shift average (8 h) exposures. Numerous laboratory studies [4–6, 35, 39] have been performed at the Missoula Fire Sciences Laboratory, Rocky Mountain Research Station, USDA Forest Service, in Missoula, Montana, U.S.A., quantifying emissions from various vegetation in pile burns using FTIR sampling in the exhaust duct of a large overhead hood. The first study in this series, performed in 1996 [39], suggested that combustion conditions and fuel type strongly effects emissions. Later studies [4–6, 35] quantified emissions for various different vegetative fuel types and reported new and interesting hydrocarbon gaseous species like furan, 1-2,-Butadiene, and isobutene. These tests, however, could not isolate burning conditions due to the rather uncontrolled pile-burn geometry.

It is well known that emissions can vary depending on both the mode of combustion and fuel type; however, there are few studies addressing these changes alongside varying FMC. Mobley [40] found fuel arrangement and moisture content are significant factors affecting the resulting emission factors (EFs) within similar fuel types. Studies conducted in the field including wildfire and prescribed fire emissions are unable to distinguish between modes of combustion, fuel type, and fuel conditions. Moreover, it is difficult to determine an appropriate location for instrumentation to sample emissions that is representative of total emissions from a fire. Emissions may also vary from location to location during a wildland fire as mixing and secondary combustion takes place within the plume. To fill these gaps, it is crucial to study emissions that result from each specific fuel type and combustion condition. One way to achieve this is through conducting small-scale laboratory studies. These studies also have the benefit of burning under controlled conditions, where properties of the fuel (like chemical composition, mass, shape, size) are known, the environment is very well controlled, and the emissions can be fully captured, measured, and analysed [39].

In laboratory-scale experiments, Chen et al. [87] investigated the impact of moisture content on emissions from various fuels, including litter, duff, soil, and aboveground shrub vegetation. After drying and re-wetting the fuels to a desired moisture content, they found that an increase in FMC led to a decrease in overall combustion efficiency. Although changes in EFs were observed with varying FMC, no clear trend was identified. May et al. [23] conducted a laboratory examination of the effect of FMC on sugar gum eucalyptus, mountain laurel, and northern bayberry. Their fire spread experiments over a 1 m^2 test surface demonstrated that FMC had a significant impact on the production of PM, CO, and CO_2. The presence of volatile oils in recently-live, moist samples, particularly eucalyptus, was hypothesized to be a factor. Possell and Bell [72] used a cone calorimeter to investigate the effects of FMC on eucalyptus emissions. Although the peak heat-release rate (HRR) increased, CO and PM emissions were observed to decrease with decreasing FMC. Similarly, Hayashi et al. [73] found that an increase in carbon species emissions occurred with an increase in FMC in experiments on the residue of rice, wheat, and barley crops. Combustion conditions and emissions differed depending on the crop type, with wheat straw undergoing long-duration

smoldering and rice and barley straw undergoing long-duration flaming. Mobley [40] also found similar results for loblolly pine needle beds burned in laboratory experiments.

Studies have extensively studied the impact of FMC on smoldering combustion for peat fires and organic soils due to their long burning durations, production of effluents, and negative health effects. In experiments conducted by Hu et al. [36, 37], peat was found to sustain smoldering combustion at high FMC levels of up to 61%. On the other hand, McMahon et al. [41] conducted laboratory-scale experiments on wet and dry soil samples and observed low emissions of NO_x, but high levels of particulate matter (PM) emissions during smoldering combustion. PM emissions were measured using a staged cascade impactor for different size ranges, and Hu et al. [36, 37] noted variations in the production rate of PM for different FMC levels under the same burning conditions. Hu et al. [36, 37] also observed blackish carbon particles during flaming combustion and a yellowish haze during smoldering combustion, which is characteristic of haze aerosols from wildland fire smoke with diameters less than 1 µm. Similarly, McMahon et al. [41] reported a bright yellow color on glass fiber filters designed to capture particulates from experiments and concluded that they were most likely oil droplets from smoldering combustion, with no evidence of soot particles. However, none of these studies conducted a comprehensive analysis on the filters to identify the chemical compounds present.

4.3 Experimental methods

Douglas fir and lodgepole pine needles were chosen as fuels for testing. Elemental analysis (dry basis) was performed at an independent lab using a Thermo Scientific Flash Smart CHNS Elemental Analyzer, based on the modified Dumas Method. The analyzer uses a combustion method to convert the sample elements into simple gases (CO_2, SO_2, H_2O, and N_2). The resulting gases go through a column where they are separated and, after separation, are detected as a function of their thermal conductivity. Both vegetative fuels were tested three times and the results provided the value of C/H/N as 52.38 ± 0.17/6.44 ± 0.09/ 1.48 ± 0.05 % for lodgepole pine and 51.39 ± 0.2/ 6.34 ± 0.07/ 1.28 ± 0.8 % for Douglas fir pine needles.

Recently-live fuel experiments were performed within 2-3 days of receiving samples. For wet and completely dry conditions, the fuel was dried in the oven as explained in Chapter 2. Following the drying process, the FMC for the samples at which the tests were performed resulted in 48.02 ± 6.95 %, 23.18 ± 2.89 %, and 3.54 ± 1.11 % for live, wet, and dry respectively. As the fuel is dried at a lower temperature and monitored for moisture content, Douglas fir consistently experienced a sudden drop to a dry condition moisture content, due to which wet conditions were not achieved for Douglas fir and are therefore not reported in this chapter.

Experiments were performed in a custom made linear tube-heater apparatus as shown in Fig.2.2. The heater temperature was set at 475°C ($\sim$ 28.82 kW/m^2 of external heat flux) for smoldering and 650°C ($\sim$ 67.95 kW/m^2 of external heat flux) for flaming experiments. Four

different diagnostic techniques were used: transient gas (Thermo Scientific Nicolet iG50 Fourier-transform infrared (FTIR)) spectroscopy and PM (DustTrak DRX Model 8534), time-averaged PM (Gravimetric filters), and video recording (GoPro camera).

4.4 Results and discussion

4.4.1 Combustion dynamics

Once the temperature and heater travelling rate are set, the fuel initially pyrolyses for a few seconds before igniting into continuous flaming or smoldering combustion, depending on the prescribed test conditions. Emissions are recorded starting 2 minutes after ignition, ensuring only continuous flaming and smoldering products are measured and the filters in the sampling probe do not become clogged with high concentrations of unburnt HCs and TPM. Figure 4.1 shows a snapshot of typical flaming and smoldering combustion conditions observed inside the quartz tube for dry lodgepole pine. These conditions remain steady throughout the duration of the experiment. Similar behavior is observed for other fuel types and test conditions as well.

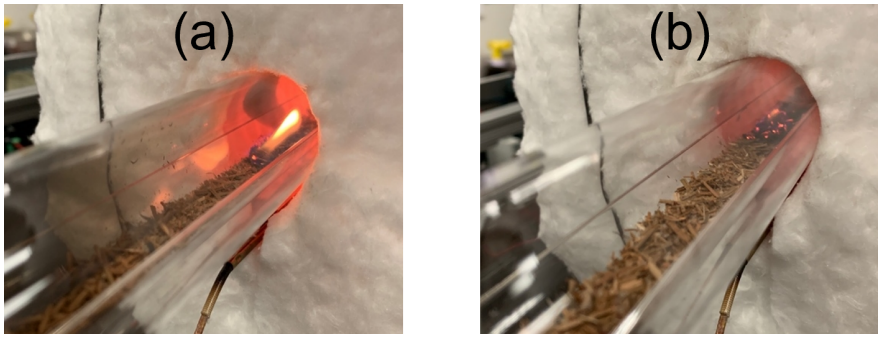

Figure 4.1: Snapshot of continuous (a) Flaming and (b) smoldering combustion throughout the duration of the experiment for dry lodgepole pine needles.

Gaseous emissions were sampled using FTIR which provides a 3D spectra of time-dependent gaseous emissions throughout the duration of an experiment. Figure 4.2 (a, c) shows this absorbance spectra for dry (Fig. 4.2a) and live (Fig. 4.2c) Douglas fir under flaming combustion. Following the spectra as a function of time, it is clear that emissions from this setup have a steady-state emissions profile throughout the duration of the test. As this spectra is relatively constant, a 2D plot of wavenumber vs. absorbance spectra is also provided in Fig. 4.2 (b, d) for live and dry flaming Douglas fir, respectively.

The FTIR instrument was carefully calibrated for all 26 gaseous species by selecting different spectral bands to avoid any discernible interference from other gaseous species. Further details about the specific spectral regions and corresponding gaseous species can

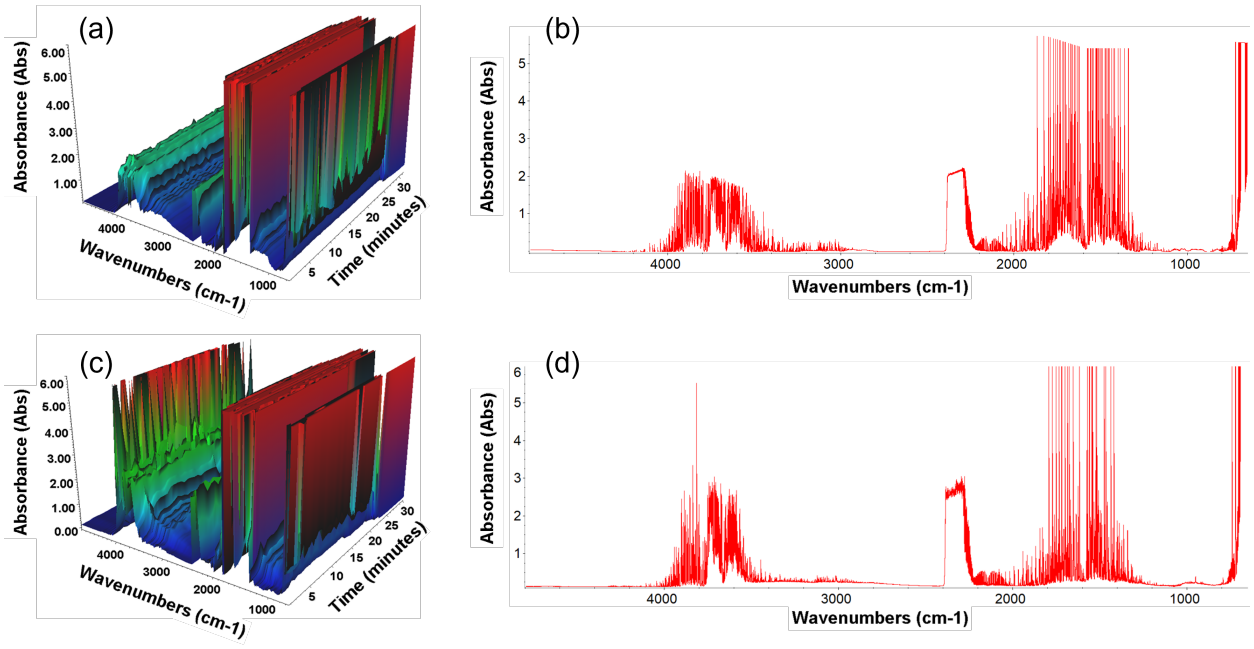

Figure 4.2: (a) 3D spectrum of live flaming Douglas fir, (b) 2d plot of live flaming Douglas fir at any given time, (c) 3D spectrum of dry flaming Douglas fir, and (d) 2d plot of dry flaming Douglas fir at any given time.

be found in the Appendix A. Notably, CO has a distinctive band from 2000 - 2250 cm^{-1}, which is clearly distinguishable in Fig. 4.2 (b, d). In contrast, the absorption from 2200 - 2400 cm^{-1} corresponds to CO_2 as well as various acids, aldehydes, hydrocarbons, and other gaseous species that exist in the range of 300 - 4000 cm^{-1} and 600 - 2000 cm^{-1}. In these plots, a higher value of absorbance for particular wavenumbers indicates a higher concentration of that particular gaseous species in the sampling stream as it has absorbed a higher amount of incident infrared light. The wide array of unknown effluents from biomass burning not present during calibrations makes it nearly impossible to completely avoid any interference; however, great care was taken to minimize these interferences as much as possible [88].

In flaming live Douglas fir (Fig. 4.2b) the absorption by CO and CO_2 is lower compared to dry Douglas fir (Fig. 4.2d). This seems reasonable as dry Douglas fir has a negligible amount of moisture leading to higher amount of carbon content (51.39% of dry fuel mass) resulting in a higher production of CO and CO_2 compared to live Douglas fir. Similarly, the concentration by various different carbon containing gases is higher for dry Douglas fir as it has the lowest moisture content. A similar comparison of the 3D spectrum between flaming and smoldering of live Douglas fir is presented in Appendix C.

To better demonstrate the steady-state nature of emissions, time-dependent concentrations of three gaseous species from flaming Doulgas-fir at 48% FMC are shown in Fig. 4.3.

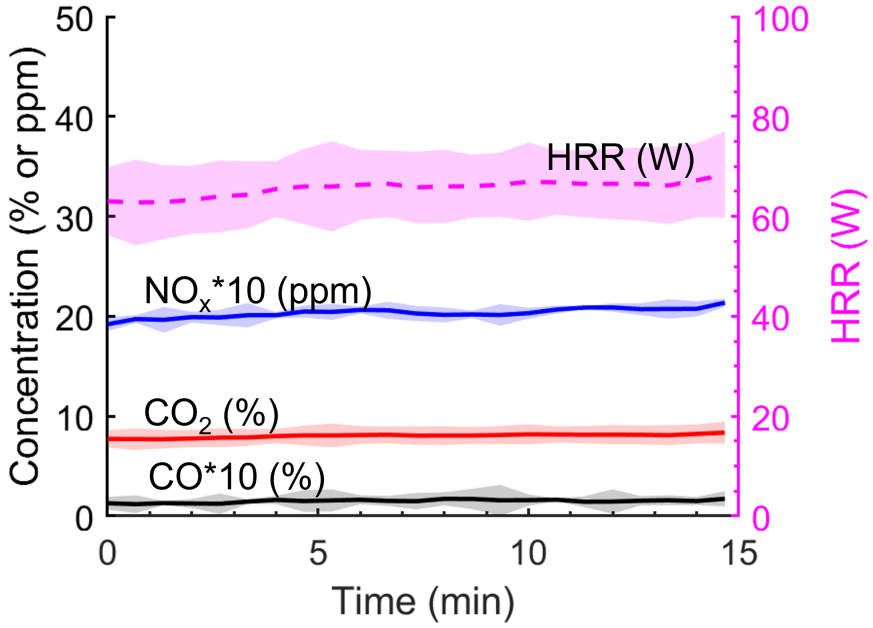

Figure 4.3: Average concentrations of CO*10 (%), CO_2 (%), NO_x*10 (ppm), and HRR (W) from flaming live Douglas fir emissions as measured directly out of the quartz tube. Note the use of %, ppm and scaling by a factor of 10 in order to highlight all species on one graph.

As mentioned earlier, due to this unique experimental setup, the emissions remain relatively constant and the standard deviation ($\pm 1\sigma$) between repetitions is small, is shown as shaded area. The heat-release rate (HRR) is also calculated using the CO and CO_2 production method [77] and is shown on right y-axis in Fig. 4.3 and average values for all different test conditions are provided in Table 4.1. Similar steady plots were found for all other experimental conditions. This concludes that this new setup is capable of producing steady-state emissions and can be employed to understand emissions from various different fuel types (vegetative as well as structural) under various fuel conditions (i.e., shape, size, FMC) and combustion conditions (i.e., pyrolysis, flaming, smoldering, mixed mode) by controlling the airflow rate, oxygen concentration in the incoming airflow, amount of fuel, temperature of the heater, and traverse rate of the heater.

4.4.2 Emission factors

4.4.2.1 Major gases and TPM

Few previous studies have considered FMC as an important parameter affecting emissions of different wildland fuels. In this study, several clear variations are observed between EFs of different species, depending on initial FMC and combustion conditions. Figure 4.4 shows

the EF of various gaseous species i.e., carbon monoxide (CO), carbon dioxide (CO_2), sulphur dioxide (SO_2), oxides of nitrogen (NO_x), ammonia (NH_3), and acohol i.e., methanol (CH_3OH) and TPM at two different FMC for Douglas fir and three different FMC for lodgepole pine. Please note that the EFs in Fig. 4.4 are scaled so that all the species appear on the same plot. Additionally, seven different hydrocarbons are summed together and plotted as 'HC', five different acids are summed together and plotted as 'Acids', and two different aldehydes are summed together and plotted as 'Aldehydes'. Detailed EFs of each species are discussed in further sections.

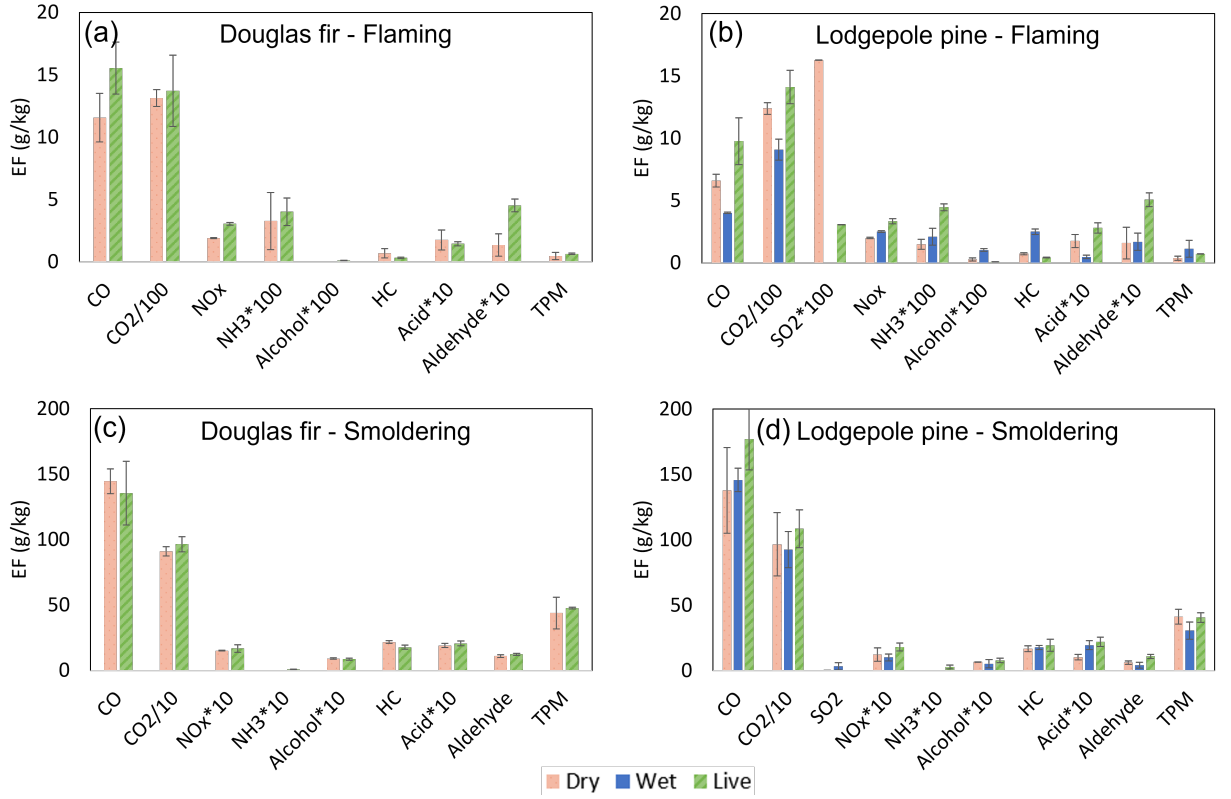

Figure 4.4: Average EFs of major gaseous species for a) Douglas fir, b) lodgepole pine under flaming combustion, c) Douglas fir, d) lodgepole pine under smoldering combustion for varying FMC.

For flaming combustion, between different vegetative fuels, Douglas fir produced a higher of CO EF than lodgepole pine. Despite coming from the same geographical region and being similar species, there are notable variations in EFs. In a previous chapter, gaseous sampling was performed using NDIR gas sensors which reported higher concentrations of CO from Douglas fir compared to lodgepole pine, as is also seen in this study using FTIR. For smoldering combustion, the EFs of various species are similar for both vegetative fuels;

however, Douglas fir did show any appreciable variation in emissions with respect to FMC whereas lodgepole pine showed some measurable differences. Moreover, SO_2 was detected only for lodgepole pine flaming and smoldering combustion, which may have occurred due to differences in the chemical makeup of the fuels.

Douglas fir showed elevated EFs for live (48%) conditions compared to dry (3.5%) for CO, CO_2, NO_x, NH_3, alcohol, aldehydes, and TPM, as well as a reduction in HC and acids during flaming combustion, shown in Fig. 4.4a. CO production was also notably higher for live conditions, which may be due to incomplete combustion, with the MCE dropping from 99% to 97% for this condition. A reduction in HC and acids is within the standard deviation and can be assumed to be roughly comparable between live and dry conditions. During smoldering combustion, Douglas fir did not show much variation with respect to FMC as the EFs are very comparable for live and dry conditions in Fig. 4.4c.

Lodgepole pine showed decreased EFs for CO and CO_2 from live (50%) to wet (23%) FMC conditions, followed by an increase from the wet (23%) to dry (3.5 %) conditions during flaming combustion (Fig. 4.4b). Similar trends were seen for acids and aldehydes. On the other hand, the EFs of alcohol, HC, and TPM first increase and then decrease. Comparing the flaming results (Fig. 4.4b) with smoldering combustion (Fig. 4.4d) for lodgepole pine, the trends for CO, CO_2, and aldehydes remains fairly similar. SO_2 was observed for dry and live conditions for flaming whereas it was only detectable under wet conditions in smoldering combustion, although it still may be present below detectable limits. Overall, the EFs for CO, TPM, and HC remain higher for smoldering compared to flaming combustion for both vegetative fuel types.

May et al. [23] measured CO, CO_2, and TPM for three different vegetative fuels under dry and live conditions. They did not distinguish between flaming and smoldering as they employed a 0.25 m^2 square spreading burn configuration under a calorimetry hood which makes a direct comparison difficult. They reported increases in CO and TPM and decreases in CO_2 from dry to live conditions. This is consistent with our results for flaming combustion with an exception for CO_2. CO_2 results are within the standard deviation of Douglas fir but are opposite for lodgepole pine. This could have occurred because May et al. [23] had mixed modes of combustion, with flaming combustion initially but different proportions of smoldering after fire spread, however results were presented as average values of the complete experiment.

Goode et al. [5] also performed laboratory pile burns of Douglas fir litter under the large calorimetry hood in Missoula, MT and reported an EF(CH_3OH) as 0.82 which is comparable to smoldering Douglas fir in this study. Selimovic et al. [6] performed laboratory pile burns of various vegetative fuels which included Douglas fir and lodgepole pine. They reported a MCE of 94% which typifies a mixed mode of combustion. They reported EF(CH_3OH) as 0.73 and 0.86 for Douglas fir and lodgepole pine, respectively. The EF(NO_x) is reported as 3.4 (Douglas fir) and 2.97 (lodgepole pine), EF(SO_2) is reported as 1.18 (Douglas fir) and 1.31 (lodgepole pine), and EF(NH_3) as 0.47 (Douglas fir) and 0.62 (lodgepole pine) by Selimovic et al. [6]. All these values are in good agreement with smoldering combustion EF (within 70%) for both vegetative fuels in this study except for the EF(SO_2) for Douglas fir.

SO_2 was not detected in emissions from Douglas fir, which could have been influenced by the initial fuel sulfur content. Sulfur, designated a plant macronutrient, is primarily taken up by higher plants from the soil in the form of sulfate [35]. As the fuel changes over time, the sulfur content may become negligible for the Douglas fir needles utilised in this study. The observed variation of ∼30% among EF of different gaseous species could result from variations in the FMC and fuel composition. Selimovic et al. [6], for instance, burnt duff, litter, and large diameter branches whereas only needles were tested in this study.

4.4.2.2 Hydrocarbons (HCs)

Incomplete combustion of vegetation can lead to the production of various hydrocarbons, which can have significant implications on fire behavior, health, and air quality. Figure 4.5 provides a detailed analysis of seven hydrocarbons that have been observed in this study, namely methane (CH_4), acetylene (C_2H_2), ethane (C_2H_6), butane (C_4H_{10}), isobutene (C_4H_8), ethene (C_2H_4), and propene (C_3H_6). These results reveal distinct patterns in hydrocarbon production, with variations observed between different fuel types and FMC levels. We also identified butane (C_4H_{10}), which had not been commonly reported in previous literature sampling gaseous species using FTIR. Further discussion on this gaseous species will be provided in this section.

For flaming combustion, live Douglas fir produced detectable levels of only one hydrocarbon i.e., butane (C_4H_{10}) whereas dry Douglas fir produced five different HCs as seen in Fig. 4.5a. Flaming lodgepole pine revealed only 4 HCs that were detectable. For live and wet lodgepole pine, only butane was detectable at appreciable levels, whereas dry flaming lodgepole pine had low levels of methane (CH_4), acetylene (C_2H_2), and higher levels of isobutene (C_4H_8). Interestingly, both Douglas fir and lodgepole pine had only butane as the detectable hydrocarbon emitted in a live state. Smaller HCs such as methane and ethane were expected but butane was repeatably identified by the calibrated FTIR even after extensive repetitions of the experiments and manual inspection of the spectra. Wet lodgepole pine also had only butane as the HC emitted. We hypothesize that, in this apparatus, the energy provided by the heater is applied towards vaporising the moisture present in live and wet vegetation, thus delaying complete combustion of the pyrolysis species, and leaning towards production of heavier hydrocarbons. Dry Douglas fir and lodgepole pine, on the other hand, showed a variety of HCs produced including methane (CH_4), acetylene (C_2H_2), and isobutene (C_4H_8) for both Douglas fir and lodgepole pine whereas additional butane (C_4H_{10}) and ethene (C_2H_4) were detected from Douglas fir.

As shown in Fig. 4.5 (c, d), the total hydrocarbon (HC) emission factors (EFs) for smoldering combustion are much higher than those for flaming combustion. This is an expected result, as smoldering is an incomplete solid-phase oxidation process that occurs at lower temperatures, resulting in a higher production of unburnt HCs. In contrast, flaming combustion consists of high-temperature, gas-phase complete combustion that produces less HC emissions. The variation between live and dry HC EFs is not significant for smoldering Douglas fir, as can be observed in Fig. 4.4c unlike flaming combustion where significant

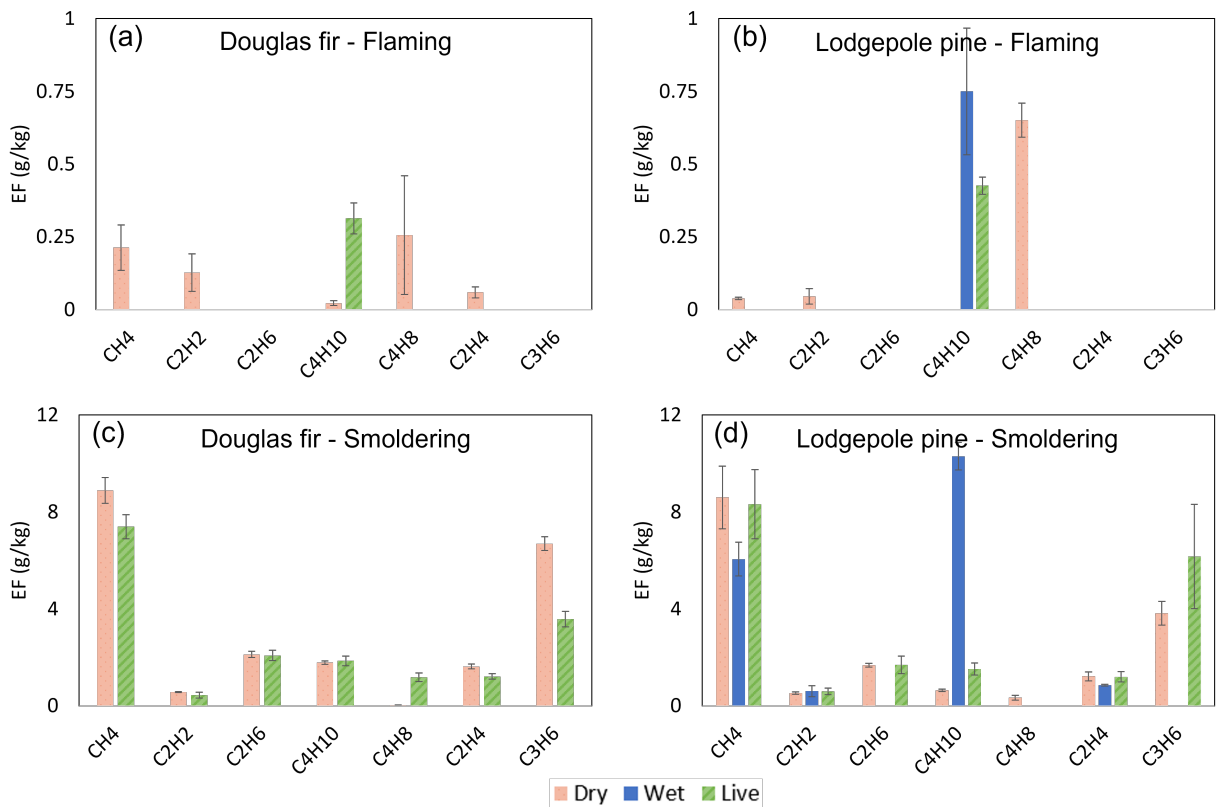

Figure 4.5: Average EFs of various hydrocarbons for a) Douglas fir, b) lodgepole pine at flaming combustion, c) Douglas fir, d) lodgepole pine at smoldering combustion for varying moisture contents.

changes are observed. For smoldering Douglas fir, methane (CH_4) and propene (C_3H_6) have the highest EFs compared to acetylene (C_2H_2), ethane (C_2H_6), butane (C_4H_{10}), isobutene (C_4H_8), and ethene (C_2H_4). Figure 4.4d shows that for smoldering lodgepole pine, there is a higher variation in emission factors (EF) when compared to Douglas fir, as the FMC changes. Dry lodgepole pine emits all seven speciated hydrocarbons (HC), whereas live lodgepole pine emits six (excluding isobutene). Wet lodgepole pine, on the other hand, only emits four. Among the four HC emitted by wet lodgepole pine during flaming combustion, butane (C_4H_{10}) has the highest EF, followed by methane (CH_4), and the lowest EF is seen for acetylene (C_2H_2) and ethene (C_2H_4).

Some previous studies [8, 89] have reported butane (C_4H_{10}) in the literature using FTIR. One study [7], which conducted open combustion of biomass in the laboratory, reported that canister gas samples were analyzed for C_4 hydrocarbons, namely butene (C_4H_8) and n-butane (C_4H_{10}). However, they only briefly mentioned that the contribution from C_2 - C_4 HCs was 1.3 $\pm$ 1.9% in the total carbon balance, without providing any details on the

observed C_4 HCs or their EFs. Additionally, a number of studies [84, 86] provided EFs for higher carbon chains like C_6 and C_8 found during field measurements, explaining that higher carbon molecules could be present in the emissions. In our study, butane was calibrated for the spectral wavenumbers range of 2995 - 2695 cm^{-1}, and it was observed in all repetitions of the experiments.

Goode et al. [5] reported the presence of isobutene (C_4H_8) in laboratory grass fires spreading as a backing fire over a flat bed and ponderosa pine needles spreading as a backing fire at a 40% slope, with reported EFs of 0.644 and 0.17, respectively. Our study shows a similar EF range of 0.34 - 0.65 for lodgepole pine, which is within close proximity to that reported by Goode et al. Additionally, while Goode et al. reported isobutene (C_4H_8) below detection limit for Douglas fir, our study found significant values for both flaming and smoldering Douglas fir. Bertschi et al. [4] conducted experiments using Douglas fir and pine grass and reported EF(CH_4) as 7.4, EF(C_2H_4) as 1.53, EF(C_2H_2) as 0.23, and EF(C_3H_6) as 0.53 with a Modified Combustion Efficiency (MCE) of 90.4. The EF for CH_4, C_2H_4, and C_2H_2 align well with the results for smoldering Douglas fir in our study, but the EF(C_3H_6) in our study was 6 - 12 times higher than that reported by Bertschi et al. The discrepancies between studies could be attributed to variations in fuel type, experimental apparatus, sampling techniques, or data analysis methods.

4.4.2.3 Acids

Figure 4.6 presents a detailed analysis of five acids detected, including hydrogen cyanide (HCN), hydrogen chloride (HCl), hydrogen bromide (HBr), nitrous acid (HNO_2), and formic acid (CH_2O_2).

During flaming combustion of Douglas fir and lodgepole pine, only three acids were identified: hydrogen cyanide (HCN), hydrogen bromide (HBr), and formic acid (CH_2O_2). For Douglas fir, both HCN and HBr decreased with an increase in FMC, whereas the opposite was observed for CH_2O_2. For lodgepole pine, only CH_2O_2 was observed under wet conditions, while CH_2O_2 and HBr were observed under live conditions and all three acids were emitted under very dry conditions. Variations were observed in the acids released with a change in FMC for flaming lodgepole pine.

During smoldering combustion, live Douglas fir emitted all five acids, but HBr was not observed under dry conditions. There was variation in the emission factors (EF) of the individual acids, but when the total EF of all acids was compared, the values are very similar (see Fig. 4.4c). Therefore, it is important to study the different acids individually and report their values. For lodgepole pine, dry conditions produced HCN, HBr, HNO_2, and CH_2O_2, wet conditions produced HCN, HNO_2, and CH_2O_2, while live conditions produced HCN, HCl, HNO_2, and CH_2O_2. HCl was observed only under live conditions, and HBr was observed only under dry conditions. The other three acids were observed for all three different FMC levels, and the EF showed significant variation with a change in FMC.

This study has identified HBr for the first time in wildland fuels, which has not been reported in the literature before. According to McKenzie et al. [90], bromine and chlorine

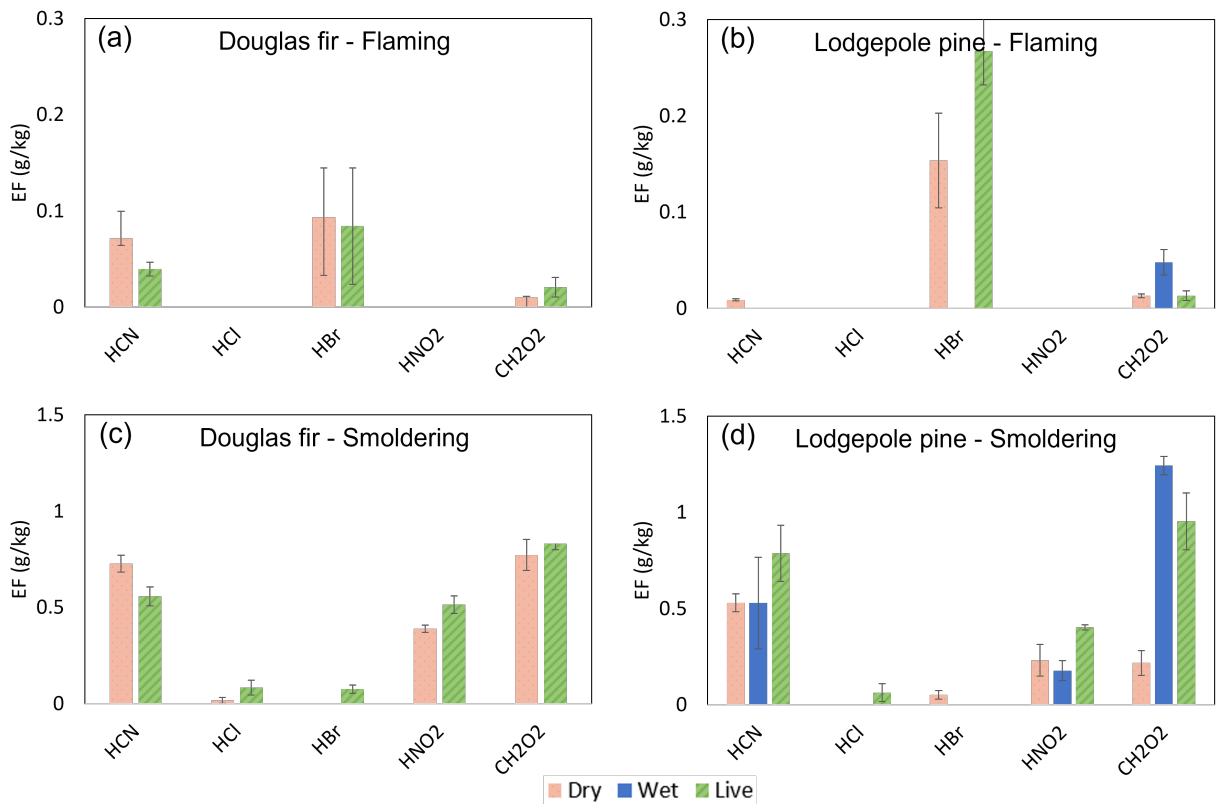

Figure 4.6: Average EFs of various acids for a) Douglas fir, b) lodgepole pine at flaming combustion, c) Douglas fir, d) lodgepole pine at smoldering combustion for varying moisture contents.

are present in vegetation as bromide and chloride, respectively. Chlorine is an essential micronutrient, while bromine is not considered an essential nutrient, but it may replace chlorine when chlorine is deficient. Biomass burning typically emits chlorine and bromine as CH_3Cl and CH_3Br, which has been reported in the literature [91] for three wildland fires in the western US. The FTIR was calibrated for spectral bands in the range of 2470 - 2640 cm^{-1}, and a high concentration of HBr was observed for flaming combustion compared to smoldering combustion for both Douglas fir and lodgepole pine. We would like to highlight that the detection of HBr may have potentially occurred due to interference from other gaseous species present in the fire emissions, such as CH_3Br, which has been previously reported in the literature. Alternatively, calibration issues could also have contributed to the detection. However, despite conducting a thorough literature search, we were unable to find any relevant information regarding potential interferences.

Burling et al. [35] conducted laboratory measurements for various vegetative fuel types, not including Douglas fir and lodgepole pine, and reported EFs for HCl and HNO_2 in the

range of 0.02 - 0.07 with an MCE of approximately 94%. Both of these acids were only identified for smoldering combustion in this study, and the values are consistent with those reported in the literature. However, a proper comparison cannot be made as no previous studies have considered FMC as an important parameter or distinguished between different combustion conditions, as was done in this study. Bertschi et al. [4] performed experiments using Douglas fir and pine grass and reported EF(HCN) as 0.47 and EF(CH_2O_2) as 0.39 with an MCE of 90.4%. The value of EF(HCN) is close to that of smoldering combustion of Douglas fir, whereas the value of EF(CH_2O_2) is twice the value reported by Bertschi et al. [4] for smoldering combustion of Douglas fir. Bertschi et al. [4] burned two different vegetative fuels together, and the FMC is unknown, which may have resulted in an imperfect comparison with the literature. Overall, the values found in this study are comparable to what is found in literature, except for HBr.

4.4.2.4 Aldehydes

Figure 4.7 presents the analysis of two types of aldehydes i.e., acrolein (C_3H_4O) and formaldehyde (CH_2O) found in this study. Acrolein and formaldehyde are respiratory irritants and exposure beyond the limit can cause lung injury. Formaldehyde is also classified as carcinogens [10]. Quantification of EFs of these two aldehydes is very important as they have major health effects on wildland firefighters and near by population.

Under all test conditions, acrolein (C_3H_4O) and formaldehyde (CH_2O) were produced, and variations were observed with changes in FMC. During flaming combustion, EF(C_3H_4O) was significantly higher for live conditions in both Douglas fir and lodgepole pine compared to other FMCs. Similarly, EF(CH_2O) was also high for live conditions in both vegetative fuels. This behavior could be attributed to the unique chemical composition of FMC present in live fuels. For smoldering combustion, live conditions produced the highest EF, and the least variation was observed in EF with changes in FMC of Douglas fir. However, a higher variation was observed in EF with changes in FMC for lodgepole pine, indicating differences among fuel species.

In literature, only one study [85] has reported acrolein as a pyrolysis combustion product from prescribed fires using infrared spectroscopy. They used a spectral region from 1100 - 1200 cm^{-1} for detection whereas the spectral region from 2680 - 2699 and 2705 - 2725 cm^{-1} is used in this study. Direct comparison of the EF is not possible as they reported as emission ratios to CO and EFs were not calculated. Another study [4] reported EF (CH_2O) as 0.74 which is again comparable to the smoldering EF.

4.4.3 Emission factor using mass loss rate (EF) and carbon balance (EF_{cb})

In order to validate our EFs, its important to compare them with studies performed in the field during prescribed and wildland fires, as well as pile burns at laboratory scale. Instead of using an EF based on mass loss rate (MLR) (Eq. 1.1) as used in this work, a carbon

Table 4.1: MCE (%), HRR (W), and EFs (g/kg) for different fuel types under both flaming and smoldering combustion conditions
DF, Douglas fir; LPP, lodgepole pine; L, live; W, wet; D, dry.

	Flaming					Smoldering				
	DF-D	DF-L	LPP-D	LPP-W	LPP-L	DF-D	DF-L	LPP-D	LPP-W	LPP-L
MCE (%)	98.7 ± 0.01	97.8 ± 0.02	99.2 ± 0.01	99.2 ± 0.01	98.8 ± 0.01	80.0 ± 0.03	81.8 ± 0.02	81.8 ± 0.02	77.6 ± 0.09	79.7 ± 0.01
HRR (W)	109 ± 16.07	65.6 ± 12.76	100.2 ± 11.41	59.96 ± 11.04	64.83 ± 7.40	31.15 ± 4.34	109 ± 1.55	33.15 ± 5.39	24.02 ± 8.70	18.29 ± 3.36
TPM (g/kg)	0.46 ± 0.29	0.63 ± 0.06	0.38 ± 0.16	1.13 ± 0.68	0.72 ± 0.01	43.80 ± 12.10	47.70 ± 0.61	41.30 ± 5.68	30.60 ± 6.62	40.60 ± 3.70
CO (g/kg)	11.56 ± 1.95	15.53 ± 2.08	6.59 ± 0.51	4.01 ± 0.05	9.76 ± 1.89	144.5 ± 9.35	135.5 ± 24.42	137.8 ± 32.73	145.7 ± 8.94	176.9 ± 23.53
CO_2 (g/kg)	1312 ± 67.8	1371 ± 286.4	1239 ± 47.2	909.1 ± 84.6	1411 ± 134	909.6 ± 35.3	964.1 ± 56.7	966.1 ± 241.3	925.4 ± 138.5	1086 ± 145
SO_2 (g/kg)	0	0	0.16 ± 0.00	0	0.03 + 0.00	0	0	0.36 ± 0.01	3.46 ± 2.72	0
NO_x (g/kg)	1.89 ± 0.05	3.05 ± 0.11	2.01 ± 0.05	2.52 ± 0.07	3.33 ± 0.20	1.51 ± 0.02	1.67 ± 0.28	1.23 ± 0.51	1.01 ± 0.27	1.82 ± 0.31
NH_3 (g/kg)	0.03 ± 0.02	0.04 ± 0.01	0.02 ± 0.00	0.02 ± 0.00	0.04 ± 0.00	0	0.09 ± 0.02	0	0	0.28 ± 0.15
CH_3OH (g/kg)	0	∼0	0.003 ± 0.00	0.01 ± 0.00	0.001 ± 0.00	0.90 ± 0.06	0.86 ± 0.08	0.67 ± 0.00	0.53 ± 0.31	0.78 ± 0.17
CH_4 (g/kg)	0.21 ± 0.08	0	0.04 ± 0.00	0	0	8.88 ± 0.53	7.39 ± 0.49	8.59 ± 1.30	6.05 ± 0.70	8.32 ± 1.42
C_2H_2 (g/kg)	0.13 ± 0.06	0	0.05 ± 0.03	0	0	0.57 ± 0.02	0.44 ± 0.12	0.52 ± 0.05	0.61 ± 0.23	0.59 ± 0.14
C_2H_6 (g/kg)	0	0	0	0	0	2.12 ± 0.12	2.08 ± 0.21	1.68 ± 0.08	0	1.68 ± 0.36
C_4H_{10} (g/kg)	0.02 ± 0.01	0.31 ± 0.05	0	0.75 ± 0.22	0.43 ± 0.03	1.78 ± 0.07	1.85 ± 0.20	0.64 ± 0.05	10.30 ± 0.57	1.52 ± 0.25
C_4H_8 (g/kg)	0.26 ± 0.20	0	0.65 ± 0.06	0	0	0.03 ± 0.01	1.18 ± 0.18	0.34 ± 0.10	0	0
C_2H_4 (g/kg)	0.06 ± 0.02	0	0	0	0	1.62 ± 0.10	1.21 ± 0.11	1.22 ± 0.18	0.85 ± 0.04	1.20 ± 0.21
C_3H_6 (g/kg)	0	0	0	0	0	6.69 ± 0.28	3.57 ± 0.32	3.82 ± 0.49	0	6.16 ± 2.15
HCN (g/kg)	0.07 ± 0.03	0.04 ± 0.01	0.01 + 0.00	0	0	0.73 ± 0.04	0.56 ± 0.05	0.53 ± 0.05	0.53 ± 0.24	0.79 ± 0.15
HCl (g/kg)	0	0	0	0	0	0.02 ± 0.02	0.08 ± 0.04	0	0	0.06 ± 0.05
HBr (g/kg)	0.09 ± 0.05	0.08 ± 0.06	0.15 ± 0.05	0	0.27 ± 0.04	0	0.08 ± 0.02	0.05 ± 0.02	0	0
HNO_2 (g/kg)	0	0	0		0	0.39 + 0.02	0.51 ± 0.05	0.23 ± 0.08	0.18 ± 0.05	0.40 ± 0.01
CH_2O_2 (g/kg)	0.01 ± 0.00	0.02 ± 0.01	0.01 ± 0.00	0.05 ± 0.01	0.01 ± 0.00	0.77 ± 0.08	0.83 ± 0.03	0.22 ± 0.06	1.24 ± 0.05	0.95 ± 0.15
C_3H_4O (g/kg)	0.11 ± 0.08	0.38 ± 0.07	0.13 ± 0.12	0.12 ± 0.06	0.43 ± 0.05	9.56 ± 0.96	10.16 ± 0.09	6.01 ± 1.22	3.50 ± 2.07	9.35 ± 1.35
CH_2O (g/kg)	0.02 ± 0.01	0.07 ± 0.04	0.03 ± 0.01	0.05 ± 0.01	0.07 ± 0.01	1.36 ± 0.16	2.11 ± 0.62	0.18 ± 0.04	0.65 ± 0.26	1.54 ± 0.17

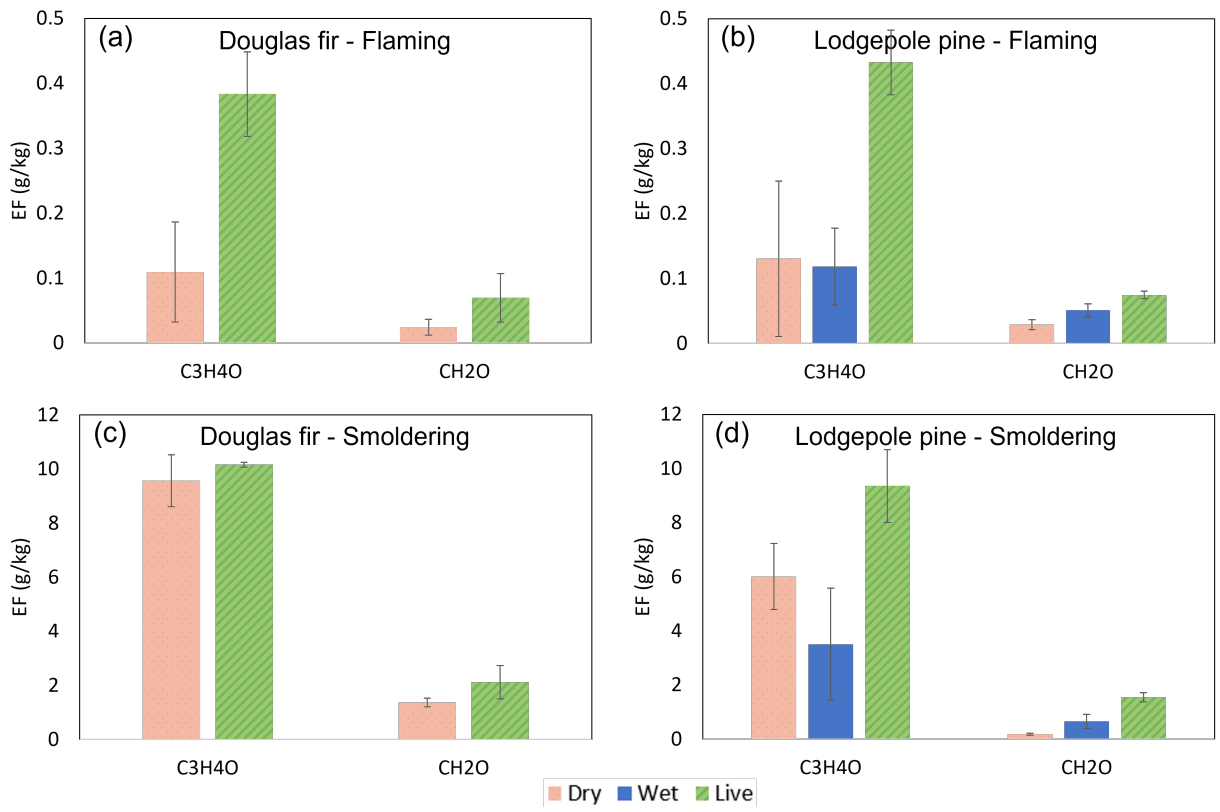

Figure 4.7: Average EFs of various aldehydes for a) Douglas fir, b) lodgepole pine at flaming combustion, c) Douglas fir, d) lodgepole pine at smoldering combustion for varying moisture contents.

balance approach is widely used in literature [3, 92] to calculate the EF of gas species in the field. This approach assumes all of the major carbon-containing emissions have been measured and use the following equation,

$$EF_{cb,i}\ (g/kg) = F_c * 1000(g/kg) * \frac{MM_i}{12} * \frac{C_i}{C_T} \tag{4.1}$$

where F_c is the carbon content in the vegetative fuel (%, on dry mass basis), MM_i is the molar mass of species i, C_i is the number of moles of species i, and C_T is the total number of moles of carbon emitted. A considerable number of publications have reported EF_{cb} values [3, 4, 6, 7, 39], while studies investigating EF based on MLR have remained scarce [5, 22, 23, 36, 37]. This is because obtaining MLR is challenging and often impossible for field studies. However, as the emissions produced in this study are steady-state, it was easy to calculate EF_{cb}. Therefore, the EFs reported in this study were compared to EF_{cb} for both Douglas fir and lodgepole pine and are shown in Figs. 4.8 and 4.9, respectively.

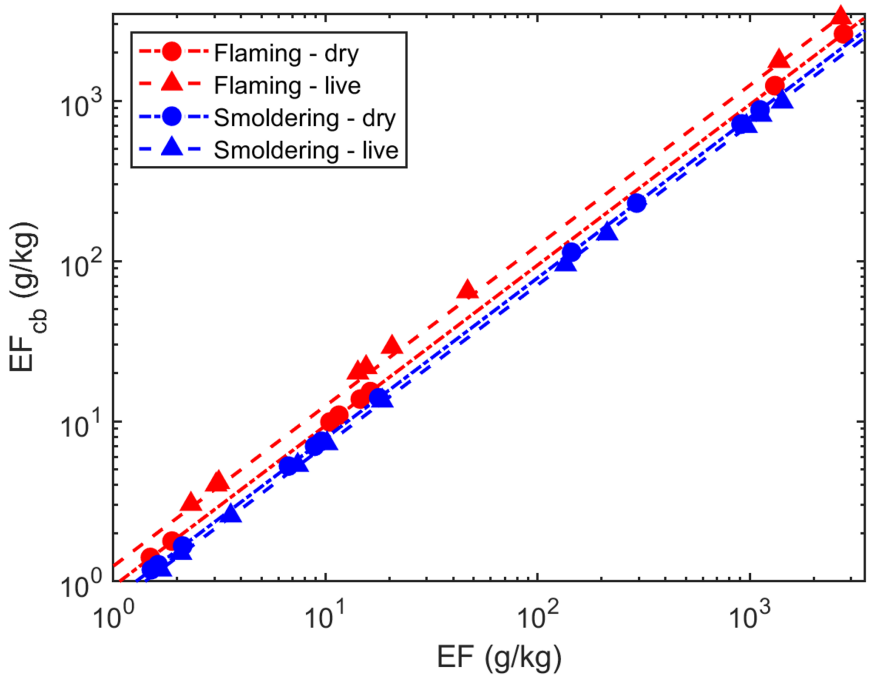

Figure 4.8: Comparison of EF using mass loss rate (EF) with a carbon balance approach (EF_{cb}) for Douglas fir.

EF and EF_{cb} are linearly correlated for all experimental conditions studied, with an R^2 = 0.99, which helps to justify using the proposed method for EF_{cb}. However, EF_{cb} values specifically lie between 95 - 125% of EF for flaming and 70 - 115% for smoldering. This is mainly because EF_{cb} relies on the carbon balance assumption which fails to take into account the carbon from unidentified higher molecular species, leading to slight deflation of EF_{cb} values. The uncertainty of ± 10% from the FTIR data could also have resulted in slight inflation of EF_{cb}.

4.4.4 Literature Comparison of EF vs. MCE

The EFs calculated using a carbon balance approach (EF_{cb}) were further used to compare the results from various literature studies conducted at field scale [3, 8] and laboratory scale [4–7], including one study performed in a similar apparatus but run in an opposite concurrent configuration [9]. This is important both to see whether results follow trends with MCE, as has been shown in previous studies, and to validate that results from this small-scale apparatus align with actual wildland fire emissions. Most studies chosen for comparison used Douglas fir or lodgepole pine as one of there vegetative fuels [3–9]. None of the studies compared have explicitly varied FMC; however, as MCE vaires during combustion it provides

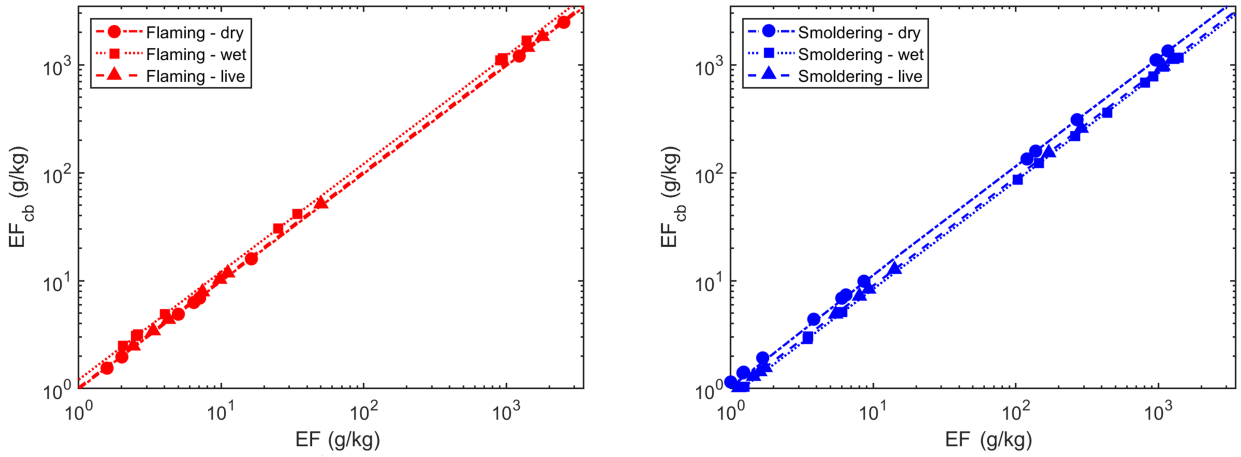

Figure 4.9: Comparison of EF using mass loss rate (EF) with a carbon balance approach (EF_{cb}) for (a) flaming and (b) smoldering combustion of lodgepole pine.

a clearer method to compare combustion behavior.

Figure 4.10 illustrates the relationship between the EF_{cb} of CO_2, CO, TPM, and CH_4 with MCE found in this study alongside those from previous literature (calculated based on the carbon balance method). Trends are fitted with a linear function with R^2 values of 0.48, 0.90, 0.80, and 0.56 for CO_2, CO, TPM, and CH_4, respectively. CO shows the strongest correlation with MCE. This is expected as CO is a strong measure of smoldering combustion and is used in the calculation of MCE. It is interesting to note that field studies generally lie between fully smoldering and flaming conditions. This mixed mode often occurs due to forward flaming combustion followed by 'post-frontal' smoldering of fuels after the main fire front has passed. This indicates that real fires typically incorporate mixed modes of combustion that cannot always be well documented in the field but can be studied in more detail in a small-scale setup, such as the one developed in this study. The current study and one previous [9] are unique in their ability to produce fully smoldering or flaming conditions, necessary for a more detailed physical understanding of the fire emissions process.

A weaker correlation was found between the MCE and CO_2 (R^2 = 0.48) and CH_4 (R^2 = 0.56) as shown in Figure 4.10. This could have resulted due to the different chemical composition of the vegetative fuel type as it changes over time, different analytical methods, sampling approaches, and experimental conditions. EFs of other gaseous species were not correlated with MCE because there was not enough literature available to compare them in a reasonable manner.

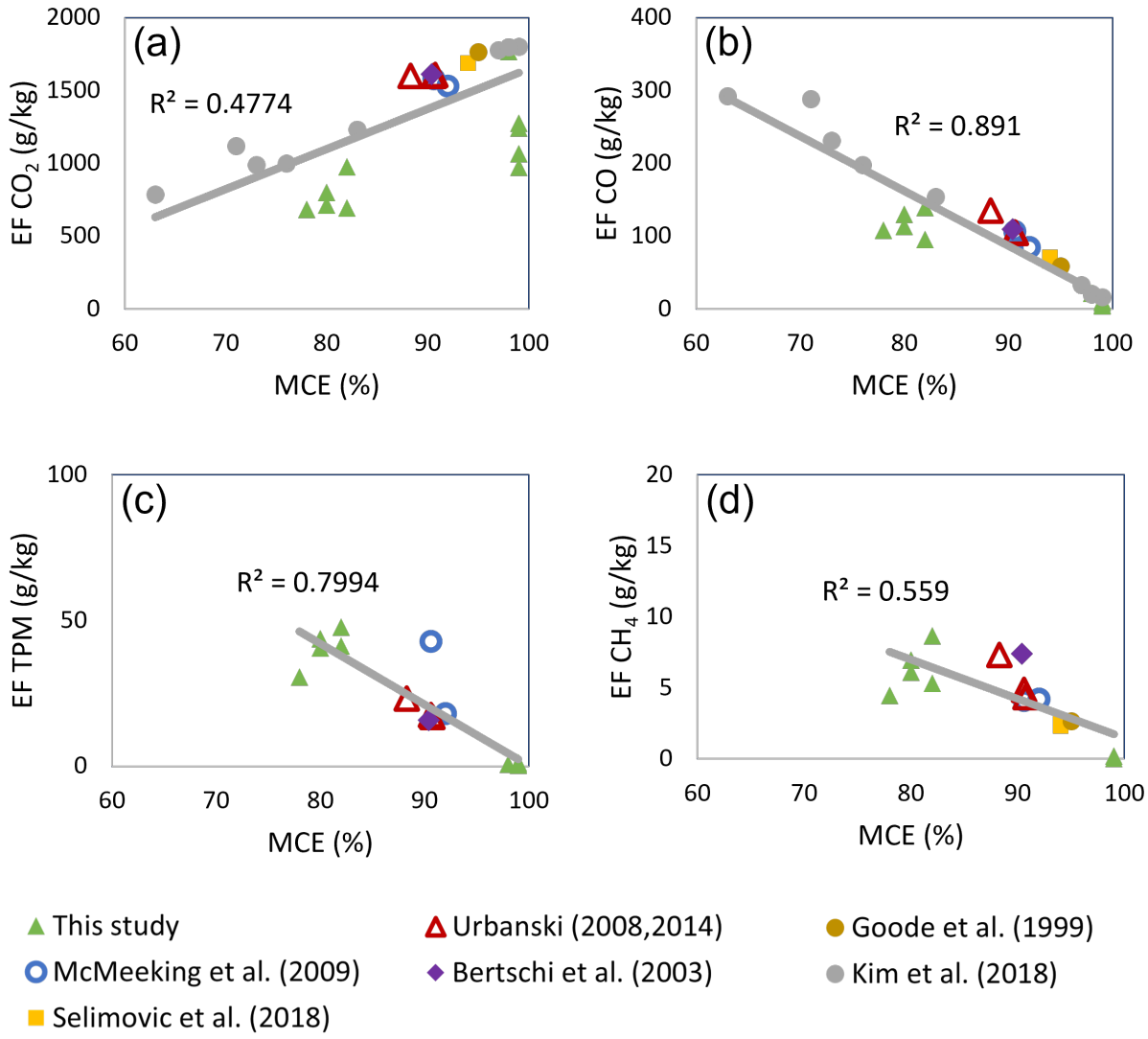

Figure 4.10: A comparison of EFs of different species during flaming and smoldering combustion vs. MCE. Results from previous studies are also shown [3–9].

4.5 Conclusions

A small-scale laboratory apparatus was designed which produced steady-state emissions from vegetation burned in the laboratory. Two different fuel types common in western wildfires, lodgepole pine and Douglas fir needles, were burned under different FMC and combustion conditions. The apparatus was able to produce steady-state emissions for long durations of the time, allowing them to be sampled for further study. The concentration of 20 gaseous species and TPM were sampled from the effluents and reported for the first time for Douglas

fir and lodgepole pine needles under varying FMC and combustion conditions i.e., flaming and smoldering.

The emissions produced during flaming combustion showed significant dependence on FMC; however, changes in effluents also varied depending on species despite the similarity between the two conifers. As expected, smoldering combustion resulted in significantly increased CO, TPM, and HC emissions compared with flaming for both fuel types. Unburnt hydrocarbons with higher emission factors produced during smoldering were CH_4, C_2H_2, C_2H_6, C_4H_{10}, C_4H_8, C_2H_4, C_3H_6, CH_2O_2, C_3H_4O, CH_2O, and CH_3OH. While smoldering combustion exhibited little variation in overall effluents depending on FMC, there were variations in specific effluents depending on fuel species, suggesting that the specific fuel type plays an important role in burning behavior and emissions. Among the effluents characterized, butane (C_4H_{10}) and hydrogen bromide (HBr) were repeatedly identified by FTIR and not commonly reported in the literature. Acrolein (C_3H_4O) was also identified and had only been reported by one previous study, and only during pyrolysis, not combustion.

Representing emissions factors using either a mass or carbon balance produced similar results that were well correlated for both flaming and smoldering. Emissions for common effluents, such as CO_2, CO, CH_4, and TPM were also seen to be reasonably correlated with MCE in agreement with previous literature.

This study has provided an important dataset of emission factors for two common wildland fuels characterizing a broad array of effluents while varying FMC and combustion conditions. The results clearly show that consideration of the FMC and fuel type is necessary in order to properly distinguish emissions. This has important implications on efforts to model emissions from wildland fuels, as a broader understanding of the processes driving emissions production must be undertaken considering variations in fuel type and FMC. This level of detail is absent in current emissions databases. This study provides important validation data that are repeatable in the laboratory and can be expanded upon to other fuels and measurement techniques in the future.

4.6 Acknowledgements

Data from this chapter, in part, is included in a manuscript titled “Variations in gaseous and particulate emissions from flaming and smoldering combustion of Douglas fir and lodgepole pine at different fuel moisture conditions”, by P. Garg, S. Wang, J. M. Oakes, C. Bellini, and M.J. Gollner, in preparation for submission and peer review in August 2023. The thesis author is the primary investigator in this publication.

Chapter 5

Limiting conditions of smoldering-to-flaming transition of cellulose powder

In real fire scenarios, both smoldering and flaming play significant roles in structure and wildland fires, and despite being fundamentally different, one can transition to and even co-exist with the other. Smoldering-to-flaming (StF) transition is an abrupt initiation of homogeneous gas-phase burning (i.e., flaming) preceded by heterogeneous solid-phase burning (i.e., smoldering), which can lead to fast spreading fires both in residential and wildland fuels. Despite its hazard, StF transition remains difficult to predict because of its sensitive nature to external conditions, the inherent variability of porous biomass fuels, and a limited understanding of its dominating mechanisms.

Work in this chapter helps to quantify limiting conditions for StF transition of cellulose powders, a major constituent of wildland fuel in a custom-made linear tube-heater apparatus that can provide a radiant heat flux of up to 60 kW/m^2 on a cellulose fuel bed. Oxygen concentrations of 10 - 21% are blown over the bed of cellulose powder with velocities of 1.5 – 10.5 cm/s. The limiting external heat fluxes for StF transition under different rates of oxygen supply were quantified. The fire phenomena, gaseous emissions, modified combustion efficiency, and the effect of fuel density are further examined to provide a detailed picture of StF transition behavior. Based on these parameters, a critical oxygen concentration and critical oxidizer flow velocity has been determined for the experimental conditions used in this study. This work advances the fundamental understanding of the StF transition, and thus helps guide the prevention of extreme fire events.

5.1 Background

Smoldering is a slow, low-temperature, flameless combustion of porous solid fuels, differing from flaming combustion in terms of chemistry, transport processes, and time scales [93–95].

For both smoldering and flaming, pyrolysis is a common prerequisite, generating gaseous pyrolyzate and solid char that are both susceptible to subsequent oxidative reactions [42]. Smoldering is more specifically a heterogenous oxidation reaction where oxygen molecules directly react with the hot surface of reactive porous fuel or char, whereas flaming is a homogenous oxidation reaction of pyrolyzate and ambient oxygen. Both modes of solid fuel burning release carbon dioxide, water, heat, other gases and by-products [96]. In general, the characteristic temperature, spread rate, and heat release rate of smoldering are much lower than those of flaming [97]. For example, smoldering generally spreads in a creeping manner, which is 2-3 orders of magnitudes smaller than that of flame spread. On the other hand, as an incomplete combustion process, emission factors of toxic gases (e.g., CO and CH_4) from smoldering are much higher than those from flaming per unit mass burned [22, 98].

In spite of its low-intensity nature, smoldering can withstand extreme conditions such as poor oxygen supply [99] and high fuel moisture content [22, 100], making it the most persistent combustion phenomenon [101]. More importantly, smoldering can be initiated by a weak heat source [42] or even self-ignition [43], providing a shortcut to flaming through smoldering-to-flaming (StF) transition, which is a rapid initiation of homogeneous gas-phase ignition (i.e., flaming) induced by a heterogenous solid surface reaction (i.e., smoldering). In this transition process, the smolder reaction acts both as the source of pyrolyzate and ignition heating. This process can lead to severe consequences through a sudden increase in spread rate, heat release, and subsequent safety hazards [44]. A typical StF transition example is the ignition of bedding and upholstery by cigarettes in residential fires, where smoldering ignition of the furnishing material from the smoldering cigarette is first achieved and then abruptly transitions to flaming when specific conditions are met. The hazard in this context is thus two-fold: toxic gases during smoldering and rapid burning following the initiation of flaming [93]. StF transition also contributes to rapid fire spread during wildland-urban-interface fires by lofting embers (i.e., firebrands). These accumulating and often smoldering embers can initiate local smoldering ignition which may later exhibit StF transition that leads to fire spread far beyond the original fire point [44–47]. Despite its important hazard, our understanding of the precise conditions for StF transition and controlling mechanisms remains limited.

Fundamentally, StF transition is controlled by a competition between oxygen supply and heat transfer to and from the reaction zone [102]. Therefore, Torero et al. [102] summarized four possible factors governing the transition from smoldering to flaming: (i) strong (secondary) char oxidation [103], (ii) acceleration of smoldering propagation (i.e., smoldering intensity) [104, 105], (iii) oxygen supply [106, 107] and (iv) sample size/heat losses [108]. Each of these factors enhances the rate and/or intensity of the smoldering reaction, which is necessary to trigger an abrupt StF transition, leading to spontaneous/piloted gas-phase ignition supported by the excess pyrolyzate, heat, and reaction from the smoldering front [109]. For example, a larger sample size could decrease interior heat losses to the ambient, leading to a robust reaction area with a higher temperature and propagation rate [110]. As a result, this robust char oxidation could provide sufficient heat to accelerate pyrolysis and ignite pyrolyzate gases, triggering the StF transition [44].

In the literature, external oxidizer flow and heat flux are often quantities of interest as they are the key parameters affecting the thresholds of StF transition [111]. For example, airflow or wind is crucial to the StF transition, because it increases both oxygen supply and heat losses [102, 112]. An increasing airflow rate increases oxygen supply to the smoldering reaction, leading to a more intense smoldering rate with more pyrolyzate and higher heat release and temperatures that support the occurrence of StF transition. At the same time, the excess airflow also increases convective heat losses from the porous fuel bed, thus decreasing the tendency for StF transition [44]. External heating compensates for heat losses to the ambient, leading to increasing reaction rates and temperatures favoring the occurrence of the StF transition. However, controlled experiments isolating the effects of external oxidizer flow and heat flux are lacking, limiting our knowledge of mechanisms controlling StF transition.

Biomass, which is the major source of fuel for residential and wildland fires, is generally composed of cellulose ($\sim$ 50%), hemicellulose ($\sim$ 25%), and lignin ($\sim$ 25%) [113]. For simplification, many laboratory studies have used powder cellulose as a simple surrogate to understand the burning behavior of biomass as it provides a homogeneous fuel bed of known properties, and is the main component that dominates the combustion process [114–119]. For example, Rogers et al. [118] studied the thermal decomposition of cellulose insulation and explored the kinetic parameters for establishing a numerical model. Ohlemiller [111] studied forward and reverse smoldering spread over cellulosic insulation bed material under varying wind speeds. They have an electrical heater covering the full width of the insulation and the temperature of the igniter was set to 375 °C for the duration of 1 hour. They found that only forward smoldering produced transition to flaming (at $\sim$ 2 m/s) at lower wind speeds when an external heat flux is added. They concluded that both kinetics, dominated by heat losses at the flame front, and the oxygen supply rate played important roles in the transition. However, to the best of authors' knowledge, few experiments have been conducted using pure cellulose to understand the process of StF transition. So, in this study pure cellulose powders are utilised to quantify the limiting conditions of the StF transition.

5.2 Experimental Methods

5.2.1 Material, setup, and controlling parameters

A commercially available microcrystalline cellulose powder provided by Thermo Fisher Scientific as shown in Fig. 5.1 was used in the experiments as a porous fuel bed. Before tests, the cellulose had a bulk density of 380 $\pm$ 20 kg/m^3, a moisture content, defined as the mass of water divided by the mass of a wet sample (expressed in %), of 3.3 $\pm$ 1.34 %, and an average particle diameter of 50 μm.

Cellulose combustion experiments were performed in a custom-made linear tube-heater apparatus, as shown in Fig. 2.2. While originally designed for toxicity exposure experiments and later adapted to generate laboratory wildland fire smoke for emissions studies, the design's unique ability to steadily generate fire spread under external heating and controlled

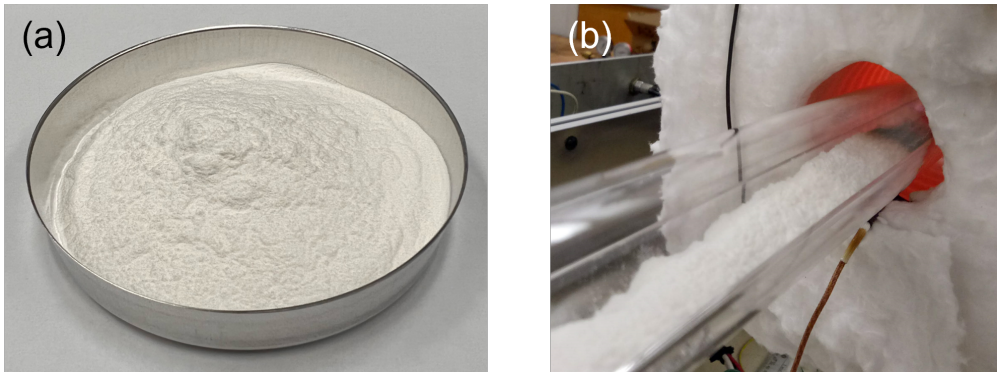

Figure 5.1: (a) Microcrystalline cellulose powder tested in this work and (b) cellulose powder shown in the quartz boat inserted in the quartz tube during an experiment.

atmosphere conditions was also ideal for studying the StF transition process.

The temperature of the annular ceramic heater (up to 700 °C) was controlled by a proportional–integral–derivative (PID) controller. Radiant heat flux on the top fuel surface from the heater was measured by a radiometer and equivalent radiant heat flux was formulated as $\dot{q}''_e = 2.8exp(0.005T)$, with $R^2 = 0.98$ as shown in Fig. 2.3. The flow rates of air and nitrogen were controlled using Alicat mass flow controllers. The experiments were performed in a counter-current direction, where the heater was traversed opposite to the wind direction in the tube. The traverse rate of the heater, which fixed the spread rate along the cellulose, was set at 2 cm/min, and was determined after performing several preliminary experiments at each condition such that the addition of external heat flux did not accelerate the spread rate along the cellulose. Three parameters were varied throughout this study to understand the effects of oxygen concentration, oxidizer flow velocity, and heat flux on the StF transition. The conditions tested were as follows:

- Oxygen concentrations (21, 19, 15, and 10%),
- Oxidizer flow velocities (1.73, 3.46, 5.2, 6.93, 8.66, and 10.39 cm/s),
- Heat fluxes (0 - 60 kW/m^2).

5.2.2 Test procedure

For each test, 15 g of cellulose powder was evenly distributed in an 80 cm-long quartz "boat", and then placed inside the quartz tube, as shown in Fig. 2.2. Afterwards, oxidizer flow was applied with a prescribed oxygen concentration and flow velocity using Alicat mass flow controllers. The heater was set to a fixed temperature and moved at a constant traverse rate of 2 cm/min along the outer side of the quartz tube for 10 minutes. This duration is equal to the length of the heater and insulation covering the heater, which is 20 cm. This timeframe

allows sufficient time for the reaction to reach a steady state. If the cellulose didn't undergo smoldering and then transition to flaming, the temperature of the heater was increased by 25 °C and allowed to run for another 10 minutes. This process was repeated until the occurrence of StF transition was observed. Visual observation of the experiments was recorded using a top-mounted digital camera which provides an angular view of the test region (as it is surrounded by an annular heater). Once a flame is observed using the camera, an ignition heat flux is defined as the transition from smoldering to flaming. Afterwards, the oxygen concentration and flow velocity of the oxidizer flow were varied to find the limiting conditions of the transition. Each experimental condition was repeated 4 times, and diagnostics which includes Enerac 700 were installed during the last two repetitions to record concentration of various different gaseous species. The standard error between the repetitions was calculated and plotted as error bars. During the experiments, the ambient temperature was 25 °C, the humidity was 50%, and the pressure was 101 kPa.

5.3 Results and Discussion

5.3.1 Fire phenomena

Once irradiation was applied, the cellulose powder began to pyrolyze and eventually blackened and initiated smoldering. By gradually adjusting the heating intensity, StF was achieved, and flaming mass burning followed up until no residual cellulose remained in the sample boat. Figure 5.2 shows some typical examples of the events when the StF transition occurred under different conditions of oxygen supply. All conditions shown here occurred in a steady-state mode of flaming combustion, meaning that the flaming continued throughout the duration of the test following the transition. Overall, as the oxygen concentration or the flow velocity decreased, the flame became blue, dim, and flat, and it floated above the burning cellulose powder. This is because the gas mixture was near its flammability limit, thus sustaining a near-limit (lean) flame [101]. On the other hand, as the weak flame covered the fuel surface, the oxygen could still diffuse into the porous char layer to maintain char oxidation. In other words, smoldering and flaming may co-exist under these conditions, similar to the near-limit blue flames observed above a cracked wood surface [120]. Reducing the oxygen further weakens the smoldering of the material and eventually results in extinguishment. Thus, the extinction of the burning smoldering-capable combustible solid can be separated into two different processes, one related to the extinction of flaming combustion and another smoldering. The former is similar to that occurring when the oxygen concentration is reduced near the Limiting Oxygen Concentration (LOC) of a non-smoldering solid combustible limit [121], but the latter has not yet been identified. An important difference in the extinction of a non-smoldering, or smoldering, material is that while in the non-smoldering case the burning of the material stops when the flame extinguishes, in the smoldering case the extinction of the flame leads to the continuation, or even intensification, of the fuel smoldering, and consequently the continuation of the fuel burning until smolder extinction occurs. Thus,

two LOC's could be defined, one at the flame extinction limit, and another at the smolder extinction limit.

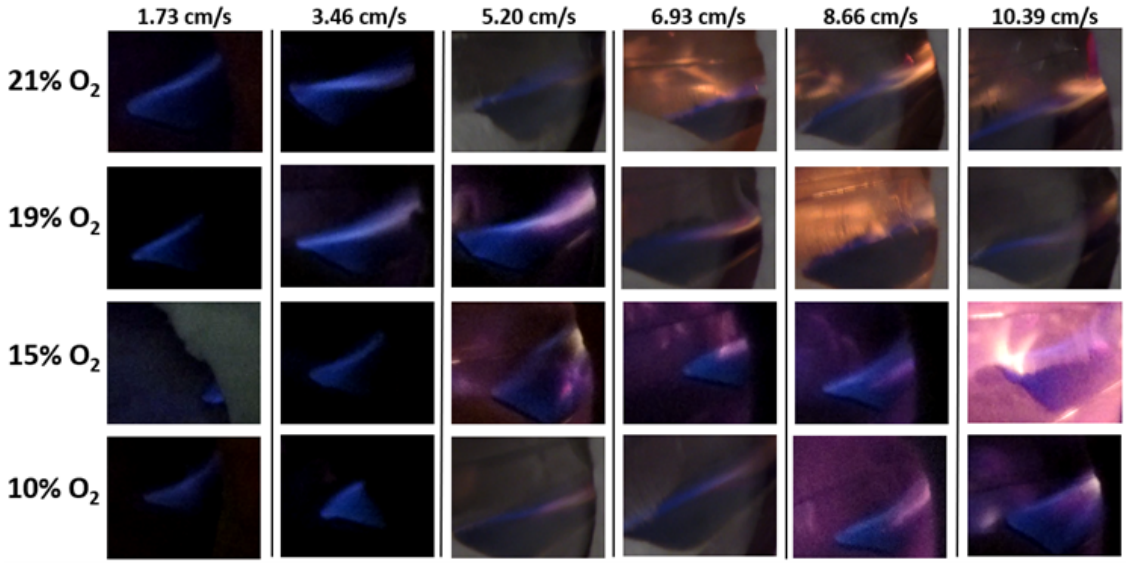

Figure 5.2: Snapshots of the moments of StF transition at different oxygen concentrations and flow velocities (size of each image is approximately 3 cm x 3 cm).

As the flow velocity and oxygen concentration increase, the flame became larger and gradually covered the entire heated fuel surface. Meanwhile, the flame color also transitioned from a completely blue to a bluish orange color flame and then to a typical orangish yellow color, indicating a stronger reaction. This could be demonstrated by a higher combustion efficiency with a higher oxygen concentration and flow rate (see more discussion in section 5.3.4).

5.3.2 Limits of smoldering-to-flaming transition

Figure 5.3 summarizes the external heat flux required for the transition from smoldering to flaming for increasing flow velocity and oxygen concentration. The dashed lines represent the averaged heat flux at which this transition occurs as a function of the flow velocity over 4 different oxygen concentrations. Above each dashed line is flaming combustion and below is smoldering combustion. Error bars represent the standard deviations between four repeated tests. The top and bottom lines represent pure flaming and smoldering conditions, respectively. The pure flaming and smoldering conditions were performed to provide a reference at fixed heating rates to compare corresponding emissions. As pure flaming and smoldering were performed at higher and lower external heat flux respectively, the standard deviation between the repetitions was zero.

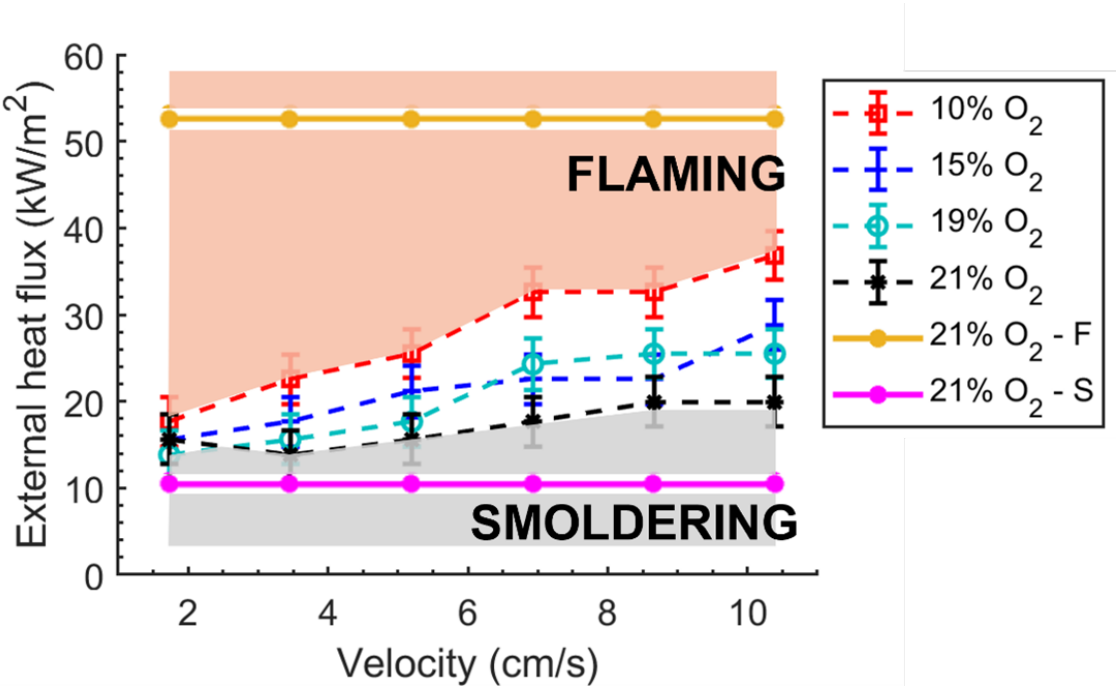

Figure 5.3: External heat flux required for StF transition of cellulose powder.

As shown in Fig. 5.3, at a given flow velocity, as the oxygen concentration increases, the heat flux required for StF transition generally decreases. For example, at a flow velocity of 5.2 m/s, the required external heat flux decreases from around 25 kW/m^2 to 16 kW/m^2, as the oxygen concentration increases from 10% to 21%. This is because the increased oxygen supply contributes to a stronger smoldering reaction [122], increasing the rate of heating and production of pyrolyzate to a sufficient level to trigger this abrupt transition. Therefore, a lower external heat flux is required to compensate for the minimum energy required for the StF transition. On the other hand, although the oxygen supply increases as the flow velocity increases, convective cooling also increases. Therefore, for a fixed oxygen concentration, as the wind velocity increases, the heat flux required for such a transition increases.

Three data points, i.e., 21% at 1.73 cm/s and 19% at 6.93 and 8.66 cm/s, exhibit a deviation from the trend explained above. Deviation from the trend was explored but the specific cause is unknown. As mentioned previously, increasing the velocity leads to enhanced convective cooling, resulting in decreased temperatures and burning rates. Simultaneously, the concentration of oxygen reaching the solid phase increases, leading to an increase in both temperature and burning rates. It appears these competing processes may not be entirely linear under reduced oxygen conditions. The trends are technically within the error bars of one another; however, the trends are repeatable in experiments and appear to be physically relevant. Moreover, at low velocities, the difference in the heat flux required for all oxygen

concentrations is within 4 W/m^2, but as the velocity increases, the difference in the heat flux required increases to $\sim$ 17 kW/m^2.

We further performed these tests at 8% and 5% oxygen concentrations with heat fluxes exceeding those shown, but no StF transition was observed. We therefore can conclude that, for this configuration and conditions, cellulose powder below a 10% oxygen concentration does not undergo StF transition.

To better understand the trends in Fig. 5.3, a simplified energy balance is applied to a reacting controlled volume of cellulose powder, where a constant minimum total heat flux when the StF transition occurs can be assumed as

$$\dot{q}''_{StF,min} = \dot{q}''_{sm} + \dot{q}''_{e} + \dot{q}''_{\infty} = constant \tag{5.1}$$

where $\dot{q}''_{StF,min}$ is the minimum total heat flux required for StF transition, $\dot{q}''_{sm}$ is the heat provided to the virgin fuel by smoldering combustion, $\dot{q}''_{e}$ is the external heat flux provided by the heater, and $\dot{q}''_{\infty}$ is the heat loss to the environment. The $\dot{q}''_{sm}$ term can be further expanded as:

$$\dot{q}''_{sm} = \dot{m}''_{c}\Delta H_{cs} = \rho_c s_c \Delta H_{cs} = \frac{\dot{m}''_{ox}}{\nu}\Delta H_c = \frac{\rho_g U Y_{O_2}}{\nu}\Delta H_c \tag{5.2}$$

where $\dot{m}''_{c}$ is the mass burning rate of the cellulose powder and $\dot{m}''_{ox}$ is oxygen mass flow rate, ΔH_{cs} is the heat of smoldering combustion of cellulose powder, ΔH_c is the heat of flaming combustion of cellulose powder, ρ_c is the density of cellulose powder, s_c is the smoldering spread rate over cellulose powder, U is the oxidizer flow velocity, ρ_g is the density of cellulose powder, ν is the oxygen stoichiometric coefficient, and Y_{O_2} is the oxygen mass fraction.

$\dot{q}''_{\infty}$ can be written as:

$$\dot{q}''_{\infty} = \epsilon\sigma(T_c^4 - T_\infty^4) + h(T_c - T_\infty) \tag{5.3}$$

where ϵ is the smoldering cellulose emissivity, σ is Stefan Boltzmann constant, T_c is the temperature of smoldering cellulose powder, T_∞ is ambient temperature, and h is the convective cooling coefficient which could be described as

$$h = Nu(k/L) \propto Nu \propto Re^m Pr^n \propto (UL/\nu)^m(\nu/\alpha)^n \propto U^m \tag{5.4}$$

where L is the characteristic length of the cellulose sample, ν is the kinematic viscosity, α is the thermal diffusivity, and $0 < m < 1$ [123]. For a given oxidizer velocity, as Y_{O_2} increases, $\dot{q}''_{sm}$ increases (Eq. 5.2). Therefore, by assuming a constant minimum total heat flux for StF transition, a smaller $\dot{q}''_{e}$ is required to compensate for the minimum energy for the StF (Eq. 5.1), agreeing well with the experimental observations.

As wind velocity increases, the smoldering intensity is controlled by a competition between smoldering heat release and environmental cooling [112], where both $\dot{q}''_{sm}$ and $\dot{q}''_{\infty}$ increases with U. However, as observed from Fig. 5.3, the required external heat flux increases as the wind velocity increases, which indicates that the StF process is more sensitive

to environmental cooling than oxygen supply by the oxidizer flow. Ohlemiller [111] also performed StF transition for cellulose insulation and reported that the rates of heat transfer and oxygen supply are tightly coupled, as observed in this study.

5.3.3 Emissions

Gaseous emissions after StF transition at varying flow rates and a constant oxygen concentration of 21% are shown in Fig. 5.4. Overall, emissions remained relatively constant for the test duration (an example plot at 21% oxygen concentration and 1.73 cm/s flow velocity can be found in the Appendix D) and the mean values with standard deviations between repeating experiments have been plotted. The trends of different emissions at concentrations of 19%, 15%, and 10% were similar to that of 21%, so only the emissions at an oxygen concentration of 21% have been plotted here and plots at 19%, 15%, and 10% can be found in the Appendix D.

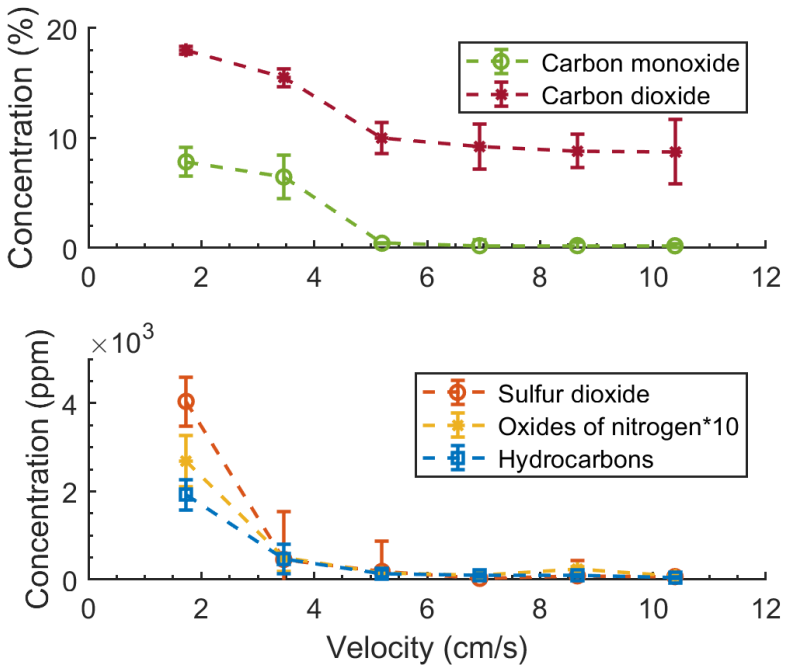

Figure 5.4: Gas emissions after StF transition at an oxygen concentration of 21%.

Figure 5.4 shows that, below 5 cm/s, although a dim blue flame was observed above the cellulose powder (see Fig. 5.2), high concentrations of CO, CO_2, NO_x, SO_2, and HC are measured. Above 5 cm/s, the concentrations of the measured gases are low and constant as a higher oxidizer velocity brings in more oxidizer and burning is no longer sensitive to the increasing flow velocity. Because such a stark change in emissions is observed at 5 cm/s,

we denoted it as a limiting velocity. This limiting velocity may change with changes in experimental parameters as, for instance, Ohlemiller [111] found a transition velocity of 2 m/s for forward StF transition experiments. This limiting velocity seems to be a critical value for StF transition. In this work, a limiting velocity of 5 cm/s was observed for all other oxygen concentrations as well. As shown in Fig. 5.2, at lower airflow velocities, the flame was weak, lean, and blue covering the fuel surface and consuming the emissions. This indicates that the reaction was weak and incomplete, allowing the oxygen to diffuse into the porous char layer and maintain the char oxidation. Consequently, an increased quantity of gaseous products from incomplete combustion were generated.

The transition from a blue to orange flame occurred at 5 cm/s as observed in Fig. 5.2, which was further supported by the emissions plotted in Fig. 5.4. The blue color observed occurs due to radiation by excited CH radicals which could have been produced by incomplete combustion and orange due to radiation from CO_2, water, and soot particles produced in complete combustion. Also noticeable is that the amount of HC produced at velocities below 5 cm/s was relatively high while almost negligible above 5 cm/s.

5.3.4 Modified combustion efficiency

To better define the StF transition from the emissions data in Fig. 5.4, we used a modified combustion efficiency (MCE) as presented in Eq. 1.3. The gas concentrations of the combustion products corresponding to the conditions in Fig. 5.4 are used to estimate the MCE and have been plotted in Fig. 5.5.

As shown in Fig. 5.5, for airflow below 5 cm/s, the MCE is less than 95%, indicating a mixed mode of combustion. This further supports the previous description where smoldering and flaming are observed to co-exist under these test conditions. Above 5 cm/s, as the flame intensifies, no smoldering is observed, and the flame covered the entire fuel surface consuming the oxygen and preventing the onset of smolder. At low velocities (1.73 and 3.46 cm/s), we also see the effect of oxygen concentration on MCE. Due to the low oxygen concentration, the fuel is not consumed completely, and the MCE is low, but as the oxygen content increases, the MCE increases.

The solid yellow line in Fig. 5.5 corresponds to experiments run at a single high heat flux generating fully flaming combustion, and the solid pink line corresponds to a low heat flux generating fully smoldering conditions. This is done to provide emission limits for comparison. It is interesting to note that below a velocity of 5 cm/s a transition in emissions is observed even for these two conditions. For fully flaming conditions, the MCE is higher than at the flammability limit for different oxygen concentrations below this velocity, suggesting that the high external heat flux helps raise the temperature of combustible gases leading to a complete reaction and improving the MCE. However, for fully smoldering conditions at low flow velocities, the residence time of oxygen is high due to the low velocity and helps to better combust the reactants, improving the MCE; but for higher velocities the residence time is low, and MCE reduces.

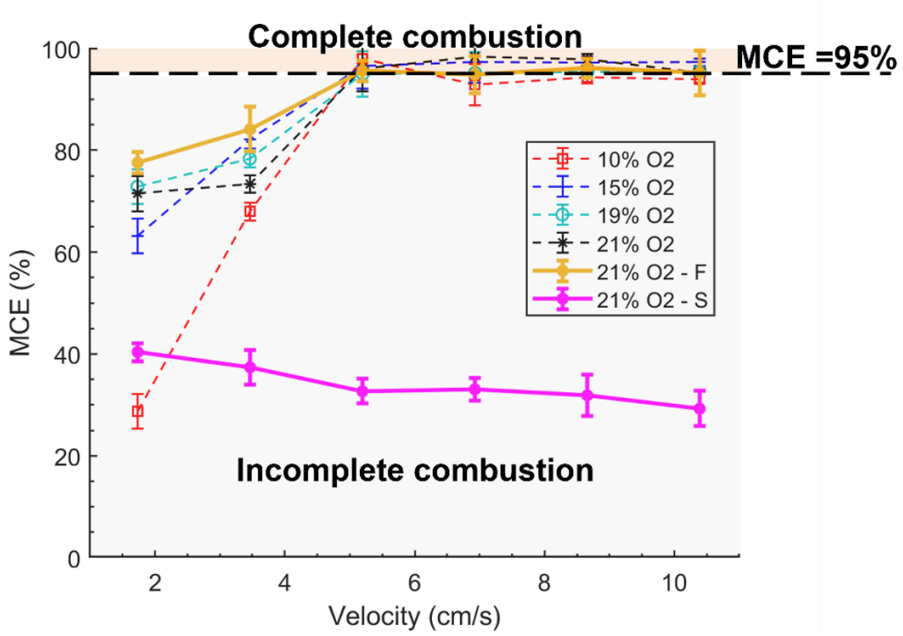

Figure 5.5: Modified combustion efficiency at the StF transition limits of cellulose.

5.3.5 Effect of density

All the above results correspond to high-density cellulose powder i.e., 380 ± 20 kg/m^3. To explore the effect of fuel density on the limiting conditions of StF transition, another type of cellulose power with a lower density of 180 ± 15 kg/m^3 was tested, and the results are shown in Fig. 5.6.

At a given flow velocity, the required external heat flux increases as the oxygen concentration decreases, agreeing with the results in Fig. 5.3. On the other hand, as the density decreases, the heat flux required for transition increases. The trend of heat fluxes required for all oxygen concentrations remain for both cellulose powders, however the slope and absolute values of heat flux vs. velocity changes. The StF transition of low-density cellulose was also not observed at oxygen concentrations below 10%.

The result that a higher cellulose density requires a lower heat flux for StF transition could be due to a higher heat conductivity of the cellulose fuel bed that results in a thicker heated layer of cellulose and corresponding increase in a larger flux of pyrolyzate. According to Eqs. 5.1 and 5.2, as the density of cellulose powder increases, the burning mass flux of cellulose powder increases, further increasing the $\dot{q}''_{sm}$ ($\dot{q}''_{sm} \propto \dot{m}''_c$ from Eq. 5.2), requiring lower external heat flux ($\dot{q}''_e$), which explains the experimental trend in Fig. 5.6.

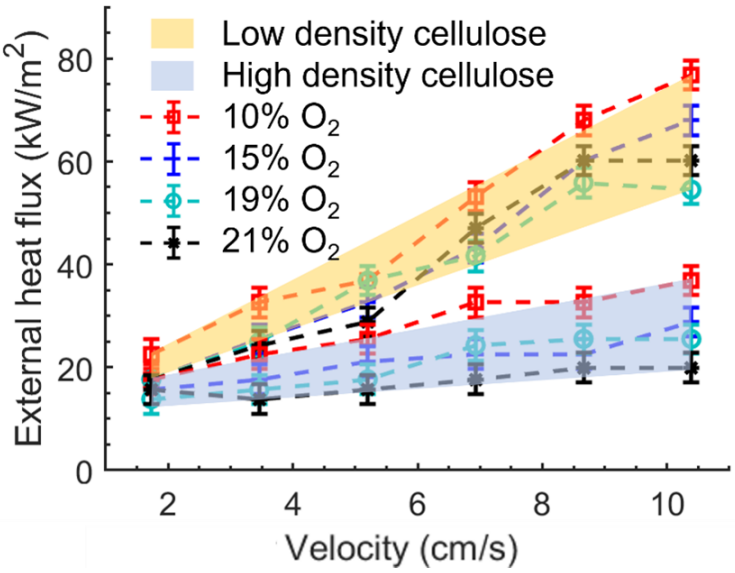

Figure 5.6: Effect of fuel density on the limiting conditions of StF transition.

5.4 Conclusions

In this study, we utilized a new experimental apparatus to study the StF transition of cellulose powder under varying environmental conditions. Conditions varied included oxidizer flow velocity (1.5 – 10.5 cm/s), oxygen concentration (21, 19, 15, and 10%), external heat flux (0 – 60 kW/m^2), and fuel density. For a fixed fuel bed density, as oxygen concentration decreases, the heat flux required for the StF transition increases, agreeing with both an energy balance analysis and phenomenological arguments. However, for fixed oxygen concentrations, the heat flux required for StF transition increases with increasing oxidizer flow velocity due to the increasing role of convective cooling. Moreover, tests conducted at oxygen concentrations of 8% and 5% did not exhibit the transition even at higher external heat fluxes, leading to a conclusion that a minimum oxygen concentration of 10% is required for StF transition. The density of the cellulose powder was also varied, and it was found that the heat flux required for StF transition increases as the density of the cellulose powder decreases.

Furthermore, a limiting oxidizer velocity of 5 cm/s has been found based on visual observations, measurements of emissions, and calculation of the modified combustion efficiency. Below 5 cm/s, smoldering may co-exist with a flame because oxygen can penetrate the weak blue flame covering the fuel surface and diffuse into the smoldering cellulose powder. Although this limiting value of the flow velocity may change with variations in some of the parameters, it appears to be a critical value for the StF transition similar to what has been

observed by previous investigators.

This work provides additional information about the StF transition under varying environmental conditions that may be present during residential and wildland fires. Future numerical simulations are needed to reveal the underlying physical and chemical processes of the StF transition.

5.5 Acknowledgements

Data from this chapter, in part, is included in a manuscript titled "Limiting conditions of smoldering-to-flaming transition of cellulose powder", by P. Garg, I. Shan, S. Lin, M.J. Gollner, and C. Fernandez-Pello, under consideration by the peer-reviewed Fire Safety Journal. The thesis author is the primary investigator in this publication.

Chapter 6

The effectiveness of filter material for respiratory protection worn by wildland firefighters

During a wildland fire event, firefighters often receive significant exposure to smoke consisting of particulate matter (PM) and gaseous emissions. Major respiratory and cardiovascular health concerns are related to inhalation of smoke and respiratory protection (RP), such as masks, are one of the most important pieces of personal protective equipment (PPE) that can be used to mitigate this exposure. One barrier to RP implementation is that the effectiveness of different PPE worn by firefighters is not well studied in the literature.

The aim of this study is to generate direct evidence on the effectiveness of common RP materials, to assess their ability to provide protection from wildland fire smoke. Six different filtering materials were tested against simulated wildland fire smoke produced by smoldering Douglas fir needles in a custom-made lab-scale apparatus. Both PM and gases were measured with and without the filter material and their effectiveness is reported in this study. As a result of this study, it is shown that some existing filter solutions (e.g., bandanas) are inappropriate, and suggest proper materials for use in future RP solutions.

6.1 Background

Over the past few decades the frequency, severity, and total area burned by wildfires has increased dramatically in many regions around the world [18–20]. In the United States, a history of aggressive wildfire suppression, leading to higher fuel loads and climate change, resulting in longer fire seasons, earlier snow melts, and prolonged droughts have contributed to these worsening trends [19–21]. Alongside potential destruction from the fire itself, wildland fires emit large amounts of gaseous emissions and particulate matter (PM) which varies depending on the vegetation type, moisture content, and state of combustion [22, 23, 33]. The smoke from these wildland fires travels long distances and can therefore impact air quality as

well as the broader earth-climate system [24]. Exposure to wildland firefighters and near-by populations, however, can occur at high concentrations, sometimes repeatedly within the same fire season, potentially leading to numerous health effects [10, 25]. The pattern of wildland firefighter smoke exposure is often very different compared to that of surrounding populations, as they have high occupational exposures over long durations, whereas population often have location-based exposures with more mitigation measures (e.g. masks or indoor filtration systems) available.

The extent to which this smoke exposure impacts both first responders and public health has been widely studied in literature. Adetona et al. [10] performed a thorough literature review on the health effects of wildfires on both firefighters and the public. Short-term health effects observed from these emissions includes asthma exacerbation, coughing, headache, hypertension, and breathlessness [26–28], while long-term health effects include respiratory and cardiovascular illness [11, 12, 17, 29].

Numerous studies have quantified emissions from wildfires [3, 30, 31], prescribed fires [32], and smaller-scale laboratory experiments [33–35]. Particulate matter (PM) is often considered the most important constituent to predict the health hazard of smoke, especially to surrounding populations, where there is more time and distance for effluent dilution. PM is classified by aerodynamic diameter: coarse (aerodynamic diameter between 2.5 and 10 μm), fine (< 2.5 μm), and ultra-fine (< 0.1 μm) [48]. Literature shows that wildland smoke is dominated by respirable particles, i.e., < 4 μm [10, 25]. Previous studies performed during periods of wildland fire events [10, 49] have measured fine PM (≤ 2.5 μm) and respirable PM (≤ 4 μm) which are small enough to penetrate into the lungs. The maximum occupational exposure limit for respirable PM by Occupational Safety and Health Administration (OSHA) is 5,000 $\mu g/m^3$; however, concentrations surrounding wildland fire events are often very high (12.5 mg/m^3 as reported by Alves et al. [50] in the immediate vicinity of fire) compared to this limit [10].

Gaseous species emitted are also a significant concern, especially closer to the fire source, as some of them are carcinogenic and can cause major health issues. Species of major concern are carbon monoxide (CO), sulfur dioxide (SO_2), nitrogen dioxide (NO_2), ozone (O_3), acrolein (C_3H_4O), formaldehyde (CH_2O), benzene (C_6H_6), toluene (C_7H_8), and xylene (C_8H_{10}) [10]. Exposure to these species beyond the established exposure limits could be deadly. OSHA in the United States has defined exposure limits for these species which should be taken into consideration by firefighters when working for days or weeks in the field [51]. For instance, CO easily binds with hemoglobin to form carboxyhemoglobin (COHb), limiting the oxygen carrying capacity of blood, resulting in short term effects like headache, dizziness, disorientation, and weakness [52]. Acrolein and formaldehyde are respiratory irritants and exposure beyond the limit can cause lung injury. Formaldehyde and benzene are classified as carcinogens and nitrogen dioxide causes a decrease in pulmonary responses [10]. Additionally, high concentrations of ozone and other gases formed downstream the fire location are also associated with acute cardiovascular effects and respiratory illness [53]. A few studies at prescribed fires and wildfires have reported measured emissions of gaseous species below the exposure limits, but this result largely depends on the location of sampling [10, 32, 54, 55].

Knowing the potential health effects of smoke exposure, it is very important for nearby populations and firefighters to protect themselves when conditions warrant by wearing proper respiratory protection (RP) equipment. Wildland firefighters work in very close proximity of fire fronts and often remain at locations which can experience heavy smoke for extended periods of time, for instance during inversion events. Therefore, having proper RP equipment can be necessary to preserve their health. Wildland firefighters, however, are often seen wearing either bandanas or nothing over their mouth and nose. Unlike structural firefighters, who use self-contained breathing apparatus (SCBA) that meet National Fire Protection Association standards [49, 56], wildland firefighters have no standard respirators available. The use of a SCBA is not feasible in wildland applications because the volume of air in cylinders does not last for long enough periods and the cylinders are too heavy for prolonged use under high temperatures and a physically-demanding workload. During the COVID-19 pandemic, the prevalence of masks and respirators has dramatically increased [57, 58], however their effectiveness specifically for wildland fire smoke has not been studied.

Despite the widespread availability and use of respirators in other applications, wildland firefighting conditions are unique due to lengthy deployments, hot weather, and extremely strenuous exercise. Present respirators are often uncomfortable to use for long durations under these conditions. According to responses at a workshop reported in the literature, some firefighters even consider smoke exposure as a necessary part of their job [124]. Despite the potential challenges of adopting respiratory protection for wildland firefighters, proper RP should be investigated because of the considerable adverse health effects proper personal protective equipmen (PPE) could alleviate. Unfortunately, strong evidence to support the efficacy of respiratory protection for use during wildland fires is lacking. At present, wildland firefighters are recruited with incomplete information about the occupational risks to health and life expectancy. In a recent call to action manuscript, Rice et al. [124] recommended a joint collaboration of scientists, fire managers, regulators, public health practitioners, and the affected public to address these health risks and to propose appropriate solutions.

The effectiveness of filter material for respiratory protection depends on several factors. First, different filter material layers can be combined to protect against particles of different sizes, volatile organic compound (VOC), carcinogenic gases, etc. For instance, melt-blown polypropylene is often used for particle filtration with electrostatic charging added for higher efficiency capturing of small particles, while activated carbon is often used to absorb small concentrations of VOCs. For similarly-sized materials, additional filter layers often enhance filtration efficiency, however it also increases breathing resistance, which makes masks difficult to wear for long durations or under strenuous exercise conditions. Second, the overall efficiency of a mask depends on the seal between the mask and the wearer, so that all respirated air is in fact filtered. A proper fit test is often required to minimise leakage and maximize filtration efficiency. In the United States, the National Institute for Occupational Safety & Health (NOISH) certifies 9 types of respirator masks with three classes, N (not resistant to oil), R (somewhat resistant to oil) and P (strongly resistant to oil), and three separate levels of efficiency (95, 99, and 99.97%) in each class. The efficiency indicates the degree to which the filter removes small (0.3 μm) particles. American Society for Testing

and Materials(ASTM) International also has developed certification tests for surgical masks, ASTM I, II, and III masks, with increasing levels of bacterial and particle filtration efficiencies as well as fluid resistance for medical applications, although the fit of these masks is not assessed and often poor without modification [125–127].

During the COVID-19 pandemic different test methods were more widely implemented and standardised to test the filtration efficiency of RP masks. NIOSH certification testing is often considered the most rigorous because it uses a charge neutralized NaCl aerosol, whose diameter is close to the most penetrating particle size and at a high flow rate, so that there is maximum penetration through the mask and the measured efficiency represents a realistic value. The Food and Drug Administration (FDA) also recognises Particulate Filter Efficiency (PFE) and Bacterial Filtration Efficiency (BFE) tests developed by ASTM [125–127]. The PFE test uses unneutralized 0.1 μm polystyrene latex particles at 0.5 to 25 cm/sec face velocities and the BFE test uses unneutralized S. aureus bacteria with a mean particle size of 3 ± 0.3 μm diameter at a flow rate of 28.3 L/min. Both PFE and BFE are done to measure the performance of different medical masks and have been widely used in literature. Leith et al.[128] performed a study to understand the inhalation and exhalation of infectious aerosol for seven different masks, most of them cloth masks with different thread count per cm. They compared protection efficiency for different conditions, like speaking vs. not speaking, different flowrates, and for both inhalation and exhalation. They found that the masks with finer fibers showed better performance with moderate flow resistance. Kodros et al.[57] developed a framework to quantify filtration efficiency of different face masks by generating particles in the size range of 0.5 - 10 μm. They correlated these results to the PM size range produced during wildland fires and found that N-95s are very efficient and can reduce exposure by more than a factor of 14, whereas cotton masks offer the lowest protection. They did not expose the masks to actual wildland fire smoke, but rather generated ammonium sulphate aerosol particles to test the efficiency of the masks.

Navarro et al.[48] presented a study on co-occurrence of exposure from smoke and COVID-19 for wildland firefighters, providing additional mitigation measures to prevent infection from both. They recommended social and physical distancing of the unit and wearing of cloth masks when operating outside the unit. De Vos et al. [56] performed a 15 min bushfire smoke study on 64 firefighters wearing 3 different types of RP masks with filters for particulate only (P), particulate/organic vapor (POV), and particulate/organic vapor/formaldehyde (POVF), and analyzed the air inside the firefighter masks. They found that higher concentrations of formaldehyde and acrolein were seen inside the P-type mask compared to POV- and POVF-type masks. Another experimental study [129] compared toxic penetration using a combined carbon cartridge/particulate pre-filter versus a simple cloth bandana and concluded that neither filter performed well and determined that further investigation is required. Khayan et al.[130] designed respiratory masks using an additional activated carbon layer to absorb toxic gases like CO_x, NO_x, and SO_x from ambient air, and the results show that a surgical mask combined with an activated carbon layer is more effective than a surgical mask alone. Soeroso et al. [131] also tested the effectiveness of three types of masks, a surgical mask, an N-95 mask, and an activated carbon mask in ambient air and observed

reduced CO levels using an N-95 and an activated carbon mask, while a fabric mask had the poorest protection from CO levels.

In this study, six different mask materials were put through testing using wildland-fire-like smoke, and their efficiency of filtration calculated for both particulate matter and gaseous species. We would expect that increasing levels of filter materials are very good at particulate filtering and increasingly good at gas filtering, though none may be 100% effective. Bandanas are the primary protection measure used today by wildland firefighters and we hypothesize that they are inappropriate for this application based on previous studies on cloth masks for viral protection [128, 132–134]. In this study we specifically focus on the effectiveness of the filter materials, not the fit, operation, or practicality, with the acknowledgement that advancements will need to be made to their implementation into practical RP.

6.2 Methodology

6.2.1 Respiratory protection materials

Six different candidate filter materials used in respiratory protection (RP) devices were selected for testing: a cotton bandana, a surgical mask, N-95, P-95, P-100-2097, and P-100-2297, as shown in Fig. 6.1. Bandanas are the most commonly worn filtering material by firefighters during a wildland fire event. Most designs currently available on the market consist of one thin layer of cotton fabric, which has been chosen for this study. Other variations using nomex are also found, but not tested in this study. Bandanas are often utilized because they are easy to carry and breathable while performing high intensity work for long periods during a wildland fire event. Many firefighters therefore use them over their mouths for respiratory protection even though they are not designed for this purpose.

During the COVID-19 pandemic, surgical masks designed for healthcare settings became widely used and were added to the list of tested materials. The surgical masks used in this study were purchased from a U.S. manufacturer (DemeTECH). They were ASTM level 3 rated face masks, consisting of 3 filter layers, with the first layer (non-woven polypropylene) providing protection against fluids, high breathability, and protection against airborne bacteria, the center consisting of a melt-blown polypropylene layer filtering 98% of airborne particles and bacteria, and the inner comfort layer (non-woven polypropylene) which enables the wearer to wear masks comfortably for long periods.

One common N-95 (3M Aura 9205+), 1 elastomeric P-95 (3M 2078) filter, and two different P-100 (2097 and 2297) masks were also tested, representing increasing levels and breadth of filtration. N-95 and P-95s are NIOSH approved and both rated to filter out 95% of the particulate matter of diameter around 0.3 μm, and P-95 are resistant to oil while N-95 masks are not oil-resistant. An N-95 has 4 layers: the mask's outer layer (non-woven polypropylene), filter layer (non-woven polypropylene, melt-blown), support layer (modacrylic), and inner layer (non-woven polypropylene) providing respiratory protection. A P-95 is made of electrostatic media to enhance the capture of airborne particles and to

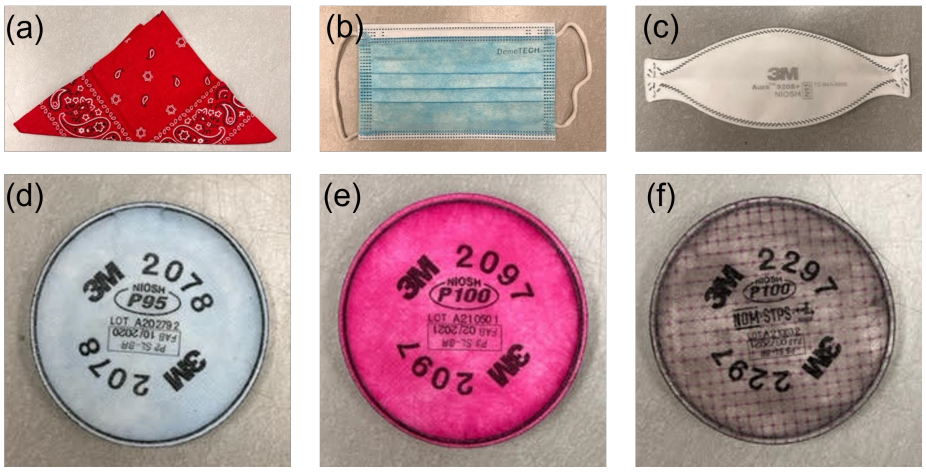

Figure 6.1: Respiratory protection (RP) mask material used in this filtration study (a) bandana, (b) surgical, (c) N-95, (d) P-95, (e) P-100-2097, and (f) P-100-2297.

reduce breathing resistance. They also have an additional layer of activated carbon providing protection against nuisance level of organic vapor and acid gases.

Finally, we tested 2 different P-100 filters used in elastomeric respirators rated to filter out 99.97% of particulate matter. The P-100-2297 can also filter out oil-based particles and has an added nuisance-level organic vapor filter, whereas the P-100-2097 does not have the added nuisance-level organic vapor filter. Both P-100's were also NIOSH approved. Another major consideration while selecting the RP material was the flatness of the mask material. As the masks were cut and fitted into the filter cassette, it was easy to get a leak-proof fitting with the flat mask compared to curved masks.

6.2.2 Determination of flow rates, area of test material, and face velocities

During a wildland fire event, physical demands on firefighters vary widely throughout a shift [135], with respiration rates estimated to range between 21 and 173 L/min for periods of low- and high-intensity physical activities based on heart rate measurements [17]. Weighting the time spent at a particular activity level as a fraction of an average shift, these values converge to an average minute volume per shift of 41 L/min, in agreement with the 22 to 60 L/min range reported in previous studies [82]. To calculate the flow rate for testing, the average respiration rate of 41 L/min is used across the effective surface area of the mask, which is approximated as 150 cm^2, according to the NIOSH N-95 certification test [136]. This gives a flow rate (face velocity) of 4.55 cm/s, which is in close agreement with several different test methods, such as those by NIOSH, FDP-PFE, and ASTM-PFE [136].

To perform the experiments, a circular section was cut from each RP material and fitted into a sample holder of diameter 3.7 cm, sealing around the edge to prevent any leak. A constant respiration rate of 41 L/min through the whole mask of area 150 cm^2 was scaled proportionally to the area of the cut circular section and the equivalent volumetric flow rate through the cut circular section came out to be 2.939 L/min. Before fitting the cut section of the mask into the sample holder, the masks were pre-conditioned by leaving them in a lab atmosphere (relative humidity of approximately 42 $\pm$ 5% and a temperature of 22 $\pm$ 1 °C) for at least 24 hrs, following the NIOSH test methods.

The breathing resistance of the material was determined by measuring the differential pressure drop using an inclined manometer across the test samples with a flowrate of 2.939 L/min (as determined by scaling), which ranged between 50 - 70 Pa for all studied masks type.

6.2.3 Experimental setup and Instrumentation

Douglas fir was completely oven dried resulting in FMC of 4% was chosen for testing. Combustion of Douglas fir was conducted in a custom made linear tube-heater apparatus as shown in Figure 6.2. To understand the effectiveness of the masks, we conducted worst case combustion condition experiments, i.e., smoldering (at 450°C), which produces significant amounts of particulate matter. 3.75 g of Douglas fir needles were evenly distributed in a 40 cm long quartz boat, which was further inserted into the quartz tube. For particulate matter (PM) measurements, effluents were drawn after dilution from stainless steel tubes inserted across the exhaust duct. Whereas for gaseous analysis, effluents were directly drawn from the quartz tube and no dilution was required (due to the higher saturation limit of the instrument) as shown in Fig. 6.2 (b,c). The data presented here corresponds to the smoke concentration at the end of the quartz tube before any dilution.

Three different diagnostic techniques were used. A DustTrak and gravimetric filters analysis for particulate matter and FTIR for gaseous emissions sampling. The FTIR used in this study was pre-calibrated for 26 gases. Out of these 26 gases, only 16 were detected at measurable levels for smoldering Douglas fir needle smoke. These 16 gaseous species are discussed in the results section (Table 6.1). The reference spectra of these 16 targeted gases were used to determine concentrations at the sampled conditions, 100°C and 650 torr, using a full-gas factory calibration. Each mask type was tested 8 times, 4 times using a DustTrak alongside a filter cassette for real-time and time-averaged PM concentrations, respectively, and 4 times using an FTIR for gaseous species. Average values from the 4 experiments and the associated standard deviation between tests are reported in this work.

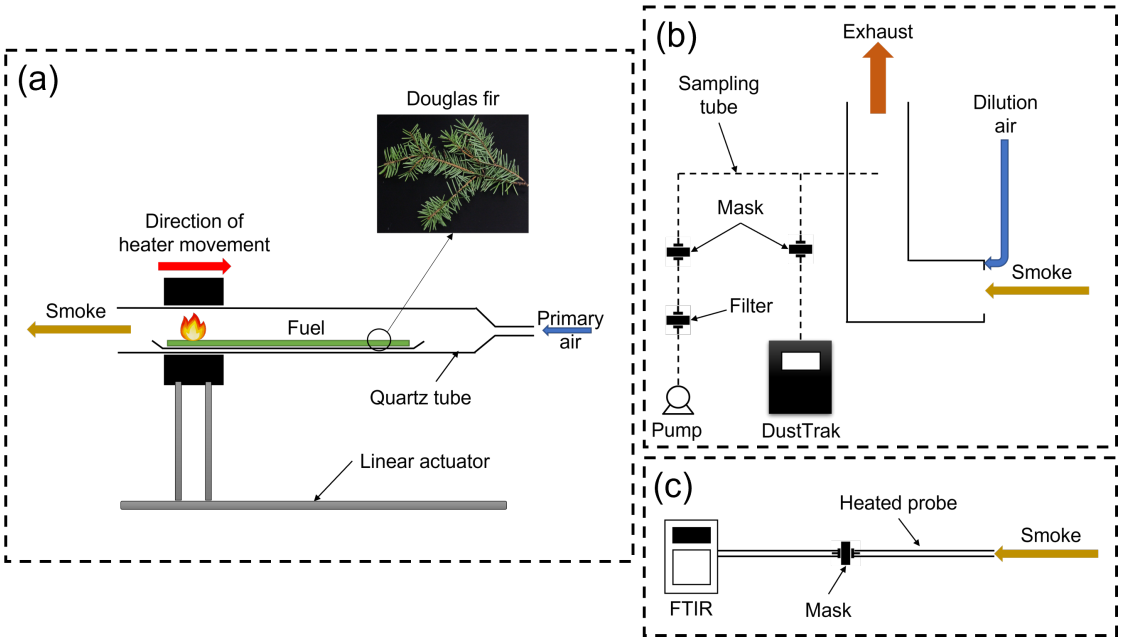

Figure 6.2: Schematic diagram of the (a) linear tube-heater smoke generator apparatus, (b) attachment for particulate matter (PM) sampling, (c) attachment for gaseous sampling.

6.3 Results and Discussion

6.3.1 Particulate matter filtration

For the fixed fuel loading, airflow, and heating temperature conditions described above, the average concentration of total particulate matter produced by smoldering Douglas fir (no mask, reference condition) was 0.125 ± 0.03 mg/s. Time-dependent concentrations of TPM after passing through different respiratory filtration masks are compared with the reference condition in Fig. 6.3. Please note that each line shown in the plot is an average of 4 experiments, with the shaded region indicating the standard deviation between 4 repeated tests. The data for N-95, P-95, P-100-2097, and P-100-2297 has not been plotted, as the 0.001 mg resolution for the DustTrak gave a zero value i.e., below the detectable limit, and analysis in the nanometer range was not possible with the instrumentation available.

Given the modularity of the experimental setup, it is interesting to note that the concentration of the TPM produced over the time is steady for the test duration with a small rise at the start of the experiment, which most likely results from the ignition of the smoldering Douglas fir, before reaching a steady state. Bandanas are commonly worn by firefighters for RP, which is troubling as the results clearly show that the particulate matter concentration rate only reduces by 0.02 mg/s compared to no mask conditions. Surgical masks, which became very common during COVID-19 pandemic, seem to provide a significant level of PM

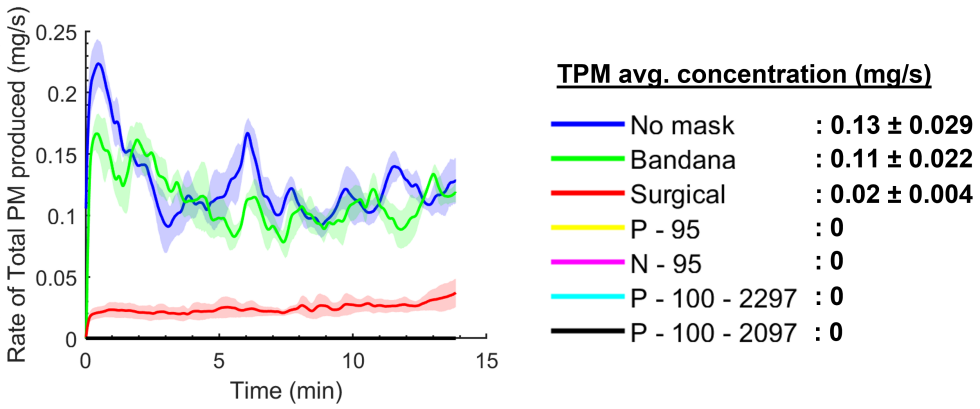

Figure 6.3: Rate of total particulate matter seen after passing through an RP filter. Note that the shaded area represents the standard deviation between 4 repetitions.

reduction compared to the bandanas (assuming only filtration, not fit), however, maximum filtration is observed for N and P type masks, which reduce PM below 0.1 mg/s after passing through the RP material.

While there are many ongoing efforts aimed at designing new RP for wildland firefighters, at present there are few, if any, requirements for their use [137, 138]. Implementing respiratory PPE that provides adequate filtration of smoke is challenging, as present solutions are difficult to wear for long durations such as the long shifts that firefighters endure working in the field. Bandanas have remained the easiest option, as they are easy to carry and breath through, but provide minimum protection against PM as seen in Fig. 6.3 and approximately 90% of TPM passes through the material. Eden et al. [17] performed a study on the size distribution of PM using the same fuel, combustion conditions, and experimental setup. They found that the size distribution of particle number concentration in smoldering Douglas fir was unimodal, with count median diameter (CMD) of 110 ± 20 nm and geometric standard deviation (GSD) of 1.47 ± 0.03 (average ± 95% confidence interval over three runs). These particle sizes fall within the respirable range of humans and can reach deep into the lungs and cause long-term cardiopulmonary diseases. Proper protective equipment should be worn by firefighters rather than bandanas as they filtered only 0.02 mg/s compared to no mask conditions, as seen in Fig. 6.3.

6.3.2 Gaseous emissions

Figure 6.4 shows the concentration of gaseous species sampled downstream of the filter material. The plot on the left shows the concentration of major species, i.e., CO_2, CO, and hydrocarbons (HC), where seven gaseous species, i.e., hydrogen cyanide (HCN), methane (CH_4), acetylene (C_2H_2), ethane (C_2H_6), butane (C_4H_{10}), ethene (C_2H_4), and propene (C_3H_6) were combined for brevity and reported as hydrocarbons (HC). In Fig. 6.4 [left], we see that the

concentration of CO_2 is higher for a bandana compared to other masks, but it is within the uncertainty between the 4 repetitions of the experiments as seen in Table 6.1. CO_2 is a non-reactive gas and the concentration should not change with the mask type. Also, the concentration of CO is constant for all the 6 different masks but the concentration of HC is lowest for P-95 and P-100's.

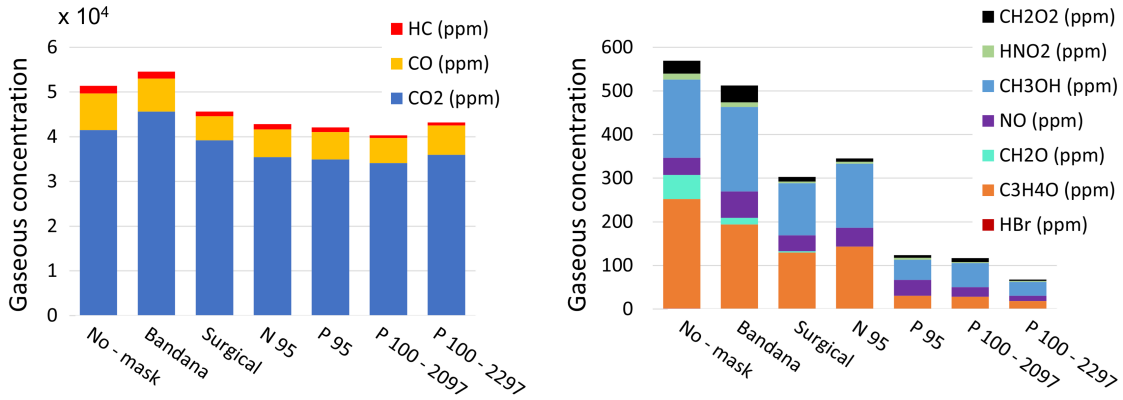

Figure 6.4: Concentration of [left] major (HC, CO, and CO_2) and [right] minor (CH_2O_2, HNO_2, CH_3OH, NO, CH_2O, C_3H_4O, and HBr) gaseous species downstream the RP mask

In Fig. 6.4 [right], the concentration of three acids, i.e., hydrogen bromide (HBr), nitrous acid (HNO_2), and formic acid (CH_2O_2), two aldehydes, i.e., acrolein (C_3H_4O) and formaldehyde (CH_2O), one alcohol, i.e., methanol (CH_3OH), and nitric oxide (NO) is presented downstream of the different mask materials tested. Out of these 7 gases, acrolein (C_3H_4O) and formaldehyde (CH_2O) are respiratory irritants and can damage lung tissues. Acrolein is a major irritant and exposure to higher concentrations can lead to major lung injury, while formaldehyde is classified as a carcinogen by the US EPA [139].

P-type masks appear to result in the lowest concentrations of hydrocarbons (HC) in the left plot (Fig. 6.4) and all the gaseous species in the right plot; p-type masks have a layer of activated carbon and the reaction with this activated carbon layer appears to effectively reduce the concentration of gaseous HC species compared to other mask types. These carbon-activated layers are not necessarily expected to last for the longer durations of wildland firefighter shifts, as they reach saturation. Following a breakthrough time, filters become ineffective because all the adsorption sites become filled, allowing gases to pass through without being adsorbed [129]. Breakthrough time is a very important parameter for carbon activated filters but its effect was not observed in this current study, as all the experiments lasted for a maximum of 15 minutes during which all the filters are expected to remain fully functional.

The FTIR used in this study was pre-calibrated for 26 gaseous species and Table 6.1 gives the reported concentrations of the 16 gaseous species that were detected. The remaining 10

Table 6.1: Concentration of different gaseous species detected by a FTIR downstream the RP mask material

Species	**No mask**	**Bandana**	**Surgical**	**N-95**	**P-95**	**P-100-2097**	**P-100-2297**
TPM (mg/L)	2.42 ± 0.03	2.21 ± 0.04	0.45 ± 0.13	0.03 ± 0.01	0.03 ± 0.01	0.02 ± 0.01	0.01 ± 0.01
Carbon Monoxide (%)	0.82 ± 0.06	0.74 ± 0.03	0.53 ± 0.03	0.62 ± 0.04	0.61 ± 0.03	0.56 ± 0.08	0.65 ± 0.04
Carbon Dioxide (%)	4.1 ± 0.4	4.5 ± 0.4	3.9 ± 0.2	3.5 ± 0.4	3.5 ± 0.2	3.4 ± 0.5	3.6 ± 0.2
Hydrogen Cyanide (ppm)	29.6 ± 3.3	27.9 ± 1.2	17.8 ± 0.8	19.7 ± 1.2	4.2 ± 0.6	2.3 ± 0.3	1.5 ± 0.2
Hydrogen Bromide (ppm)	1.7 ± 0.2	1.3 ± 0.3	0.5 ± 0.1	0.5 ± 0.1	0	0	0
Acrolein (ppm)	250.6 ± 38.8	192.9 ± 11.5	129.1 ± 8.0	142.5 ± 10.3	30.3 ± 8.0	28.3 ± 10.2	18.6 ± 6.5
Formaldehyde (ppm)	55.4 ± 5.8	14.9 ± 1.1	3.4 ± 0.5	0	0	0	0
Nitric Oxide (ppm)	39.4 ± 4.5	60.5 ± 4.0	35.8 ± 3.9	43.4 ± 4.8	36.7 ± 2.7	22.0 ± 2.0	12.0 ± 1.1
Methane (ppm)	948.3 ± 91.6	966.2 ± 77.5	667.8 ± 33.6	783.2 ± 54.6	811.4 ± 45.8	461.9 ± 69.8	495.6 ± 32.1
Acetylene (ppm)	31.7 ± 4.3	29.1 ± 2.6	21.0 ± 1.7	22.9 ± 1.8	24.3 ± 3.1	14.3 ± 2.2	17.1 ± 1.7
Ethane (ppm)	108.6 ± 11.5	114.6 ± 12.3	69.2 ± 3.7	84.1 ± 5.3	63.7 ± 7.4	46.7 ± 7.1	41.4 ± 3.2
Butane (ppm)	374.1 ± 33.6	256.4 ± 5.2	111.9 ± 10.8	133.6 ± 13.0	6.0 ± 1.6	10.9 ± 1.5	6.1 ± 1.3
Methanol (ppm)	179.4 ± 26.0	194.0 ± 13.2	119.5 ± 5.2	146.7 ± 4.8	46.2 ± 12.1	55.1 ± 13.3	31.4 ± 4.9
Nitrous Acid (ppm)	13.5 ± 1.1	10.0 ± 0.8	4.3 ± 0.2	4.6 ± 0.2	4.1 ± 0.2	2.4 ± 0.1	2.7 ± 0.2
Formic Acid (ppm)	29.0 ± 1.2	38.9 ± 3.0	10.7 ± 0.2	8.0 ± 0.2	6.0 ± 0.2	9.1 ± 0.3	3.0 ± 0.2
Ethene (ppm)	77.9 ± 7.7	73.1 ± 5.1	52.2 ± 4.7	57.6 ± 5.6	58.0 ± 7.6	34.5 ± 4.4	41.4 ± 3.9
Propene (ppm)	129.8 ± 14.4	114.0 ± 9.0	93.6 ± 3.9	110.5 ± 7.1	59.6 ± 14.2	50.4 ± 9.7	62.9 ± 17.9

gases were also searched for but their concentration remained below the detectable limits of the FTIR. All measured gases were calibrated for ppm levels, but the 10 gases that were not detected could still be present in concentrations lower than this limit. In Table 6.1, the concentration of formaldehyde has decreased by 73% for bandanas compared to no mask conditions. Foote [129] measured the concentration of formaldehyde upstream and downstream of a bandana and they reported a reduction of 20 - 30%. The 73% reduction in formaldehyde found in this study is suspicious but no errors have been identified in the FTIR measurements and results were consistent and repeatable between 4 tests. One potential explanation is that our tests run for a short duration over which formaldehyde is absorbed, and do not test for chemical or particle saturation of the filter material occurring at longer times. Similarly, we reported increases of 50% and 33% in nitric oxide and formic acid, respectively, for the bandana compared to no masks. We do not have a clear explanation for these anomalies, given their consistency and repeatability. Further study is required to fully understand these anomalies, which is currently out of scope of this study.

6.3.3 Protection efficiency (PE)

To calculate the particulate protection efficiency of the different RP mask materials, we used a simplified equation found in the literature [128, 140]. Face mask protection efficiency (PE) is then calculated as

$$PE\ (\%) = \left[1 - \frac{C}{C_0}\right] * 100 \tag{6.1}$$

where C is the concentration of particulates downstream from the mask and C_0 is the reference particulate concentration with a no-mask condition (or the concentration of particulates upstream of the mask as described in [128, 140]). The concentration of the particulates downstream from the mask, C was calculated using the weight of the gravimetric filter,

$$\text{C (mg/L)} = \frac{\text{Filter net weight (mg)}}{\text{Flowrate}\left(\frac{\text{L}}{\text{min}}\right) * \text{Runtime (min)}} \tag{6.2}$$

Figure 6.5 shows the TPM protection efficiency obtained from Eq. 6.1 for the six different mask materials utilised in this study, using a no-mask condition as the reference. The filtration efficiency for all RP masks ranged from 8.9% for the bandana to 99.5% for P-100-2297.

Following the statistical method presented by Muller et al. [140], the TPM protection efficiency across six RP masks was tested to see whether it was normally distributed. Unlike the results found by Muller et al. [140], where a non-normal distribution was found, the distribution of protection efficiency for each RP mask in this study was found to be normally distributed after performing a Shapiro-Wilk test. In this study, the probability of finding the given protection efficiency for any RP type was 0.9 ± 0.05.

Muller et al. performed experiments with two different volcanic ash samples with a mean aerodynamic diameter of approximately 100 μm and found that single layer bandanas are

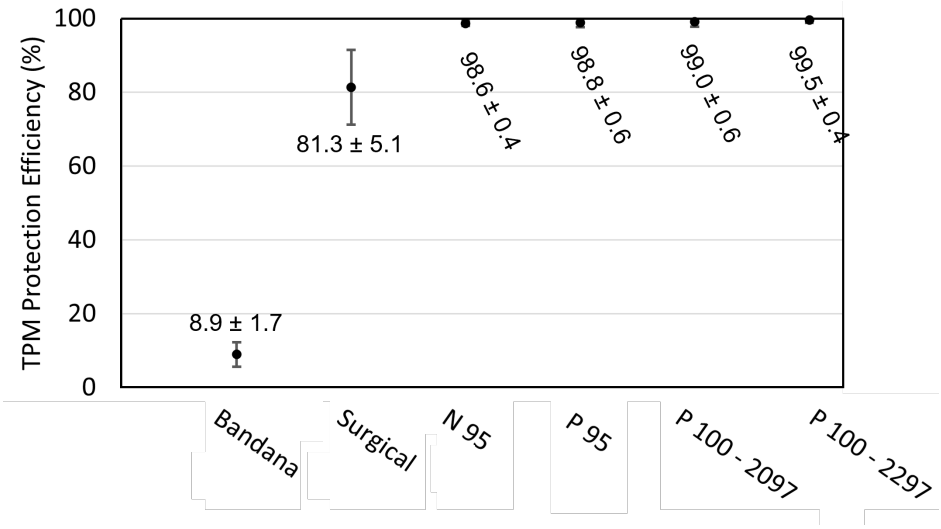

Figure 6.5: Percentage of total particulate matter from smoke by mass that would be filtered by different types of respiratory filtration mask materials. Note that the error bars represent the standard deviation between 4 repetitions

only 17.5 % efficient, which was the least efficient material among different masks tested. Similarly, the bandana is the least effective here (PF = 8.9%) against the smoke TPM produced in this study. To understand if the concentration of TPM found downstream of a bandana was significant or not compared to the no mask condition, a t-test was performed and a p-value of 0.285 was found, implying that the difference between the two data sets is statistically insignificant. However, the p-values for surgical masks, N-95, P-95, and P-100 filters compared to no-masks were found to be < 0.05, implying that their differences are statistically significant. Surgical masks that became widely used during COVID-19 showed much better filtration efficiency of 81.3% and this can be evidently seen in the reduction of TPM upstream of the mask in Fig. 6.3. Other RP materials like N-95, P-95, and P-100's had filtration efficiency above 95%, agreeing with the literature [56, 57]. It should be noted that this study was performed with a perfect seal of the mask in the cassette, which is not the case in real life. Bandanas and surgical masks are not designed to make a perfect seal around the face.

6.4 Conclusions and Limitations

In this study, we performed experiments using new linear tube-heater apparatus. Filter material samples from different masks were analyzed, which could be made available to firefighters during a wildfire event, as a means to reduce health risks from both acute and long-term exposure. Results showed that the bandanas are very ineffective as they provide

only $\sim$ 10% TPM filtration efficiency for the particle size range produced during smoldering combustion whereas, surgical, N-95, P-95, and P-100 filters were very effective at removing TPM with filtration efficiency of 81%, 98%, 99%, and 99.5% respectively. N-95, P-95, and P-100 filters were also effective at filtering some gaseous species, especially those with nuisance VOC capabilities compared to the bandana. Although this effect may not be sustained for longer durations. Results from this work can be used to support recommendations to wildland firefighters on what type of masks can be worn and how effective they actually are as personal protective equipment.

This study did not examine the fit or seal of the masks. We assume that the masks are completely sealing the face and the air is inhaled and exhaled only through the mask material, which is rarely the case especially for bandanas and surgical masks. Secondly, the experimental parameters, such as pre-conditioning, face velocity, and pressure drop mentioned by standardised procedures by NOISH, EPA, etc. were taken into consideration and values were kept within the recommended range, but the experimental setup utilized was completely different compared to any standardised method. This could result in some discrepancy in the data, since particle sizes from wildland fire smoke vary from NaCl solutions used in the standardized test methods. However, the overall message conveyed in this research, that higher-performing masks limit exposure to wildland fire smoke, is valid and can be used as a guideline for firefighters and the general public. Finally, we acknowledge that there remains a gap between finding an appropriate filtering material and designing a practical respirator that can be used for many hours in the field. It is our hope that showing the effectiveness of existing masks may spawn innovation to develop solutions that are comfortable, practical, and safe, spurring adoption.

6.5 Acknowledgements

Data from this chapter, in part, has been published in *Fire Safety Journal*, "The effectiveness of filter material for respiratory protection worn by wildland firefighters", by P. Garg, S. Wang, J. M. Oakes, C. Bellini, and M.J. Gollner (2023) 139, 103811. The thesis author is the primary investigator in this publication.

Chapter 7

Conclusions and Future Work

7.1 Conclusions

Emissions from wildland fires have been the subject of research within the fire community for many years. However, despite their well-known effects on the Earth's climate system and the health impacts on human beings, there is a lack of studies that differentiate the individual contributing parameters such as mode of combustion, fuel type, and fuel conditions. Studies conducted in the literature have attempted to quantify emissions in the field, including both wildfires and prescribed fires. However, it is challenging to accurately determine the specific source of emissions in these scenarios. Additionally, lab-scale experiments involving pile burns have not effectively distinguished between different fuel conditions and the specific mode of combustion, particularly flaming.

In this study, a custom small-scale linear tube-heater apparatus has been developed to generate steady-state emissions over extended periods of time. The design and versatility of this apparatus enable the examination of various combustion conditions, including pyrolysis, flaming, smoldering, and mixed modes. Additionally, it allows for the investigation of different fuel types, such as vegetative and structural fuels, under varying fuel conditions including shape, size, and fuel moisture content (FMC). The apparatus also facilitates the study of different external heat fluxes, oxidizer concentrations, and oxidizer flow velocities, as the environment within it can be tightly controlled. Furthermore, the emissions produced within the apparatus can be comprehensively captured, measured, and analyzed, providing valuable insights for the study.

Experiments conducted in this study focused on the Fuel Moisture Content (FMC) of four different vegetative fuels that represent wildland vegetation. Both smoldering and flaming modes of combustion were investigated, and gaseous and particulate matter emissions were recorded. Important parameters, such as Modified Combustion Efficiency (MCE) and Emission Factors (EFs), were calculated. The results revealed that CO, particulate matter, and unburned hydrocarbons showed an increase during smoldering combustion compared to flaming combustion. Furthermore, the EFs were found to be significantly correlated with

FMC for flaming combustion, whereas FMC had little effect on EFs for smoldering combustion. The emissions from the vegetative fuels, despite originating from the same location, displayed variations, highlighting the significance of fuel type. To gain a more detailed understanding of gaseous emissions, a Fourier-transform infrared (FTIR) spectroscope calibrated for 26 different gaseous species was utilized. This analysis revealed the presence of numerous hydrocarbons, acids, aldehydes, and alcohols, with their concentrations varying based on fuel type, FMC, and combustion conditions. This research also identified butane (C_4H_{10}) and hydrogen bromide (HBr) as gaseous species, which has not been commonly reported in literature. Additionally, acrolein (C_3H_4O), a known respiratory irritant, was identified for the first time during combustion in this study, whereas it had previously only been reported during pyrolysis.

Next, the experimental apparatus's versatility allowed for the quantification of the limiting conditions for the smoldering-to-flaming (StF) transition using cellulose powders, at different oxidizer flow velocities (1.5 – 10.5 cm/s), oxygen concentrations (21, 19, 15, and 10 %), and external heat fluxes (0 – 60 kW/m^2). It was found that the external heat flux required for StF transition decreases as the O_2 concentration increases from 10% to 21% at fixed flow velocities, agreeing with both phenomenological arguments and a simplified energy balance. However, for a fixed O_2 concentration, as the flow velocity increases, the required heat flux increases, due to the increased importance of convective heat losses. Furthermore, tests performed at 8% and 5% O_2 do not undergo transition even at higher heat fluxes concluding a threshold oxygen concentration of 10%. Under low-velocity conditions (airflow $<$ 5 cm/s), smoldering may still co-exist with a discrete weak blue flame because the oxygen can diffuse into reacting (smoldering) cellulose powder. An oxidizer flow velocity of 5 cm/s appears to be a limiting value for the StF transition, at least for the present experimental conditions. It was also found that increasing the density of cellulose powder required a lower external heat flux for StF transition. This work contributes to the fundamental understanding of the StF transition providing important parameters to mitigate fire events.

Finally, employing the same experimental setup with minor modifications to the sampling lines, six different respiratory protection (RP) materials were tested against the wildland fire like smoke generated by smoldering Douglas fir. The findings revealed that bandanas, which are commonly worn by wildland firefighters during wildfire events, exhibited the least effectiveness in filtering both particulate matter and gaseous emissions. Conversely, other materials demonstrated effectiveness in filtering particulate matter and some degree of effectiveness in filtering gaseous species. The outcomes of this study can be utilized to provide recommendations regarding the selection of personal protective equipment for wildland firefighters during wildfires.

7.2 Future Work

The adaptability of the small-scale, steady-state emissions apparatus developed in this study offers significant advantages for measuring a wide range of fuels under various burning con-

ditions. While this study focused solely on vegetative fuel emissions, the same apparatus can be utilized in future investigations to understand the emissions from Wildland Urban Interface (WUI) fuels. During a wildfire event, numerous homes and structures are also burned, and the emissions from the individual materials used in constructing these structures can be characterized using the same apparatus. The database resulting from such experiments will serve as valuable input for numerical models used to simulate and model emissions.

Furthermore, the experiments conducted in this study using a small-scale setup can be extrapolated to a medium-scale level. By conducting a scaling study, similar experiments can be performed to characterize the differences that arise when transitioning from small-scale to medium-scale emissions. This will contribute to a better understanding of the relationship between fire size and emissions. The findings of this study will provide valuable insights into the effects of scaling on emissions. If the scaling proves to be reasonable, this information could assist land managers in comprehending the relationship between fuel loading, moisture content, and the resulting emissions. Such knowledge can inform prescribed fire planning, predictions regarding public health in local communities, and a wide range of earth-climate studies.

Finally, although this research focuses on predicting the limiting conditions for the smoldering-to-flaming (StF) transition specifically for cellulose powder, the scope of the work could be expanded to include a variety of different fuels, starting with wood. While cellulose is the primary component of wood, wood also contains hemi-cellulose and lignin. By examining the limiting conditions for wood combustion, which represents a more realistic real-world scenario, a more comprehensive understanding can be achieved. This extension would enhance the practical applicability of the findings.

Appendix A

FTIR spectral bands

The FTIR is calibrated for 26 gaseous species at 100°C and 650 torr, utilizing specific spectral regions. Table A.1 presents the details of the specific spectral ranges employed for calibrating different gases, as well as the information regarding interference from other gases.

In the Table A.1 below, "+" means that the corresponding spectral regions are used to calibrate the corresponding gaseous species and "I" means that the gaseous species have an interference with gaseous species. For example, HCN is an interference for CO_2 at spectral region of 743.00 - 735.50 cm^{-1}.

Table A.1: Spectral bands and interferences of various gas species used during the FTIR calibration.

Spectral regions	CO	CO_2	HCN	SO_2	HCl	HF	HBr	C_3H_4O	CH_2O	NO	NO_2	NH_3	CH_4	H_2O	C_2H_2	C_2H_6	C_3H_8	C_4H_{10}	CH_3OH	C_4H_8	HNO_2	CH_3COOH	HCO_2H	C_2H_4	C_3H_6	C_5H_8
743.00 - 735.50		+	I											I												
757.00 - 766.50		+	I											I												
923.01 - 970.02		I						I	I			+		I												
993.00 - 1006.00												I							+							
1130.00 - 1095.00		I										I											+			
1250.00 - 1253.00												I	I	I							+					
1273.00 - 1275.00												I	I	I							+					
2660.00 - 2535.00					I		I	I	I				I	I								+				
1344.38 - 1346.07			I	+									I	I												
1353.50 - 1354.30			I	+									I	I												
1371.14 - 1371.86			I	+									I	I												
1375.96 - 1376.93			I	+									I	I												
1584.50 - 1588.00											+			I												
1597.00 - 1599.00											+			I												
1813.50 - 1816.00										+				I												
1851.00 - 1855.50		I								+				I												
2168.00 - 2185.00	+	I												I												
2224.00 - 2214.00	+													I												
2470.00 - 2640.00				I	I		+																			
2657.00 - 2784.00					I		I	I	+				I													

Spectral regions	CO	CO_2	HCN	SO_2	HCl	HF	HBr	C_3H_4O	CH_2O	NO	NO_2	NH_3	CH_4	H_2O	C_2H_2	C_2H_6	C_3H_8	C_4H_{10}	CH_3OH	C_4H_8	HNO_2	CH_3COOH	HCO_2H	C_2H_4	C_3H_6	C_5H_8
2680.00 - 2699.00					I		I	+	I		I		I	I								I				
2705.00 - 2725.00					I		I	+	I		I		I	I								I				
2700.00 - 2705.00					+																					
2725.00 - 2730.00					+		I						I	I												
2995.00 - 2695.00					I			I	I		I	I	I	I		+	+	+		I		I				
3075.42 - 3150.00					I								+			I	I	I								
3237.50 - 3239.50			I			I						I		I	+											
3248.00 - 3252.50			I			I						I		I	+											
3267.50 - 3269.50			I			I						I		I	+											
3304.00 - 3307.00			I			I						I		I	+											
3330.50 - 3332.00			I			I						I		I	+											
3343.50 - 3345.00			I			I						I		I	+											
3247.00 - 3249.00			+											+												
3267.00 - 3269.50			+											I												
3286.00 - 3288.00			+											I												
3329.00 - 3332.50			+											I												
3349.00 - 3354.00			+											I												
3357.50 - 3359.00			+											I												
3261.00 - 3262.40			+											I												
4107.00 - 4112.00						+	I	I						I												
4173.00 - 4175.00						+	I	I						I												
1073.91 - 855.76					I		I	I				I	I	I		I	I	I							I	I
892.88 - 906.00					I		I	I				I	I	I		I	I	I		+					+	+

Appendix B

Supplementary Material to Chapter 3

The experimental results discussed in Chapter 3 present the emission factors (EFs) for flaming and smoldering combustion of four different vegetative fuels at three different fuel moisture contents using the Enerac 700 for gaseous species and TSI DustTrak for particulate matter.

Most of the data is presented in Fig. 3.3, and the remaining smoldering EF plots are presented in Fig. B.1. Please note that live mountain laurel did not sustain smoldering combustion and has not been plotted in Fig. B.1d. Smoldering combustion did not show variation in EFs with changes in FMC, as seen for flaming combustion. In Fig. B.1, the EFs for CO_2, HC, and NO_x remain uniform, regardless of FMC, whereas some variation is seen in the EFs for TPM and CO.

For Douglas fir, as the FMC reduces from live to wet, the EF(TPM) also reduces and remains similar for wet and dry conditions (within the standard deviation of the values). Similar results were found for EF(TPM) for lodgepole pine, pitch pine, and mountain laurel. For EF(CO), the variation is very small for Douglas fir, lodgepole pine, and mountain laurel, whereas a very high EF is seen for live pitch pine compared to wet and dry conditions. This could be due to the volatiles present in the moisture of the fuel and incomplete burning behavior.

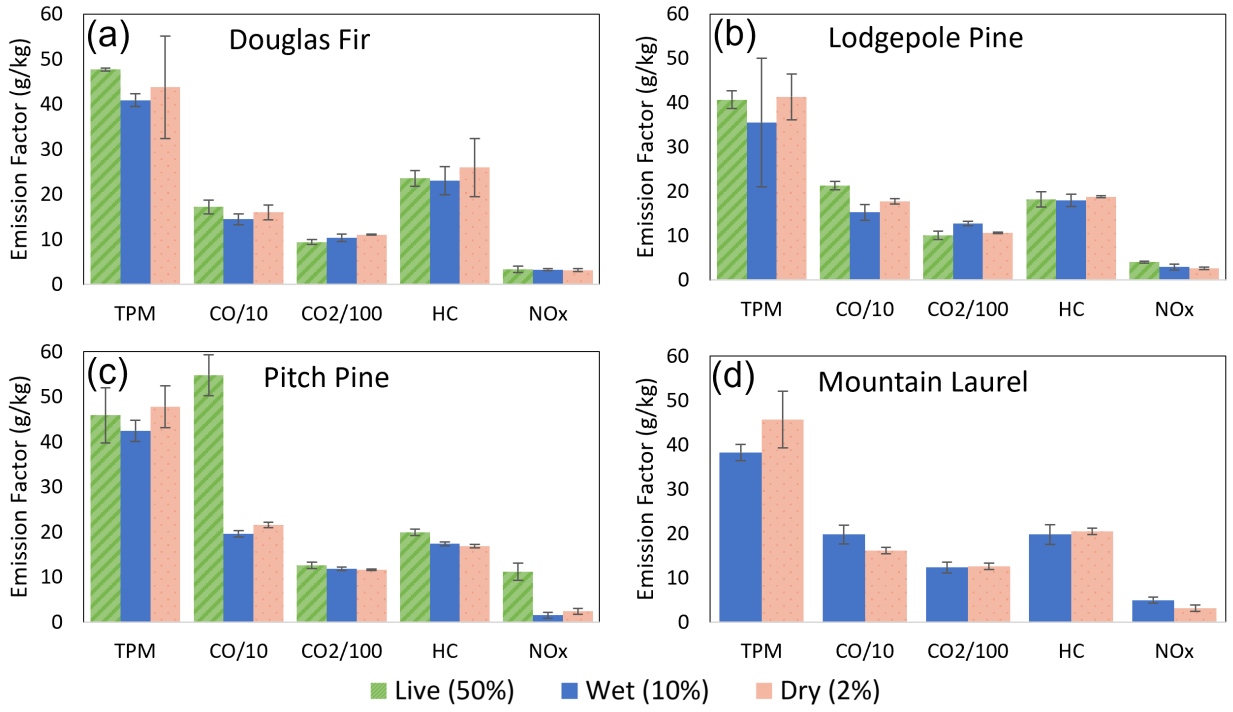

Figure B.1: Average EFs of different species during smoldering combustion of different fuels at 3 FMC conditions. Error bars represent the standard deviation between averages from different tests.

Appendix C

Supplementary Material to Chapter 4

Improved grammar: Figure C.1 (a,c) shows the variation in the 3D spectra of flaming and smoldering of live Douglas fir, respectively. Smoldering emits a higher concentration of unburnt hydrocarbons, which can be clearly seen at wavenumbers 4000 - 2500 cm^{-1} in Fig. C.1(d). Additionally, a higher concentration of CO can be observed at 2200 - 2400 cm^{-1}.

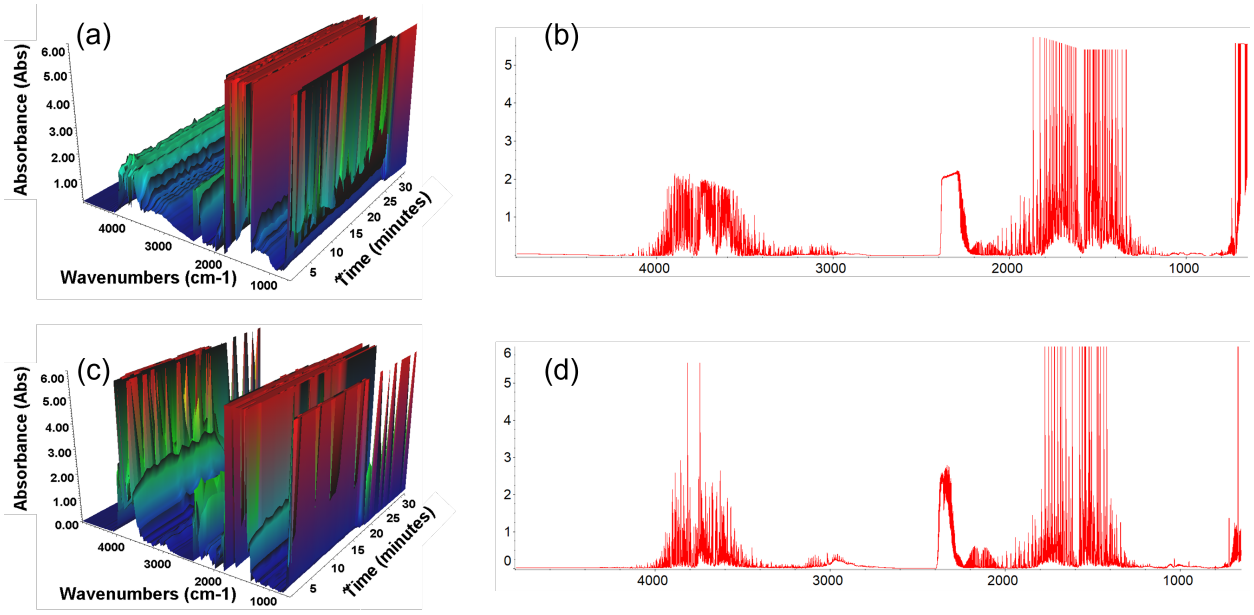

Figure C.1: (a) 3D spectrum of live flaming Douglas fir, (b) 2d plot of live flaming Douglas fir at any given time, (c) 3D spectrum of live smoldering Douglas fir, and (d) 2d plot of live smoldering Douglas fir at any given time.

Appendix D

Supplementary Material to Chapter 5

The smoldering-to-flaming transition was studied for cellulose powder to gain a better understanding of limiting conditions. Figure D.1 presents the emissions, which remained steady throughout the duration of the experiment. The concentration of CO started at approximately 15% and took about 2 minutes to reach a steady state. This occurred because the experiment required a few seconds initially to ignite, and a similar trend can be observed for HC as well. However, all other gaseous species, namely CO_2, SO_2, and NO_x, exhibited a steady state trend.

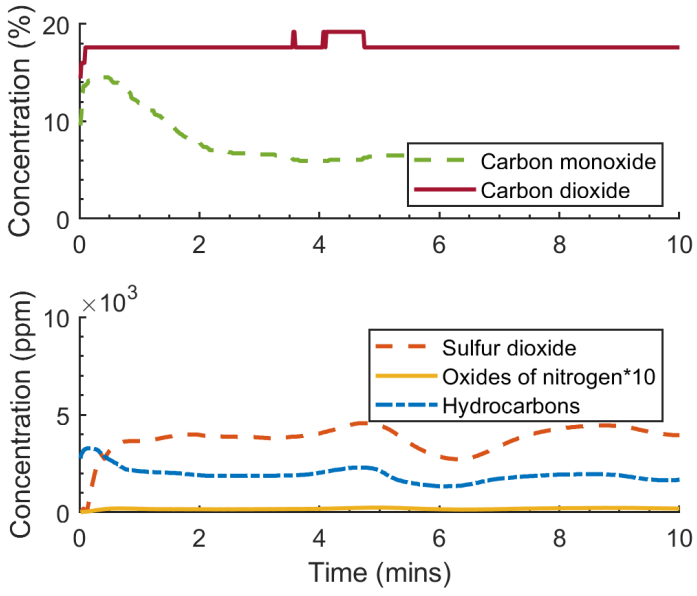

Figure D.1: Gas emissions over time at an oxygen concentration of 21% and oxidizer flow velocity of 1.73 cm/s.

Chapter 5, Section 5.3.3 discuss the trends of gaseous emissions at various 21% O_2 concentration and at varying flow velocities. Similar trends were observed for 19%, 15%, and 10% O_2 concentration ans has been plotted in Fig. D.2, D.3, and D.4 respectively.

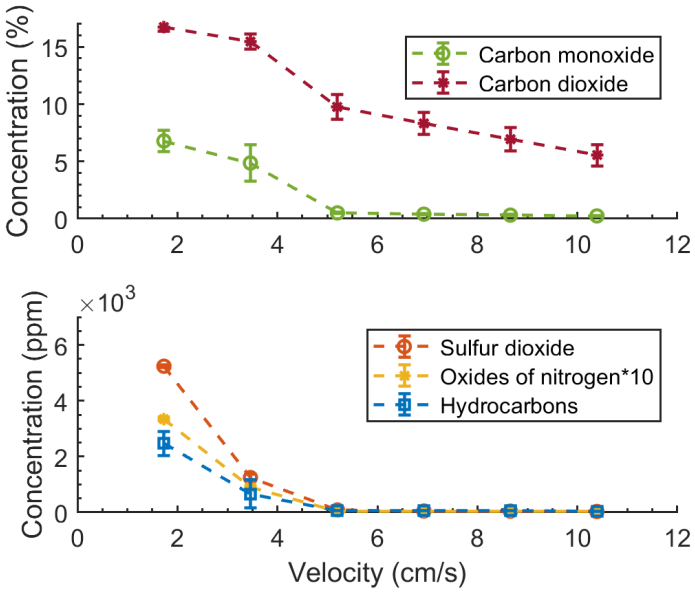

Figure D.2: Gas emissions after StF transition at an oxygen concentration of 19%.

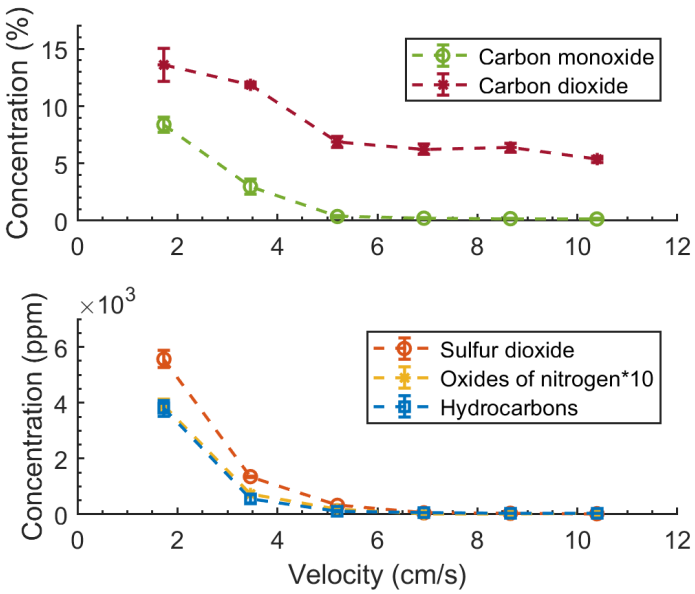

Figure D.3: Gas emissions after StF transition at an oxygen concentration of 15%.

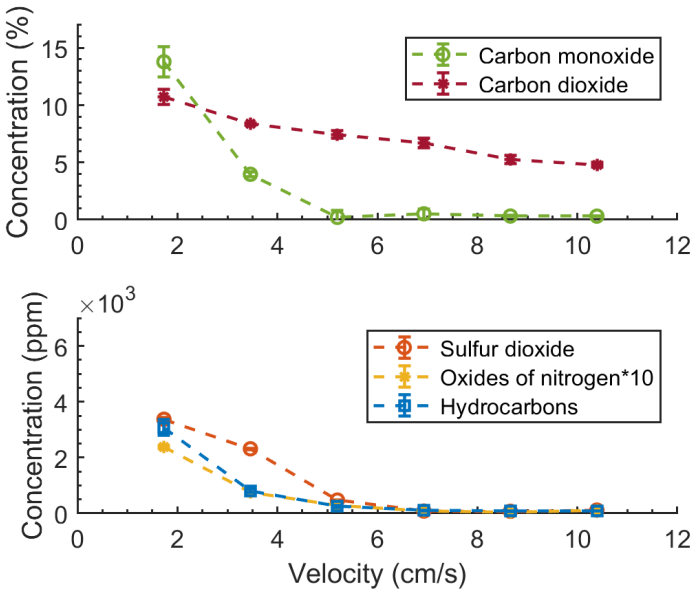

Figure D.4: Gas emissions after StF transition at an oxygen concentration of 10%.

Bibliography

[1] Enerac-Incorporated, Gas Analyzer Enerac 700.

[2] TSI-Incorporated, DUSTTRAK DRX AEROSOL MONITOR 8534.

[3] S. Urbanski, Wildland fire emissions, carbon, and climate: Emission factors, For. Ecol. Manag. 317 (2014) 51–60.

[4] I. Bertschi, R. J. Yokelson, D. E. Ward, R. E. Babbitt, R. A. Susott, J. G. Goode, W. M. Hao, Trace gas and particle emissions from fires in large diameter and belowground biomass fuels, Journal of Geophysical Research: Atmospheres 108 (D13) (2003).

[5] J. G. Goode, R. J. Yokelson, R. A. Susott, D. E. Ward, Trace gas emissions from laboratory biomass fires measured by open-path fourier transform infrared spectroscopy: Fires in grass and surface fuels, Journal of Geophysical Research: Atmospheres 104 (D17) (1999) 21237–21245.

[6] V. Selimovic, R. J. Yokelson, C. Warneke, J. M. Roberts, J. De Gouw, J. Reardon, D. W. Griffith, et al., Aerosol optical properties and trace gas emissions by pax and op-ftir for laboratory-simulated western us wildfires during firex, Atmos. Chem. Phys 18 (4) (2018) 2929–2948.

[7] G. R. McMeeking, S. M. Kreidenweis, S. Baker, C. M. Carrico, J. C. Chow, J. L. Collett Jr, W. M. Hao, A. S. Holden, T. W. Kirchstetter, W. C. Malm, et al., Emissions of trace gases and aerosols during the open combustion of biomass in the laboratory, Journal of Geophysical Research: Atmospheres 114 (D19) (2009).

[8] S. P. Urbanski, W. M. Hao, S. Baker, Chemical composition of wildland fire emissions, Developments in environmental science 8 (2008) 79–107.

[9] Y. H. Kim, S. H. Warren, Q. T. Krantz, C. King, R. Jaskot, W. T. Preston, B. J. George, M. D. Hays, M. S. Landis, M. Higuchi, et al., Mutagenicity and lung toxicity of smoldering vs. flaming emissions from various biomass fuels: implications for health effects from wildland fires, Environmental health perspectives 126 (1) (2018) 017011.

[10] O. Adetona, T. E. Reinhardt, J. Domitrovich, G. Broyles, A. M. Adetona, M. T. Kleinman, R. D. Ottmar, L. P. Naeher, Review of the health effects of wildland fire

smoke on wildland firefighters and the public, Inhalation toxicology 28 (3) (2016) 95–139.

[11] A. G. Rappold, S. L. Stone, W. E. Cascio, L. M. Neas, V. J. Kilaru, M. S. Carraway, J. J. Szykman, A. Ising, W. E. Cleve, J. T. Meredith, et al., Peat bog wildfire smoke exposure in rural north carolina is associated with cardiopulmonary emergency department visits assessed through syndromic surveillance, Environmental health perspectives 119 (10) (2011) 1415–1420.

[12] C. E. Reid, M. Jerrett, I. B. Tager, M. L. Petersen, J. K. Mann, J. R. Balmes, Differential respiratory health effects from the 2008 northern california wildfires: A spatiotemporal approach, Environmental research 150 (2016) 227–235.

[13] A. L. Westerling, H. G. Hidalgo, D. R. Cayan, T. W. Swetnam, Warming and earlier spring increase western us forest wildfire activity, science 313 (5789) (2006) 940–943.

[14] W. M. Jolly, M. A. Cochrane, P. H. Freeborn, Z. A. Holden, T. J. Brown, G. J. Williamson, D. M. Bowman, Climate-induced variations in global wildfire danger from 1979 to 2013, Nature communications 6 (1) (2015) 1–11.

[15] R. Barbero, J. T. Abatzoglou, N. K. Larkin, C. A. Kolden, B. Stocks, Climate change presents increased potential for very large fires in the contiguous united states, International Journal of Wildland Fire 24 (7) (2015) 892–899.

[16] M. Goss, D. L. Swain, J. T. Abatzoglou, A. Sarhadi, C. A. Kolden, A. P. Williams, N. S. Diffenbaugh, Climate change is increasing the likelihood of extreme autumn wildfire conditions across california, Environmental Research Letters 15 (9) (2020) 094016.

[17] M. J. Eden, J. Matz, P. Garg, M. P. Gonzalez, K. McElderry, S. Wang, M. J. Gollner, J. M. Oakes, C. Bellini, Prolonged smoldering douglas fir smoke inhalation augments respiratory resistances, stiffens the aorta, and curbs ejection fraction in hypercholesterolemic mice, Science of The Total Environment (2022) 160609.

[18] M. Burke, A. Driscoll, S. Heft-Neal, J. Xue, J. Burney, M. Wara, The changing risk and burden of wildfire in the united states, Proceedings of the National Academy of Sciences 118 (2) (2021) e2011048118.

[19] P. E. Dennison, S. C. Brewer, J. D. Arnold, M. A. Moritz, Large wildfire trends in the western united states, 1984–2011, Geophysical Research Letters 41 (8) (2014) 2928–2933.

[20] A. L. Westerling, Increasing western us forest wildfire activity: Sensitivity to changes in the timing of spring, Philosophical Transactions of the Royal Society B: Biological Sciences 371 (1696) (2016) 20150178.

[21] D. A. Jaffe, S. M. O'Neill, N. K. Larkin, A. L. Holder, D. L. Peterson, J. E. Halofsky, A. G. Rappold, Wildfire and prescribed burning impacts on air quality in the united states, Journal of the Air & Waste Management Association 70 (6) (2020) 583–615.

[22] P. Garg, T. Roche, M. Eden, J. Matz, J. M. Oakes, C. Bellini, M. J. Gollner, Effect of moisture content and fuel type on emissions from vegetation using a steady state combustion apparatus, International Journal of Wildland Fire 31 (1) (2021) 14–23. doi:10.1071/WF20118.

[23] N. May, E. Ellicott, M. Gollner, An examination of fuel moisture, energy release and emissions during laboratory burning of live wildland fuels, Int. J. Wildland Fire 28 (3) (2019) 187–197.

[24] Y. Liu, S. Goodrick, W. Heilman, Wildland fire emissions, carbon, and climate: Wildfire–climate interactions, Forest Ecology and Management 317 (2014) 80–96.

[25] S. M. Holm, M. D. Miller, J. R. Balmes, Health effects of wildfire smoke in children and public health tools: a narrative review, Journal of exposure science & environmental epidemiology 31 (1) (2021) 1–20.

[26] F. H. Johnston, R. J. Webby, L. S. Pilotto, R. S. Bailie, D. L. Parry, S. J. Halpin, Vegetation fires, particulate air pollution and asthma: a panel study in the australian monsoon tropics, International journal of environmental health research 16 (6) (2006) 391–404.

[27] F. H. Johnston, A. M. Kavanagh, D. M. Bowman, R. K. Scott, Exposure to bushfire smoke and asthma: an ecological study, Medical Journal of Australia 176 (11) (2002) 535–538.

[28] M. A. Arbex, P. H. N. Saldiva, L. A. A. Pereira, A. L. F. Braga, Impact of outdoor biomass air pollution on hypertension hospital admissions, Journal of Epidemiology & Community Health 64 (7) (2010) 573–579.

[29] J. Unosson, A. Blomberg, T. Sandström, A. Muala, C. Boman, R. Nyström, R. Westerholm, N. L. Mills, D. E. Newby, J. P. Langrish, et al., Exposure to wood smoke increases arterial stiffness and decreases heart rate variability in humans, Particle and fibre toxicology 10 (1) (2013) 20.

[30] T. E. Reinhardt, R. D. Ottmar, Smoke exposure at western wildfires, USDA FS PNRS Report No. PNW-RP-525 (2000) (2000).

[31] B. B. Palm, Q. Peng, C. D. Fredrickson, B. H. Lee, L. A. Garofalo, M. A. Pothier, S. M. Kreidenweis, D. K. Farmer, R. P. Pokhrel, Y. Shen, et al., Quantification of organic aerosol and brown carbon evolution in fresh wildfire plumes, Proceedings of the National Academy of Sciences 117 (47) (2020) 29469–29477.

[32] F. Reisen, D. Hansen, M. P. Meyer, Exposure to bushfire smoke during prescribed burns and wildfires: Firefighters' exposure risks and options, Environ. Int. 37 (2) (2011) 314–321.

[33] P. Garg, S. Wang, M. J. Gollner, Transient gas and particulate emissions from douglas-fir and lodgepole pine at two different moisture contents, 13th United States National Combustion Meeting (2023).

[34] P. H. Freeborn, M. J. Wooster, W. M. Hao, C. A. Ryan, B. L. Nordgren, S. P. Baker, C. Ichoku, Relationships between energy release, fuel mass loss, and trace gas an aerosol emissions during laboratory biomass fires, J. Geophys. Res. D. 113 (1) (2008) 1–17.

[35] I. R. Burling, R. J. Yokelson, D. W. T. Griffith, T. J. Johnson, P. Veres, J. M. Roberts, C. Warneke, S. P. Urbanski, J. Reardon, D. R. Weise, W. M. Hao, J. De Gouw, Laboratory measurements of trace gas emissions from biomass burning of fuel types from the southeastern and southwestern United States, Atmos. Chem. Phys. 10 (22) (2010) 11115–11130.

[36] Y. Hu, E. G. Christensen, H. M. F. Amin, T. E. L. Smith, G. Rein, Experimental study of moisture content effects on the transient gas and particle emissions from peat fires, Combust. Flame 209 (2019) 408–417.

[37] Y. Hu, E. Christensen, F. Restuccia, G. Rein, Transient gas and particle emissions from smouldering combustion of peat, Pro. Comb. Inst. 37 (3) (2019) 4035–4042.

[38] S. P. Urbanski, Combustion efficiency and emission factors for wildfire-season fires in mixed conifer forests of the northern rocky mountains, US, Atmos. Chem. Phys. 13 (2013) 7241–7262.

[39] R. J. Yokelson, D. W. Griffith, D. E. Ward, Open-path fourier transform infrared studies of large-scale laboratory biomass fires, Journal of Geophysical Research: Atmospheres 101 (D15) (1996) 21067–21080.

[40] H. E. Mobley, C. Barden, A. Crow, D. Fender, D. Jay, R. Winkworth, Southern forestry smoke management guidebook, USDA Forest Service, South-eastern Forest Experiment Station, General Technical Report SE-10.(Asheville, NC) (1976).

[41] C. McMahon, D. Wade, S. Tsoukalas, Combustion characteristics and emissions from burning organic soils, in: 73rd Annual Meeting of the Air Pollution Control Association, Montreal, Quebec, 1980, pp. 22–27.

[42] S. Lin, P. Sun, X. Huang, Can peat soil support a flaming wildfire?, International Journal of Wildland Fire 28 (8) (2019) 601–613.

[43] M. Schmidt, C. Lohrer, U. Krause, Self-ignition of dust at reduced volume fractions of ambient oxygen, Journal of loss prevention in the process industries 16 (2) (2003) 141–147.

[44] M. A. Santoso, E. G. Christensen, J. Yang, G. Rein, Review of the transition from smouldering to flaming combustion in wildfires, Frontiers in Mechanical Engineering 5 (2019) 49.

[45] S. L. Manzello, S. Suzuki, M. J. Gollner, A. C. Fernandez-Pello, Role of firebrand combustion in large outdoor fire spread, Progress in energy and combustion science 76 (2020) 100801.

[46] A. C. Fernandez-Pello, Wildland fire spot ignition by sparks and firebrands, Fire Safety Journal 91 (2017) 2–10.

[47] M. Hajilou, S. Hu, T. Roche, P. Garg, M. J. Gollner, A methodology for experimental quantification of firebrand generation from wui fuels, Fire technology 57 (2021) 2367–2385.

[48] K. M. Navarro, K. A. Clark, D. J. Hardt, C. E. Reid, P. W. Lahm, J. W. Domitrovich, C. R. Butler, J. R. Balmes, Wildland firefighter exposure to smoke and covid-19: A new risk on the fire line, Science of The Total Environment 760 (2021) 144296.

[49] K. Gibos, Protecting wildland firefighters from smoke exposure: a review of the literature (2005).

[50] C. Alves, C. Gonçalves, M. Evtyugina, C. Pio, F. Mirante, H. Puxbaum, Particulate organic compounds emitted from experimental wildland fires in a mediterranean ecosystem, Atmospheric Environment 44 (23) (2010) 2750–2759.

[51] O. Safety, H. Administration, Permissible exposure limits – annotated tables Available at `https://https://www.osha.gov/annotated-pels/table-z-1` [Online; accessed 27-Mar-2023] (2021).

[52] L. Stawovy, B. Balakrishnan, The threat of wildfires and pulmonary complications: A narrative review, Current Pulmonology Reports (2022) 1–7.

[53] R. J. Yokelson, I. R. Burling, J. B. Gilman, C. Warneke, C. E. Stockwell, J. De Gouw, S. K. Akagi, S. P. Urbanski, P. Veres, J. M. Roberts, W. C. Kuster, J. Reardon, D. W. T. Griffith, T. J. Johnson, S. Hosseini, J. W. Miller, D. R. Cocker, H. Jung, D. R. Weise, Coupling field and laboratory measurements to estimate the emission factors of identified and unidentified trace gases for prescribed fires, Atmospheric Chemistry and Physics 13 (1) (2013) 89–116. doi:10.5194/acp-13-89-2013.

[54] A. I. Miranda, V. Martins, P. Cascão, J. H. Amorim, J. Valente, C. Borrego, A. J. Ferreira, C. R. Cordeiro, D. X. Viegas, R. Ottmar, Wildland smoke exposure values and exhaled breath indicators in firefighters, Journal of Toxicology and Environmental Health, Part A 75 (13-15) (2012) 831–843.

[55] M. Evtyugina, A. I. Calvo, T. Nunes, C. Alves, A. P. Fernandes, L. Tarelho, A. Vicente, C. Pio, Voc emissions of smouldering combustion from mediterranean wildfires in central portugal, Atmospheric Environment 64 (2013) 339–348.

[56] A. J. De Vos, A. Cook, B. Devine, P. J. Thompson, P. Weinstein, Effect of protective filters on fire fighter respiratory health during simulated bushfire smoke exposure, American journal of industrial medicine 49 (9) (2006) 740–750.

[57] J. K. Kodros, K. O'Dell, J. M. Samet, C. L'Orange, J. R. Pierce, J. Volckens, Quantifying the health benefits of face masks and respirators to mitigate exposure to severe air pollution, GeoHealth 5 (9) (2021) e2021GH000482.

[58] D. Leith, C. L'Orange, J. Mehaffy, J. Volckens, Design and performance of upas inlets for respirable and thoracic mass sampling, Journal of Occupational and Environmental Hygiene 17 (6) (2020) 274–282.

[59] M. Rahimmalek, S. A. H. Goli, Evaluation of six drying treatments with respect to essential oil yield, composition and color characteristics of thymys daenensis subsp. daenensis. celak leaves, Industrial Crops and Products 42 (2013) 613–619.

[60] F. X. Jervis, G. Rein, Experimental study on the burning behaviour of pinus halepensis needles using small-scale fire calorimetry of live, aged and dead samples, Fire and Materials 40 (3) (2016) 385–395.

[61] F. J. Matt, M. A. Dietenberger, D. R. Weise, Summative and ultimate analysis of live leaves from southern us forest plants for use in fire modeling, Energy & Fuels 34 (4) (2020) 4703–4720.

[62] H. J. Einbrodt, J. Hupfeld, F. H. Prager, H. Sand, The suitability of the din 53436 test apparatus for the simulation of a fire risk situation with flaming combustion, J. Fire Sciences 2 (1984) 427–438.

[63] F. H. Proger, Assessment of fire model din 53436, J. Fire Sciences 6 (1988) 3–24.

[64] M. I. Gilmour, Y. H. Kim, A. Hays, M.and Farraj, D. D., The role of composition and particle size on the toxicity of wildfire emissions, JFSP Report No. 14-1-04-16 (2018).

[65] A. A. Stec, T. R. Hull, K. Lebek, Characterisation of the steady state tube furnace (ISO TS 19700) for fire toxicity assessment, Poly. Degradation and Stab. 93 (11) (2008) 2058–2065.

[66] W. Seiler, P. J. Crutzen, Estimates of gross and net fluxes of carbon between the biosphere and the atmosphere from biomass burning, Climatic change 2 (3) (1980) 207–247.

[67] D. E. Ward, C. C. Hardy, Smoke emissions from wildland fires, Environ. Int. 17 (2-3) (1991) 117–134.

[68] T. E. Reinhardt, R. D. Ottmar, Baseline measurements of smoke exposure among wildland firefighters, J. Occup. Environ. Hyg. 1 (9) (2004) 593–606.

[69] D. E. Ward, Particulate matter emissions for fires in the palmetto-gallberry fuel type, Forest science 29 (4) (1983) 761–770.

[70] S. F. F. L. (Macon, Ga.), S. F. E. S. (Asheville, Southern forestry smoke management guidebook, Vol. 10, Southeastern Forest Experiment Station, 1976.

[71] L.-W. Chen, P. Verburg, A. Shackelford, D. Zhu, R. Susfalk, J. Chow, J. Watson, Moisture effects on carbon and nitrogen emission from burning of wildland biomass, Atmospheric Chemistry and Physics 10 (14) (2010) 6617–6625.

[72] M. Possell, T. L. Bell, The influence of fuel moisture content on the combustion of Eucalyptus foliage, Int. J. Wildland Fire 22 (3) (2013) 343–352.

[73] K. Hayashi, K. Ono, M. Kajiura, S. Sudo, S. Yonemura, A. Fushimi, K. Saitoh, Y. Fujitani, K. Tanabe, Trace gas and particle emissions from open burning of three cereal crop residues: Increase in residue moistness enhances emissions of carbon monoxide, methane, and particulate organic carbon, Atmospheric Environment 95 (2014) 36–44.

[74] B. M. Butler, J. Palarea-Albaladejo, K. D. Shepherd, K. M. Nyambura, E. K. Towett, A. M. Sila, S. Hillier, Mineral–nutrient relationships in african soils assessed using cluster analysis of x-ray powder diffraction patterns and compositional methods, Geoderma 375 (2020) 114474.

[75] D. R. Weise, J. Palarea-Albaladejo, T. J. Johnson, H. Jung, Analyzing wildland fire smoke emissions data using compositional data techniques, Journal of Geophysical Research: Atmospheres 125 (6) (2020) e2019JD032128.

[76] D. R. Weise, H. Jung, J. Palarea-Albaladejo, D. R. Cocker, Compositional data analysis of smoke emissions from debris piles with low-density polyethylene, Journal of the Air & Waste Management Association 70 (8) (2020) 834–845.

[77] M. J. Hurley, D. T. Gottuk, J. R. Hall Jr, K. Harada, E. D. Kuligowski, M. Puchovsky, J. M. Watts Jr, C. J. WIECZOREK, et al., SFPE handbook of fire protection engineering, Springer, 2015.

[78] S. McAllister, M. Finney, Convection ignition of live forest fuels, Fire Safety Science 11 (2014) 1312–1325.

[79] J. Engstrom, J. Butler, S. Smith, L. Baxter, T. Fletcher, D. Weise, Ignition behavior of live california chaparral leaves, Combustion Science and Technology 176 (9) (2004) 1577–1591.

[80] T. H. Fletcher, B. M. Pickett, S. G. Smith, G. S. Spittle, M. M. Woodhouse, E. Haake, D. R. Weise, Effects of moisture on ignition behavior of moist california chaparral and utah leaves, Combustion Science and Technology 179 (6) (2007) 1183–1203.

[81] A. M. Smith, W. T. Tinkham, D. P. Roy, L. Boschetti, R. L. Kremens, S. S. Kumar, A. M. Sparks, M. J. Falkowski, Quantification of fuel moisture effects on biomass consumed derived from fire radiative energy retrievals, Geophysical Research Letters 40 (23) (2013) 6298–6302.

[82] K. M. Navarro, M. T. Kleinman, C. E. Mackay, T. E. Reinhardt, J. R. Balmes, G. A. Broyles, R. D. Ottmar, L. P. Naher, J. W. Domitrovich, Wildland firefighter smoke exposure and risk of lung cancer and cardiovascular disease mortality, Environmental research 173 (2019) 462–468. doi:10.1016/j.envres.2019.03.060.

[83] P. Garg, S. Wang, J. M. Oakes, C. Bellini, M. J. Gollner, The effectiveness of filter material for respiratory protection worn by wildland firefighters, Fire Safety Journal (2023) 103811.

[84] E.-A. Guérette, C. Paton-Walsh, M. Desservettaz, T. E. Smith, L. Volkova, C. J. Weston, C. P. Meyer, Emissions of trace gases from australian temperate forest fires: emission factors and dependence on modified combustion efficiency, Atmospheric Chemistry and Physics 18 (5) (2018) 3717–3735.

[85] N. K. Scharko, A. M. Oeck, T. L. Myers, R. G. Tonkyn, C. A. Banach, S. P. Baker, E. N. Lincoln, J. Chong, B. M. Corcoran, G. M. Burke, R. D. Ottmar, J. C. Restaino, D. R. Weise, T. J. Johnson, Gas-Phase Pyrolysis Products Emitted by Prescribed Fires in Pine Forests with a Shrub Understory in the Southeastern United States, Atmospheric Chemistry and Physics Discussions (2019) 1–46doi:10.5194/acp-2019-174.

[86] S. Akagi, I. R. Burling, A. Mendoza, T. J. Johnson, M. Cameron, D. W. Griffith, C. Paton-Walsh, D. Weise, J. Reardon, R. J. Yokelson, Field measurements of trace gases emitted by prescribed fires in southeastern us pine forests using an open-path ftir system, Atmospheric Chemistry and Physics 14 (1) (2014) 199–215.

[87] L.-W. A. Chen, P. Verburg, A. Shackelford, D. Zhu, R. Susfalk, J. C. Chow, J. G. Watson, Moisture effects on carbon and nitrogen emission from burning of wildland biomass, Atmospheric Chemistry and Physics 10 (14) (2010) 6617–6625. doi:10.5194/acp-10-6617-2010.
URL `https://acp.copernicus.org/articles/10/6617/2010/`

[88] A. A. Stec, P. Fardell, P. Blomqvist, L. Bustamante-Valencia, L. Saragoza, E. Guillaume, Quantification of fire gases by FTIR: Experimental characterisation of calibration systems, Fire Safety Journal 46 (5) (2011) 225–233. doi:10.1016/j.firesaf.2011.02.004.

[89] M. O. Andreae, Emission of trace gases and aerosols from biomass burning–an updated assessment, Atmospheric Chemistry and Physics 19 (13) (2019) 8523–8546.

[90] L. M. McKenzie, D. E. Ward, W. M. Hao, Chlorine and bromine in the biomass of tropical and temperate ecosystems, Biomass burning and global change 1 (1996) 241–248.

[91] X. Liu, L. G. Huey, R. J. Yokelson, V. Selimovic, I. J. Simpson, M. Müller, J. L. Jimenez, P. Campuzano-Jost, A. J. Beyersdorf, D. R. Blake, et al., Airborne measurements of western us wildfire emissions: Comparison with prescribed burning and air quality implications, Journal of Geophysical Research: Atmospheres 122 (11) (2017) 6108–6129.

[92] D. Ward, L. Radke, Emissions measurements from vegetation fires: A comparative evaluation of methods and results, Fire in the Environment: The Ecological, Atmospheric and Climatic Importance of Vegetation Fires 13 (1993) 53–76.

[93] T. J. Ohlemiller, Modeling of smoldering combustion propagation, Progress in energy and combustion science 11 (4) (1985) 277–310.

[94] G. Rein, Smoldering combustion, in: SFPE Handbook of Fire Protection Engineering, Springer, 2016, pp. 581–603.

[95] K. Palmer, Smouldering combustion in dusts and fibrous materials, Combustion and Flame 1 (2) (1957) 129–154.

[96] H. D. R. Jiang, F. J. Miller, A. C. Fernandez-Pello, J. L. Torero, D. Walther, Mechanisms of flame spread and smolder wave propagation, Microgravity Combustion: Fire in Free Fall (2001) 299.

[97] G. Rein, Smouldering fires and natural fuels, Fire phenomena and the Earth system: an interdisciplinary guide to fire science (2013) 15–33.

[98] Y. Hu, N. Fernandez-Anez, T. E. Smith, G. Rein, Review of emissions from smouldering peat fires and their contribution to regional haze episodes, International Journal of Wildland Fire 27 (5) (2018) 293–312.

[99] Y. Qin, Y. Chen, S. Lin, X. Huang, Limiting oxygen concentration and supply rate of smoldering propagation, Combustion and Flame 245 (2022) 112380.

[100] X. Huang, G. Rein, Computational study of critical moisture and depth of burn in peat fires, International Journal of Wildland Fire 24 (6) (2015) 798–808.

[101] J. G. Quintiere, Fundamentals of fire phenomena (2006).

[102] J. L. Torero, J. I. Gerhard, M. F. Martins, M. A. Zanoni, T. L. Rashwan, J. K. Brown, Processes defining smouldering combustion: Integrated review and synthesis, Progress in Energy and Combustion Science 81 (2020) 100869.

[103] O. Putzeys, A. Bar-Ilan, G. Rein, A. C. Fernandez-Pello, D. L. Urban, The role of secondary char oxidation in the transition from smoldering to flaming, Proceedings of the Combustion Institute 31 (2) (2007) 2669–2676.

[104] Z. Wang, N. Liu, H. Yuan, H. Chen, X. Xie, L. Zhang, G. Rein, Smouldering and its transition to flaming combustion of polyurethane foam: An experimental study, Fuel 309 (2022) 122249.

[105] A. Bar-Ilan, G. Rein, A. C. Fernandez-Pello, J. Torero, D. Urban, Forced forward smoldering experiments in microgravity, Experimental thermal and fluid science 28 (7) (2004) 743–751.

[106] N. Moussa, T. Toong, C. Garris, Mechanism of smoldering of cellulosic materials, in: Symposium (International) on Combustion, Vol. 16, Elsevier, 1977, pp. 1447–1457.

[107] O. Kadowaki, M. Suzuki, K. Kuwana, Y. Nakamura, G. Kushida, Limit conditions of smoldering spread in counterflow configuration: Extinction and smoldering-to-flaming transition, Proceedings of the Combustion Institute 38 (3) (2021) 5005–5013.

[108] D. T. Stephen, A. Carlo, F. Nde-Pello, K. Miyasaka, Controlling mechanisms in the transition from smoldering to flaming of flexible polyurethane foam, in: Symposium (International) on Combustion, Vol. 26, Elsevier, 1996, pp. 1505–1513.

[109] J. Yang, N. Liu, H. Chen, W. Gao, Smoldering and spontaneous transition to flaming over horizontal cellulosic insulation, Proceedings of the Combustion Institute 37 (3) (2019) 4073–4081.

[110] S. Lin, H. Yuan, X. Huang, A computational study on the quenching and near-limit propagation of smoldering combustion, Combustion and Flame 238 (2022) 111937.

[111] T. J. Ohlemiller, Forced smolder propagation and the transition to flaming in cellulosic insulation, Combustion and Flame 81 (3-4) (1990) 354–365.

[112] S. Lin, T. H. Chow, X. Huang, Smoldering propagation and blow-off on consolidated fuel under external airflow, Combustion and Flame 234 (2021) 111685.

[113] N. Boonmee, J. Quintiere, Glowing ignition of wood: the onset of surface combustion, Proceedings of the Combustion Institute 30 (2) (2005) 2303–2310.

[114] F. Richter, G. Rein, Pyrolysis kinetics and multi-objective inverse modelling of cellulose at the microscale, Fire Safety Journal 91 (2017) 191–199.

[115] A. Sullivan, R. Ball, Thermal decomposition and combustion chemistry of cellulosic biomass, Atmos. Environ. 47 (2012) 133–141.

[116] F. Richter, G. Rein, The role of heat transfer limitations in polymer pyrolysis at the microscale, Frontiers in Mechanical Engineering 4 (2018) 18.

[117] L. Burhenna, J. Messmer, T. Aicher, M. P. Laborie, The effect of the biomass components lignin, cellulose and hemicellulose on tga and fixed bed pyrolysis, J. of Analytical and Applied Pyrolysis 101 (2013) 177–184.

[118] F. E. Rogers, T. J. Ohlemiller, Cellulosic insulation material i. overall degradation kinetics and reaction heats, Combustion Science and Technology 24 (1980) 129–137.

[119] S. Wang, C. Zou, H. Yang, C. Lou, S. Cheng, C. Peng, C. Wang, H. Zou, Effects of cellulose, hemicellulose, and lignin on the combustion behaviours of biomass under various oxygen concentrations, Bioresource Technology 320 (2021) 124375.

[120] S. Lin, X. Huang, Extinction of wood fire: Modeling smoldering and near-limit flame under irradiation, Fire Technology (2022) 1–18.

[121] A. S. for Testing, M. C. D.-. on Plastics, Standard Test Method for Measuring the Minimum Oxygen Concentration to Support Candle-like Combustion of Plastics (Oxygen Index)., ASTM International, 2010.

[122] J. Yang, N. Liu, H. Chen, W. Gao, R. Tu, Effects of atmospheric oxygen on horizontal peat smoldering fires: Experimental and numerical study, Proceedings of the Combustion Institute 37 (3) (2019) 4063–4071.

[123] S. Wang, S. Lin, Y. Liu, X. Huang, M. J. Gollner, Smoldering ignition using a concentrated solar irradiation spot, Fire safety journal 129 (2022) 103549.

[124] M. B. Rice, S. B. Henderson, A. A. Lambert, K. R. Cromar, J. A. Hall, W. E. Cascio, P. G. Smith, B. J. Marsh, S. Coefield, J. R. Balmes, et al., Respiratory impacts of wildland fire smoke: Future challenges and policy opportunities. an official american thoracic society workshop report, Annals of the American Thoracic Society 18 (6) (2021) 921–930.

[125] J. C. Corbin, G. J. Smallwood, I. D. Leroux, J. Norooz Oliaee, F. Liu, T. A. Sipkens, R. G. Green, N. F. Murnaghan, T. Koukoulas, P. Lobo, Systematic experimental comparison of particle filtration efficiency test methods for commercial respirators and face masks, Scientific Reports 11 (1) (2021) 1–16.

[126] P. Forouzandeh, K. O'Dowd, S. C. Pillai, Face masks and respirators in the fight against the covid-19 pandemic: An overview of the standards and testing methods, Safety science 133 (2021) 104995.

[127] S. Rengasamy, R. Shaffer, B. Williams, S. Smit, A comparison of facemask and respirator filtration test methods, Journal of occupational and environmental hygiene 14 (2) (2017) 92–103.

[128] L. David, L. Christian, V. John, Quantitative protection factors for common masks and face coverings, Enviromental Science and Technology 55 (5) (2021) 3136–3143. doi:10.1021/acs.est.0c07291.

[129] K. L. Foote, Determination of toxic material penetrations for wildland respirator filters, San Jose State University, 1994.

[130] K. Khayan, T. Anwar, S. Wardoyo, W. Lakshmi Puspita, Active carbon respiratory masks as the adsorbent of toxic gases in ambient air, Journal of toxicology 2019 (2019).

[131] N. N. Soeroso, T. K. Intan, M. Ichwan, M. H. Fadlurrahman, F. R. Ananda, Four-type of masks and its effectiveness based on reduced level of expiratory carbon-monoxide, Medical Archives 74 (5) (2020) 342.

[132] L. E. Bowen, Does that face mask really protect you?, Applied Biosafety 15 (2) (2010) 67–71. doi:10.1177/153567601001500204.

[133] A. Tcharkhtchi, N. Abbasnezhad, M. Z. Seydani, N. Zirak, S. Farzaneh, M. Shirinbayan, An overview of filtration efficiency through the masks: Mechanisms of the aerosols penetration, Bioactive materials 6 (1) (2021) 106–122.

[134] C. D. Zangmeister, J. G. Radney, E. P. Vicenzi, J. L. Weaver, Filtration efficiencies of nanoscale aerosol by cloth mask materials used to slow the spread of sars-cov-2, ACS nano 14 (7) (2020) 9188–9200.

[135] J. S. Cuddy, J. A. Sol, W. S. Hailes, B. C. Ruby, Work patterns dictate energy demands and thermal strain during wildland firefighting, Wilderness & environmental medicine 26 (2) (2015) 221–226. doi:10.1016/j.wem.2014.12.010.

[136] S. Rengasamy, R. Shaffer, B. Williams, S. Smit, A comparison of facemask and respirator filtration test methods, Journal of Occupational and Environmental Hygiene 14 (2) (2017) 92–103. doi:10.1080/15459624.2016.1225157.

[137] NFPA 1984 - standard respirators for wildland fire-fighting and wildland urban interface operations (2022).

[138] DHS S&T seeks respiratory protection suitable for wildland firefighting, Forest Ecology and Management (2022).

[139] U. E. P. Agency, Health effects of formaldehyde Available at `https://www.epa.gov/formaldehyde` [Online; accessed 27-Mar-2023] (2022).

[140] W. Mueller, C. J. Horwell, A. Apsley, S. Steinle, S. McPherson, J. W. Cherrie, K. S. Galea, The effectiveness of respiratory protection worn by communities to protect from volcanic ash inhalation. part i: Filtration efficiency tests, International journal of hygiene and environmental health 221 (6) (2018) 967–976.